Reduction and sintering of copper nano-particles by non-equilibrium atmospheric pressure plasma jet

Guiling Zhang

Supervisor: Professor Shin-ichi Kuroda

Department of production science and technology

Graduate school of engineering

Gunma University

Contents

Chapter 1 General introduction 1
1.1 Definition of plasma 1
1.2 Atmospheric pressure non-equilibrium plasma 1
1.2.1 Dielectric barrier discharge 3
1.2.2 Corona discharges 4
1.2.3 Cold plasma torch 4
1.2.4 Atmospheric pressure plasma jet 4
1.3 Application of atmospheric pressure plasma jet 6
1.4 Reduction and sintering of copper nano-particles 7
1.5 Objectives of this study 9
References 10
Chapter 2 Reduction and sintering of copper nano-particles by atmospheric pressure plasma jet 19
2.1 Introduction 19
2.2 Experimental details 20
2.2.1 Non-equilibrium atmospheric pressure plasma device 20
2.2.2 Sample preparation 20
2.2.3 Plasma diagnostics 22
2.2.4 Analysis of surface characterization 23
2.3 Results and discussion 23
2.3.1 Electrical characterization of APC plasma jet 23
2.3.2 OES analysis of APC plasma jet 24
2.3.3 XPS analysis of copper particles 25
2.3.4 SEM observation of copper particles 27
2.3. 5 Electrical resistances 28
2.4 Conclusions 28
References 29
Character 3 Reduction and sintering of copper nano-particles by non-equilibrium atmospheric pressure plasma jet generated by “beam plasma torch” 45
3.1 Introduction 45
3.2 Experimental details 46
3.2.1 Non-equilibrium atmospheric pressure plasma device and experimental procedures 46
3.2.2 Sample preparation 47
3.2.3 Plasma diagnostics 47
3.2.4 Characterization of the copper nano-particles surface 48
3.3 Results and discussion 48
3.3.1 Electrical characterization of plasma 48
3.3.2 Optical emission spectra of plasma jet generated by beam plasma torch 50
3.3.3 Application on surface treatment of copper nano-paste 53
3.4 Conclusions 56
References 57
Chapter 4 Reduction and sintering of copper nano-particles by atmospheric pressure plasma

generated by beam plasma torch with air-cooling 78
4.1 Introduction 78
4.2 Experimental details 79
4.2.1 Non-equilibrium atmospheric pressure plasma device and experimental procedures 79
4.2.2 80
Sample preparation 80
4.2.3 Plasma diagnostics 80
4.2.4 Characterization of the copper nano-particles surface 81
4.3 results and discussion 81
4.3.1 Effect of air-cooling system of electrode on the electrical characterization of plasma jet 81
4.3.2 Effect of air-cooling of electrode on the OES characteristics of plasma jet 83
4.3.3 Effect of air-cooling of electrode on the temperate of Ar/H_2 plasma jet 85
4.3.4 The OES characteristics of beam plasma torch with air-cooling system 86
4.4 Application on reduction and sintering of copper nano-particles 87
4.4.1 XPS analysis 88
4.4.2 Observation by SEM 89
4.4 Conclusions 90
References 91
Chapter 5 Important factors affecting the reduction and sintering of copper nano-particles through plasma-treatment 112
5.1 Introduction 112
5.2 The effect of treatment distance down from the plasma torch on the sintering of copper nano-particles 113
5.3 The decisive gas emission intensity for sintering of copper nano-particles 115
5.4 Relationship between treatment time and the emission intensity from the Ar/H_2 plasma generated by the beam plasma torch with air-cooling 116
5.5 The effect of H_2 flow rate on the sintering of copper nano-particles through plasma-treatment by beam plasma torch with air-cooling 117
5.6 Discussion 120
5.7 Conclusions 121
References 121
Chapter 6 Summary 134
List of publications 137
Acknowledgements 138

Chapter 1 General introduction

1.1 Definition of plasma

Plasma is a neutral ionized gas containing electrons, ions and neutrals, separate from the traditional solids, liquids, and gases [1, 2]. In 1879, it was first identified by Sir William Crookes in a crookes tube, and called “radiant matter”. In 1897, the British physicist Sir J.J. Thomson identified the nature of the matter as “cathode ray”. The term of “plasma” was dubbed in 1928 by Irving Langmuir. It constitutes more than 99% in the universe. Electrons and photons are usually called as “light” species and the other constituents are called as “heavy” species.

1.2 Atmospheric pressure non-equilibrium plasma

The properties of plasma change in terms of electronic density or temperature depending on the type of energy supply and the amounts of energy transferred to the plasma. These two parameters distinguish plasmas into different categories, shown in Fig. 1.1 [1]. Basing on the relative energetic levels of electrons and heavy species of the plasma, and generated condition, plasma can be generally classified as two categories, thermal equilibrium plasma (thermal plasma) and non-thermal equilibrium plasma (non-equilibrium plasma or cold plasma) [2]. In thermal plasma, transitions and chemical reactions are controlled by collisions and not by radiative processes. Moreover, collision phenomena are micro-reversible in thermal plasma, suggesting that each kind of collision is balanced by its inverse (excitation/de-excitation; ionization/recombination; kinetic

balance) [3]. Therefore, in thermal plasma the electron temperature is equal to the gas temperature (depending on the temperature of heavy particles).

The electron temperature (T_e) and heavy particle temperature (T_h) are used to describe the characteristics of non-equilibrium plasma (cold plasma). Because of the huge mass difference between electrons and heavy particles, the plasma temperature (or gas temperature) is determined by T_h. On the other hand, the electron-induced de-excitation rate of the atom is generally lower than the corresponding electron-induced excitation rate because of a significant radiative de-excitation rate. Therefore, the density distribution of excited atoms in cold plasma is possible to depart from Boltzmann distribution, suggesting that the gas temperature is much lower than the electron temperature [4-7].

The effect of gas pressure on electron temperature (T_e) and gas temperature (T_g) is shown in Fig. 1.2 [8]. At relatively lower pressure (10^{-4} - 10^{-2} kPa) gas temperature is much lower than electron temperature. The heavy particles are excited or ionized through inelastic collisions with electrons. These inelastic collisions do not raise the temperature of heavy particles. However, collisions in the plasma intensify when the gas pressure becomes higher. They lead to both plasma chemistry (by inelastic collisions) and heavy particles heating (by elastic collisions). Then, the difference between T_e and T_g decreases; plasma state is close to the thermal equilibrium state. How to prevent heavy particles from achieving thermal equilibrium is crucial to generate non- thermal equilibrium plasma at atmospheric pressure. It was found that the density of the feeding power affects the plasma state (thermal equilibrium or not) at a large extent. Namely, a high power density induces atmospheric pressure thermal equilibrium plasma, e.g. arc plasma, and a low density of feeding power or a pulsed power supply lead to atmospheric pressure non-equilibrium

plasma.

The atmospheric pressure plasma, unlike low-pressure or vacuum plasma, does not require vacuum or low-pressure devices, which is very expensive on vacuum equipment and its maintenance.

1.2.1 Dielectric barrier discharge

The DBDs unique combination of non-equilibrium and quasi-continuous behavior has drawn great interest in a wide range of application and fundamental studies [9]. It is also usually called as "silent" [10]. In addition, the metal surface treatment processes using dielectric barrier discharges (DBDs) have also attracted a great deal of attention in various industrial applications [11]. DBDs are based on the use of a dielectric barrier in the discharge gap. It was used to stop electric currents and prevents the formation.

As shown in Fig. 1.3 (a), the planar and cylindrical electrode arrangements are used in DBDs. [12]. No matter what kind of electrode arrangement is employed, the presence of at least one dielectric layers between the metallic electrodes across the discharge gap is essential for the discharge [9]. DBDs use a dielectric covering over one or both of the electrodes of which one is typically low frequency, radio frequency or alternating current driven while the other is grounded [12] Depending on the construction and the operating conditions, three different types of DBDs can be distinguished, called the filamentary DBDs, the patterned DBDs and the diffuse DBDs [13]. In most cases filamentary DBDs are generated. If the local electric field strength in the gas spacing gap reaches the ignition level, the breakdown occurs at many points followed by the development of filaments, named microdischarges [14, 15].

1.2.2 Corona discharges

The schematic diagram of corona discharge is shown in Fig.1.3 (b). It is a non-arcing, non-uniform plasma that ignites adjacent to the high electric filed generated by the sharp points of the electrode [12]. The corona discharge is basically a Townsend discharge. It occurs prior to the electrical breakdown. Corona discharge consists of a cathode-wire and an anode (the treated material), the DC power supply is pulsed. The plasma creates a lighting crown around the wire, that is why the discharge is called "corona" [1].The corona is dark at lower currents while the active region becomes visible and looks like a glow discharge at higher current [12].

1.2.3 Cold plasma torch

In 1992, a "cold" plasma torch was first decribed by H. Koinuma [1, 10]. The schematic diagram is shown in Fig.1.3 (c). Generally its construct is a RF electrode and quartz tubing as the insulator between both the electrodes to ensure both plasma stability and homogeneity. The outer electrode is grounded, and the working gas flows into the gap between the cathode and the dielectric tube [10].The material of the RF electrode is usually SUS, and Koinuma and coworkers measured the electron temperature and indicated that the gas composition plays an important role in determining the electron temperature [1].

1.2.4 Atmospheric pressure plasma jet

The atmospheric pressure plasma jet operates in a capacitive configuration using RF power and produces a stable, uniform glow discharge between two bare metallic electrodes, without any

dielectric in between. Basically, there are three geometric configurations of atmospheric pressure plasma jets, as shown in Fig.1.3 (d), one plasma source with concentric electrodes and two types of sources with parallel electrodes. In the latter the electrodes are solid in one case, and perforated in the other [13].

Fig.1.4 (a) shows an original design of APPJ consisting of two concentric cylindrical electrodes, and RF power is applied to the inner electrode. Fig.1.4 (b) shows the most frequently used design consisting two solid parallel planar electrodes. In this design, the gas flows along the electrodes through the rectangular cross section between them. Because the electrodes may be rather large, it is sometimes called as large area APPJ [13]. Fig.1.4 (b) shows the most recently developed design by Surfx Technologies, consisting of two parallel perforated metal electrodes. The gas flow through the perforated electrodes requires vary high throughput.

Both of dielectric barrier discharges (DBDs) and RF discharges can be used to generate atmospheric pressure plasma jets. In DBDs, dielectric materials are used to cover one or both electrode, and the high voltage in the frequency range of several kHz is employed to ignite the discharge. It would cause a drop of the voltage across the plasma with charging accumulation on the dielectric layer, which covers the electrodes, Therefore, DBDs are self-pulsed discharges that can restrict the discharge current and avoid arcing. Radio frequency (RF) discharges have also been used to generate atmospheric pressure cold plasma jet with devices that are similar to DBDs or with devices where the electrodes are bare metal [15-18]. With bare metal electrodes, glow-to-arc transition occurs easily; therefore, the electrodes have to be cooled and the gas flow rate has to be adjusted to a certain level to minimize the risk of glow-to-arc transition. RF driven plasma devices require impedance matching between the power source and the plasma to optimize

the dissipated power in the plasma and minimize the reflected power.

It has been a hot topic to study the RF discharge [19-22]. There are two important discharge regimes of RF discharge observed in atmospheric pressure plasma jets called α-mode and the γ-mode [23-26]. In the α-mode, also called as "low-current discharge", the ionization is supported by the bulk plasma electrons. The electrons are oscillating with drifting amplitude and are trapped in the bulk plasma region. The α-sheath, where electrons are depleted, forms since the electrodes serve as a tank for electrons. For helium atmospheric pressure plasma, the thickness of the α-sheath is in the order of 0.25 mm. In the γ-mode, also called as "high current discharge", the ionization is maintained by secondary electron emission from the electrode surface. The sheath thickness in the γ-mode is at least one order of magnitude smaller than that of the α-mode.

According to Raizer [27], when the product of gas spacing and gas pressure exceeds a critical value, the α-mode discharge becomes instable and α-mode discharge transits into γ-mode or a coexisting α and γ mode discharge. Depending on the plasma device and the operating conditions, an upper discharge current or discharge power limit exists for the α-mode discharge, where the breakdown of the α-sheath occurs. The decrease in sheath thickness is followed by a decrease in the discharge voltage. When the voltage needed to sustain the γ-mode discharge is far below the voltage needed to sustain the α-mode discharge, only a pure γ-mode will be observed [23-26]. However, when the γ-mode discharge voltage is comparable to that of the α-mode discharge, then a coexisting α-mode and γ-mode discharge will be observed

1.3 Application of atmospheric pressure plasma jet

In recent years, atmospheric pressure plasma has become a very popular tool in various fields

[28-36], especially surface treatment as shown in Fig. 1.5. The materials that can be treated by plasma is in varieties filed. High-density polyethylene (HDPE) and polytetrafluoroethlene (PTFE) was treated by capacitively coupled DBD atmospheric pressure remote glow discharge plasma, as reported by Y. Iriyama [28]. As reported by U. Lommatzsch. *et al*. [29], an atmospheric pressure plasma jet was also used for the surface treatment and lead to the different results with changing the working gas from air to nitrogen. The working gas and the additive gas play an important role in determining the characteristic of plasma. As for the surface treatment on metal, the SUS and copper were plasma-treated in the study reported by M.C.Kim *et al*. [30], resulting in the improvement of contact angles. Cold atmospheric pressure plasma has the potential to replace many traditional, vacuum based, plasma processing practices as well as open up entirely new plasma applications. It is because of its ability to inexpensively treat the low-value items as well as the materials incompatible with vacuum processing owing to their high vapor pressure or cumbersome shape or size.

1.4 Reduction and sintering of copper nano-particles

Copper is the most significant circuit material for electronic devices and components [31, 37-41]. It has a great significance in all industries, particularly in the electrical sector due to low cost and high conductivity [42]. However, copper is easily oxidized in the air to form a thin copper oxide which is believed to be mechanically weak [31]. The oxidation of copper has always been a serious problem in the process of wiring circuit boards by soldering [43].

Copper nano-particles have been synthesized and characterized by different methods. Stability and reactivity are the two important factors that impede the use and development of metal cluster

in a new generation of nano-electronic device [42]. In order to obtain higher stability of the copper nano-particles, most of the copper nano-particles were oxidized before used.

In order to reduce and sinter copper nano-particles, various methods were used. K. Takeda [44] reported that at around 90 ℃ the copper sheet was reduced by atmospheric pressure remote Argon (Ar)/Hydrogen (H_2) plasma. According to his study, the electron density was enhanced with increasing the concentrate of hydrogen. J.H.Hsieh *et al*. investigated that it has a positive effect on cleaning copper lead frame to enhance the adhesion strength between the lead frame and the molding compound by Ar/H_2 low pressure plasma [44]. However, the size of nano-particles plays an important role in determining its melting. Also, Y. Sawada. *et al*. [36] expressed that copper oxide thin films were reduced by a dielectric barrier glow discharge He/H_2 plasma, and the reduction gradually shifts from the surface into the inner region. Summary, addition of H_2 to Ar plasma or Helium (He) plasma could lead it easier to reduce the copper oxide in various plasma sources.

On the other hand, in order to sinter the copper nano-particles, many methods are performed in various fields. However, the melting point of the metal nano-particles is generally determined by their size. For the different size of the nano-particles, many methods have been tied by researches. J. Liu *et al*. [45] successfully tried to used spark plasma to sinter the nano-particles of $(BaTiO_3)_{0.6}(SrTiO_3)_{0.4}$ mixture. The size of the nano-particles was 60-80 nm and the sintering temperature was around 1000 ℃. D.S.Seo. *et al*. [46] sintered the silver nano-paste with Pb-free frit at 400 - 550 ℃, for the particles size of 20 - 50 nm. D.S.Seo indicates that the glass frit played an important role in sintering the nano-particles. However, in this study, the diameter of copper nano-particles used is 700 - 900 nm, whose melting point is considered as close to that of bulk

copper, around 1000 ℃.

1.5 Objectives of this study

In order to widely apply the copper nano-particles in electronic components area, e.g. the circuit board industry, to reduce the production cost and improve the performance, the objectives of this study are to overcome the shortcoming that copper is easily to be oxidized in atmosphere, reduce and sinter the copper nano-particles at relatively low temperature to improve the conductivity of the copper nano-paste, and investigate the mechanism and important factors affecting the reduction and sintering of the copper nano-particles by non-equilibrium atmospheric pressure plasma jet. The diameter of the copper nano-particles in the copper nano-paste used in this study is 700- 900 nm. A capacitive coupled RF plasma device and three kinds of plasma torches with different characteristics were used in this study. Optical emission spectroscopy (OES) and digital phosphor oscilloscope were used to investigate the plasma characteristics used in experiments. Thermogravimetry analysis (TGA) was carried out to determine the decomposition temperature of the polymer additive in the copper nano-paste used in this study. In order to study the surface morphology and elemental composition on the surface of sample, whereby investigate the changes by plasma-treatment with various plasma torches. The measurements by scanning electron microscope (SEM) and X-ray photoelectron spectroscopy (XPS) were performed. Additionally, the temperature of plasma jet was measured by a thermocouple and the resistance of the copper nano-paste treated by APC plasma torch was measured by using two terminals method.

Chapter 2 shows the construction of "APC plasma torch" and the experimental setup used for plasma diagnosis and plasma-treatment. It described the image from TG-DTA and determined the

temperature of the heat-treatment for the samples used in this study. The electrical and optical characterization of pure Ar plasma and Ar/H_2 plasma were studied under various experimental conditions. Samples were plasma-treated at 425 ℃ and analyzed by XPS and SEM, as well as the changes of resistance were maintained. The role of H_2 in Ar/H_2 plasma was also investigated.

Chapter 3 describes the construction of “the beam plasma torch” with a diameter of 1 mm plasma nozzle and the experimental setup used for plasma-treatment in the atmosphere of absent of oxygen. Also the electrical and optical characteristics of plasma were investigated under various gas flow rate. It clarifies the difference from the APC plasma torch. In this chapter, the samples were treated at 425 ℃ and ambient temperature, respectively, and compared by XPS and SEM. The temperature of plasma jet was measured with increasing the RF power and gas flow rate.

Chapter 4 describes the construction of “beam plasma torch with an air-cooling system on the electrode”. The electrical and optical properties were also investigated to characterize the effect of electrode-air-cooling on the electrical and optical properties. In this chapter, the samples were plasma-treated at ambient temperature.

Chapter 5 describes the effect of emission intensity from excited Ar and H atoms on the sintering of copper nano-particles. The emission intensity ratio of Ar/H_2 was focused to reveal sintering mechanism of copper nano-particles by the non-equilibrium atmospheric pressure plasma jet.

References

[1] C. Tendero, C. Tixier, P. Tristant: *Spectrochimica Acta Part B*, **61**, 2 (2006)

[2] M. Moreau, N. Orange, M. G. J. Feuilloley: *Biotechnol. Adv.*, **206**, 610 (2008)

[3] M. Moisan, M. D. Calzada, A. Gamero, A. Sola: *J. Appl. Phys.,* **80**, 46 (1996)

[4] R. H. Huddlestone, S. L. Leonard: *Plasma Diagnostic Techniques, Academic Press, New York*, **26**, 1685 (1965)

[5] H. R. Griem, *Plasma Spectroscopy*, McGraw-Hill, New York, 1964.

[6] W. Lochte-Holtgreven, *Plasma Diagnostics*, North-Holland, Amsterdam, 1968.

[7] M. Mitchner, C. H. Kruger, Partially Ionized Gases, Wiley, New York, 1973.

[8] M. I. Boulos, P. Fauchais, E. Pfender, T*hermal Plasmas: Fundamental and Applications*. Volume I, Plenum Press, New York, ISBN: **0-306-44607-3**, 452 (1994)

[9] V. Nehra, A. Kumar, H. K. Dwivedi: *Int. J. Eng.*, **2**, 53 (2008)

[10] A. Schütze, J. Y. Jeong, S. E. Babayan, J. Park, G. S. Selwyn, and R. F. Hicks: *IEEE Trans. Plasma Sci.*, **26**, 1685 (1998)

[11] H. S. Kim, W. S. Kang, G. H. Kim, S. H. Hong: *Thin Solid Films*, **518**, 6394 (2010)

[12] G. S. Selwyn, H. W. Herrmann, J. Park, I. Henins: *Physics Division Progress Report*, **189**, 1999–2000

[13] J. Laimer, Herbert Störi: *Plasma Process. Polym.*, **4**, 266 (2007)

[14] K. V. Kozlov, H-E. Wagner, R. Brandenburg, P. Michel: *J. Phys. D: Appl. Phys.*, **34**, 3164 (2001)

[15] X. Fei: *Characterization, Comparison and Application of Two Types of Atmospheric Pressure Cold Argon Plasma Jets*, Doctoral Thesis, Kiryu, Gunma University, 2011

[16] J. Laimer, H. Störi: *Plasma Process. Polym.*, **3**, 573 (2007)

[17] J. J. Shi, M. G. Kong: *IEEE. Trans. Plasma Sci.*, **33**, 624 (2005)

[18] J. Park, I. Henins, H. W. Herrmann, G. S. Selwayn: *J. Appl. Phys.*, **89**, 20 (2001)

[19] G. Dinescu, B. Mitu, E. Aldea, M. Dinescu: *Vacuum*, **56**, 83 (2000)

[20] E.R. Ionita, G. Dinescu: *33rd EPS Conference on Plasma Phys.* Rome, 19 - 23 June 2006 ECA, **301**, P-4.010 (2006)

[21] X. Yang, M. Moravej, G. R. Nowling, J. P. Chang, R. F. Hicks: *IEEE T. Plasma Sci.*, **33**, 294 (2005)

[22] C. Martínez, S. Kyrsta, R. Cremer, D. Neuschütz: *Surf. Interface Anal.*, **34**, 396 (2002)

[23] Y. H. Choi, J. H. Kim, K. H. Paek, W. T. Ju, Y. S. Hwang: *Surf. Coat. Technol.*, **193**, 319 (2005)

[24] S. Youn Moon, J. K. Rhee, D. B. Kim, W. Choe: *Phys. Plasmas*, **13**, 033502 (2006)

[25] X. Yang, M. Moravej, G. R. Nowling, S. E. Babayan, J. Panelon, J. P. Chang, R. F. Hicks: *Plasma Sources Sci. Technol.*, **14**, 314 (2005)

[26] J. Laimer, S. Haslinger, W. Meissl, J. Hell, H. Stǒri: *Vacuum*, **79**, 209 (2005)

[27] Y. P. Raizer, M. N. Shneider, and N. A. Yatsenko: *Radio-Freqeuncy Capacitive Discharges*, CRC, Boca Raton, FL, 1995.

[28] Y. Iriyama: *J. Photopolym. Sci. Technol.*, **23**, 599 (2010)

[29] U. Lommatzsch, D. Pasedag, A. Baalmann, G. Ellinghorst, H. Wagner: *Plasma Process. Polym.*, **4**, S1041(2007)

[30] M. C. Kim, S. H. Yang, J. H. Boo, J. G. Han: *Surf. Coat. Technol.*, **174 –175**, 839–844 (2003)

[31] Y. Sawasa, H. Tamaru, M. Kogoma, M. Kawase, K. Hashimoto, *J. Phys. D: Appl. Phys.*, **29**, 2539(1996)

[32] D. H. Shin, C. U. Bang, J. H. Kim, *et al.*: *IEEE T. Plasma Sci.*, **36**, 1241(2006)

[33] S. Ono, S. Teii, Y. Suzuki, T. Suganuma: *Thin Solid Films*, **518**, 981 (2009)

[34] J. H. Hsieh, C. Li: *Thin Solid Films*, **504**, 101 (2006)

[35] J. H. Hsieh, L. H. Fong, S. Yi, G. Metha: *Surf. Coat. Technol.*, **112**, 245 (1999)

[36] Y. Sawada, N. Taguchi, K. Tachibana: *Jpn. J. Appl. Phys.*, **38**, 6506 (1999)

[37] J. Y. Park, Y. S. Jung, J. Cho, W. K. Choi: *Appl. Surf. Sci.*, **252**, 5877 (2006).

[38] M. Ghoranneviss, F. Yaghobian, M. Farbod, M. Eshghabadi: *Curr. Appl. Phys.*, **9**, S124 (2009)

[39] W. K. Han , J. W. Choi, G. H. Hwang, S. J. Hong, J. S. Lee, S. G. Kang: *Appl. Surf. Sci.*, **252**, 2832 (2006)

[40] W. Wang, Y. Zhuang, L. Li: *Mater. Lett.*, **62**, 1724 (2008)

[41] Z. Zhang, Z. Cui, K. Chen, Y, Wang, Y. Ning: *Chinese Sci. Bull.*, **42**, 1535 (1997)

[42] P. K. Khanna, S. Gaikwad, P. V. Adhyapak, N. Singh, R. Marimuthu: *Mater. Latt.*, **61**, 4711(2007)

[43] A. Manara, V. Sirtori, L. Mammarella, *Surf. Interface Anal.*, **18**, 32 (1992)

[44] K. TakedaP, H. InuiP, H. KondoP, K. Ishikawa, M. Sekine, M. Hori: *30th ICPIG*, Belfast, Northern Ireland, UK , August 28th – September 2nd 2011

[45] J. Liu, Z. Shen, M. Nygren, B. Su, T. W. Butten: *J. Am. Ceram. Soc.*, 89, 2689 (2006)

[46] D. S. Seo, S. H. Park, J. K. Lee: *Curr. Appl. Phys.*, **9**, S72 (2009)

[47] Christine M. Welch. Richard G. Compton: *Anal Bioanal Chem.*, **384**, 601 (2006)

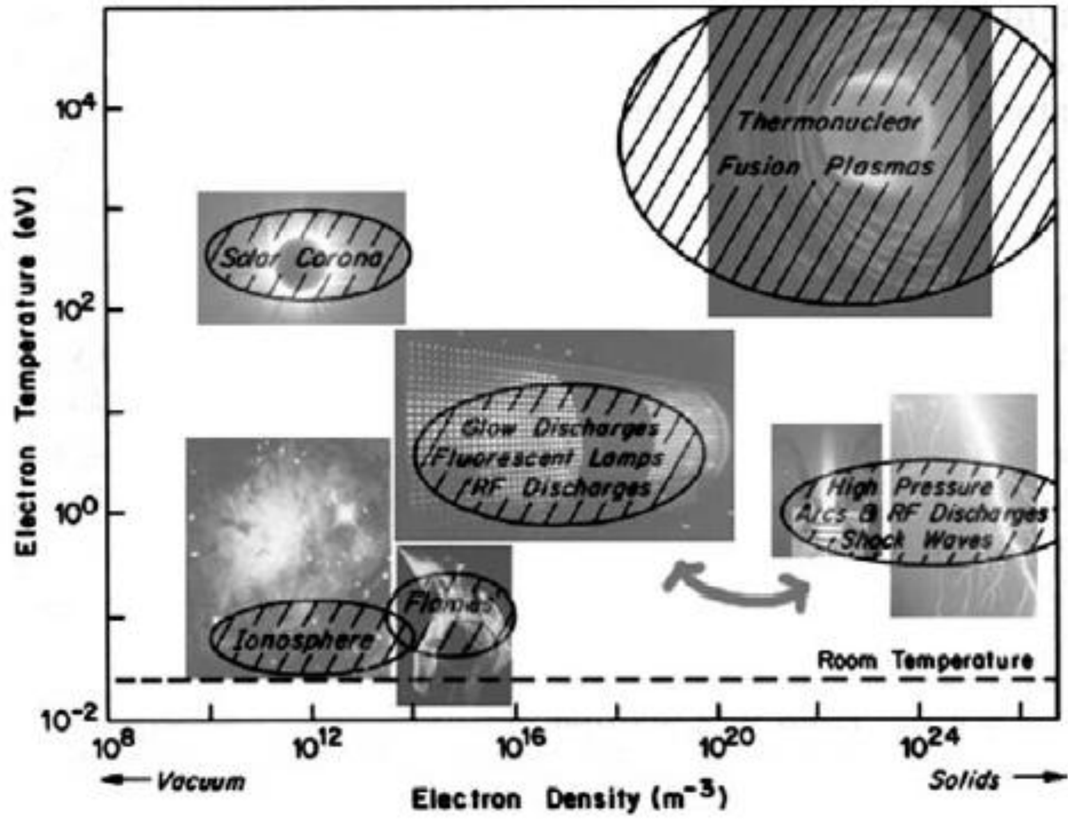

Fig. 1.1 Schematic of plasma classification [1]

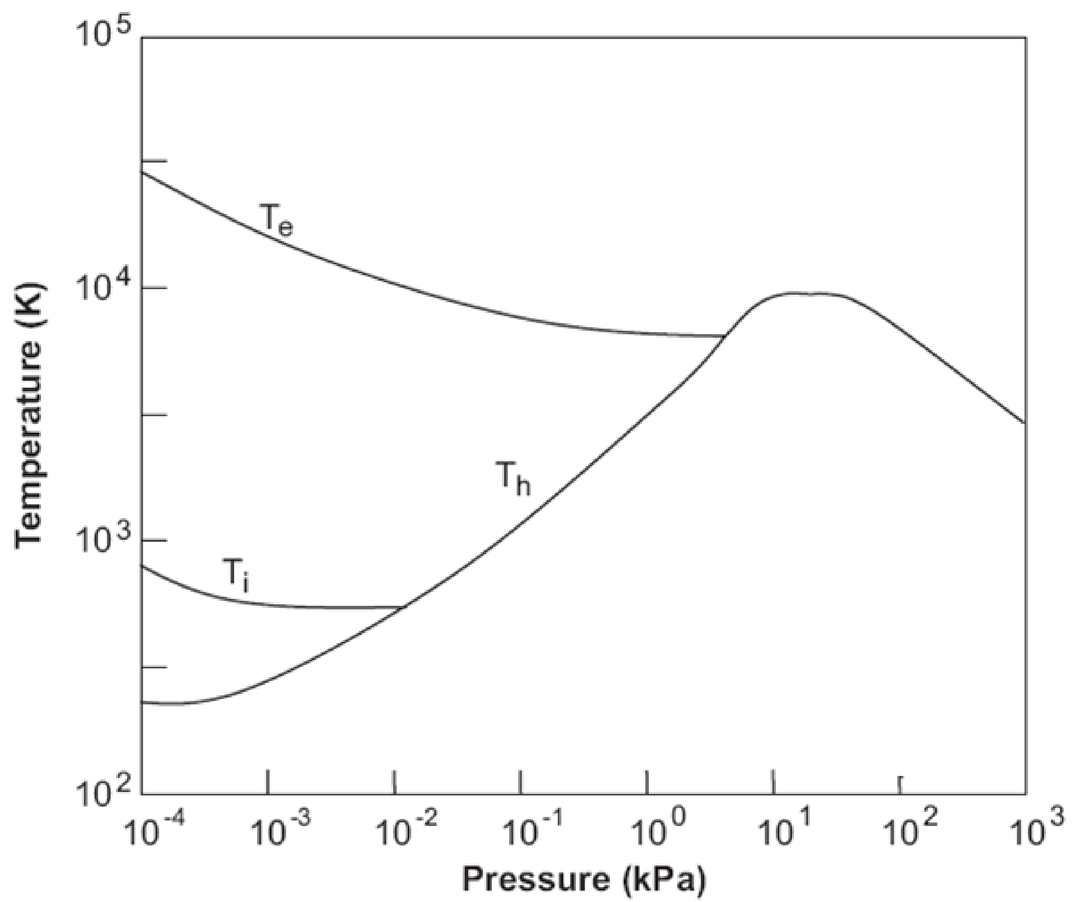

Fig. 1.2 Variation of electron and heave particle temperature with pressure [8].

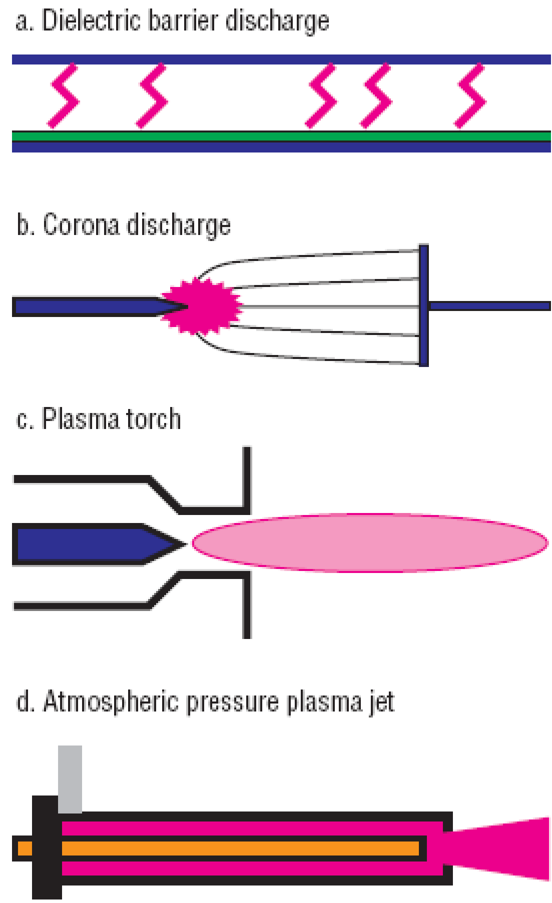

Fig.1.3 Schematic diagrams of four kinds of atmospheric pressure plasma sources. [12]

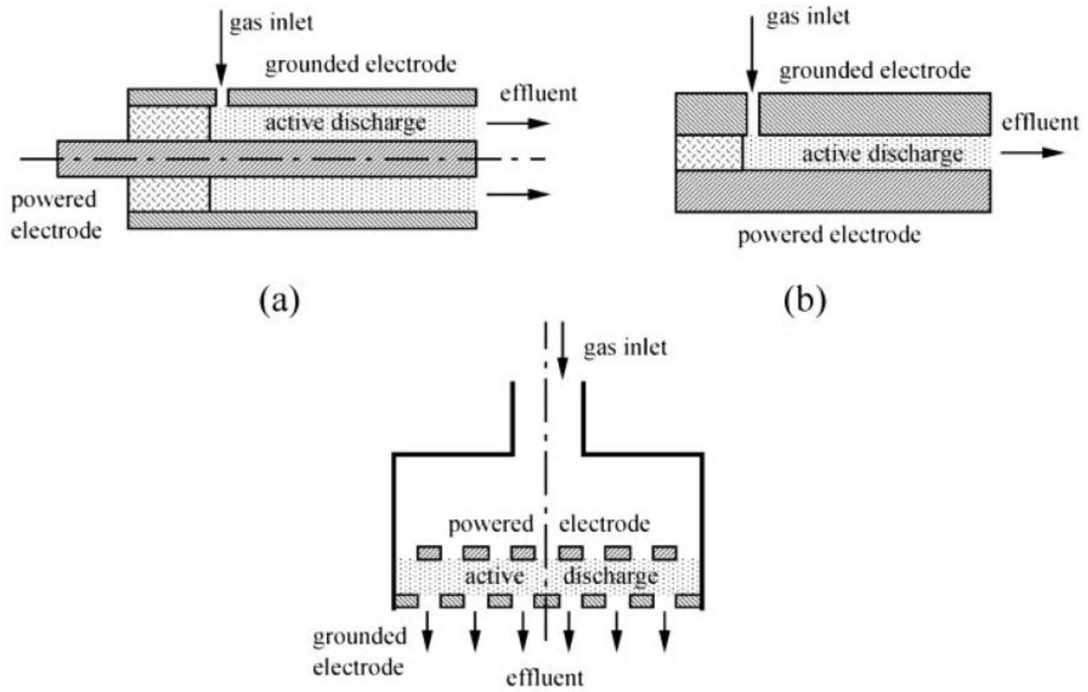

Fig. 1.4 Schematic diagrams of the configurations of atmospheric pressure plasma jet. Concentric electrodes (a), Solid parallel plate electrodes (b), perforated parallel plate electrodes (c) [13]

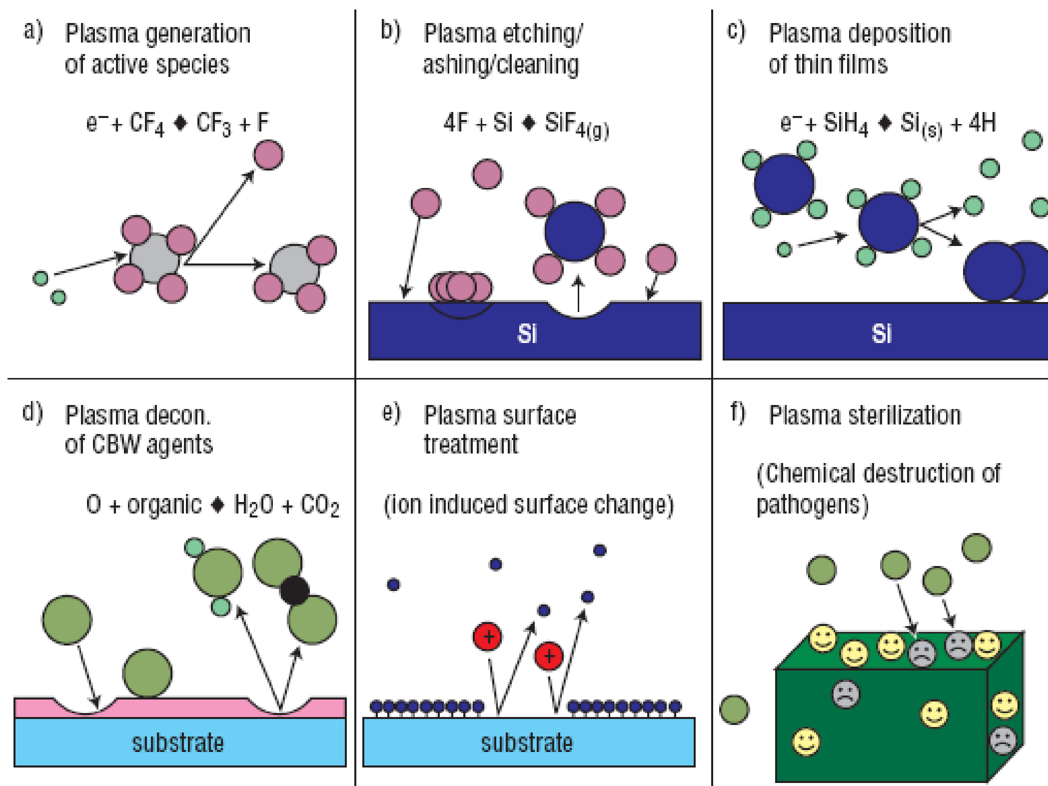

Fig. 1.5 Schematic diagram of the fundamental processed used in plasma processing of materials [12]

Chapter 2 Reduction and sintering of copper nano-particles by atmospheric pressure plasma jet

2.1 Introduction

Recently non-equilibrium atmospheric pressure plasma has been attracted great attention owing to its low cost and simple structure [1-5]. It could be effectively used to treat metal and polymer materials in the atmospheric condition. A variety of atmospheric pressure plasma jet were developed, amount of them, dielectric barrier discharges is one of the most frequently and basic way of plasma discharge [6, 7]. Traditionally, helium (He) as working gas is used to operate plasma. However it has a drawback of high cost.

As for the metallic materials, it is very interesting that the characteristics of the nano-particles are very different from those of bulk. Nowadays, the production of the electronic circuit with metal nano-particles is widely researched. The nano-particles are always sintered at high temperature or with high energy device such as laser [5, 8]. Among the various metallic materials copper is one of the most important circuits material for its high conductivity and low-cost [9, 10]. Copper nano-particles have the trend to replace the most commonly used silver nano-particles not only due to its low resistivity but also better electro-migration-resistance. Recently, various novel ways to clean and reduce the copper and copper nano-particles, such as atmospheric pressure plasma, have been developed [11-13]. However, the methods for sintering the copper nano-particles are still limited.

In this study, Ar was used instead of He gas for the working gas as it is relatively lower in cost. The Ar/H_2 non-equilibrium atmospheric pressure plasma was used to treat the thin films of copper

nano-particles in atmosphere. The electrical characterization of the plasma jet generated was investigated to confirm the discharge behavior. Optical emission spectra were also collected to investigate to changes of active species in plasma jet. The samples treated under various conditions were analyzed by X-ray photoelectron spectroscopy (XPS) and scanning emission microscopy (SEM). Also the resistance changes of the sample were measured.

2.2 Experimental details

2.2.1 Non-equilibrium atmospheric pressure plasma device

A RF capacitive coupled plasma system called "APC" developed by Cresur Corporation was used as the plasma generating device [11, 14]. The APC plasma torch consists of two parallel perforated Al electrodes and the inner electrode is connected to a RF power source with frequency of 27.12 MHz through an impedance matching network, while the outer electrode is grounded as shown in Fig.2.1. The electrode diameter was 15 mm. The diameter of the perforated holes as the plasma nozzles is 1.3 mm and the distance between them is 3.2 mm. The insulator between the electrodes is ceramics and the gap spacing between the two electrodes is 1.5 mm. The experimental conditions used were: 20 L/min of Ar and 0-10 mL/min of H_2 with RF power set at 100 W without reflect power, and the distance between the plasma torch head and sample was 3 mm.

2.2.2 Sample preparation

The processes of the metal nano-particles sintering are shown in Fig. 2.2 [15]. In fact, as shown in Fig. 2.2 (a), in order to stable the copper nano-particles, usually the polymeric dispersant was added into the copper nano-paste as the additive, which would greatly reduce the conductivity of the copper

nano-paste and prevent the nano-particles sintering. To remove the polymer additives in the paste, heat-treatment is generally carried out, as shown in Fig. 2.2 (b). Heating the sample at an appropriate temperature, the polyer dispersant would be decomposed as shown in Fig 2.2 (c), which is considered as one of the most important process for metal nano-particles sintering. Fig. 2.2 (d) shows the sintered state of the metal nano-particles, which requires much energy.

The schematic diagram of the sample used in this study is shown in Fig.2.3. The "copper nano-paste" developed by Mitsuboshi Belting Ltd. was composed of copper particles with the diameter of 700 - 900 nm and the polymer additives as the binder. The copper nano-paste was printed on alumina substrates with the thickness of 30 μm, and the printed films were dried at 100 ℃ in an oven for 30 minutes. In order to remove the polymer dispersant in the copper nano-pasted, the dried films were heated at 280 ℃ for 10 minutes. The treated temperature was determined by TGA experiment as described follow. The resistance of the copper films and the substrate between the two pieces of copper nano-films was measured. In the whole process of this study, the alumina substrates kept insulation.

TGA (a thermal analyzer TG/DTA 6200) developed by Seiko Instruments Inc. was used to measure the decomposition temperature of the polymer additive in the copper nano-paste. On the one hand, 5.959 mg sample was placed in an open aluminum pan and heated at a constant scan rate of 10 ℃/min under an air purge of 300 mL/min from ambient temperature to 500 ℃ and held at 500 ℃ for 10 minutes. On the other hand, in order to verify whether the decomposition of polymer additives have done or not, 7.661 mg sample was heated at a constant scan rate of 10 ℃/min under a nitrogen purge of 250 mL/min from ambient temperature to 500 ℃ and held at 500 ℃ for 10 minutes. Fig.2.4 shows the TGA profiles of the sample untreated. It displays that the weight loss of the sample was most obvious at 280 ℃, subsequently the weight gain of the sample was taken place rapidly. It indicates that the polymer additive in the paste

was almost decomposed at 280 ℃. And after that the copper nano-particles without organic-coating were oxidized in the atmosphere of air leading to the weight gain. The heat-treatment at 280 ℃ for 10 minutes is considered could result in the complete decomposition of the polymer additives in the copper nano-paste in this study.

In the experiment, the sample was place on the X-Y stage, which kept a slight movement of 2 mm/s forth and back in order to maintain the uniformity of the surface treatment. The schematic diagram of the experimental setup is shown in Fig. 2.6. The temperature in this study that the sample heated at was controlled by a hot plate and a resistor.

2.2.3 Plasma diagnostics

In order to characterize the plasma used in this study, electrical characterization and optical emission spectrometry (OES) measurements were carried out, the schematic diagram of the experimental setups for plasma diagnosis is shown in Fig. 2.6

Electrical characterization was investigated by using a Tekronix TDS3012C digital phosphor oscilloscope. The waveform of discharge voltage was measured with a 10:1 voltage probe (Tektronix P6139 10X Passive Probe 063-0870-05) and that of the RF current was monitored with a wide band current monitor (PearsonTM current monitor) developed by Pearson Electronics Inc., Palo Alto, California, U.S.A..

OES (optical emission spectra) was collected by C7460 plasma monitor developed by Hamamatsu Photonics K. K. at the position of 3 mm down from plasma torch head and 2 mm side from plasma jet end.

2.2.4 Analysis of surface characterization

XPS (X-ray photoelectron spectroscopy) measurements were performed to analyze the surface composition of the copper nano-paste with using Perkin Elmer ESCA 5600. Mg Kα radiation was employed as an X-ray source (15 KV, 400 W). The base pressure of system was near below 5.0×10^{-8} Torr.

Hitachi S-3000N scanning electron microscope (SEM) was utilized to observe the microstructures of the nano-particles and the printed films.

Electrical resistance was measured by a two-point probe approach. The distance of measurement is maintained as 1 cm in the experiment.

2.3 Results and discussion

2.3.1 Electrical characterization of APC plasma jet

The waveform of the discharge voltage and the RF current of Ar plasma and Ar/H_2 plasma under different flow rate of H_2 are shown in Fig. 2.7 (a) and (b). As the Ar gas flow rate of 20 L/min without addition of H_2, both the waveforms of discharge voltage and RF current in Ar plasma are purely sinusoidal, and the phase between the discharge voltage and the RF current is about 90°. With the addition of H_2 into the Ar plasma, the waveforms and the phase between the voltage and the current didn't changed and kept smooth and complete sinusoidal. It indicates that the present experimental condition resulted in the α-mode discharge [7, 16].

Fig. 2.8 shows effect of H_2 flow rate on electrical property of plasma jet generated by APC plasma torch at RF power of 100 W and with the constant Ar flow rate of 20 L/min. Amplitude of voltage

and current was used. With increasing the H_2 flow rate, both the amplitude of voltage and current decreased slightly. It indicates that the addition of H_2 results the reducing of electron intensity for the plasma discharge.

On the other hand, we measured the temperature of the Ar/H_2 plasma with different flow rate of H_2 by a thermocouple as shown in Fig. 2.9, with increasing the flow rate of H_2, the temperature of plasma increased from 150 ℃ to 175 ℃ as the RF power set at 100 W and the constant Ar flow rate of 20 L/min. It is considered that with the addition of H_2 into Ar plasma, the RF impedance matching would be disturbed, resulting in an increase in dissipated RF power [16,17]. This is assumed to be the reason of the increasing the the temperature. In the previous study in [11], the similar phenomenon ws also observed in Ar/N_2 plasma and Ar/O_2 plasma, respectively.

2.3.2 OES analysis of APC plasma jet

It is reported that when hydrogen gas was added into Ar plasma, the Ar plasma emission would be greatly quenched [18]. In the present experiment, we also found the similar phenomenon. As shown in Fig. 2.10, the optical emission spectra of Ar/H_2 plasma jets with the constant flow rate of Ar as 20 L/min and with changing the flow rate of H_2 from 0 mL/min to 15 mL/min were compared. With increasing the flow rate of H_2, the emission intensity from Ar emission decreased. The main emission lines observed in Ar/H_2 plasma generated by APC plasma torch are shown in Table 2.1, the position of the spectra collected at 3 mm down from the plasma torch head and 2 mm side from plasma jet end. The integration time was 100 ns for the APC plasma torch. And the peaks shown in Fig. 2.10 were mainly assigned to Ar emission, while the peaks due to H atoms (434.0 nm [18], 486.1 nm, 656.3 nm [19]) were

not obvious. The H atoms, which should play an important role to reduce CuO, are considered to be resulted from the dissociation of H_2 by the following reaction [19]:

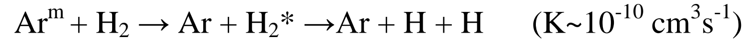

$$Ar^m + H_2 \rightarrow Ar + H_2^* \rightarrow Ar + H + H \qquad (K\sim10^{-10}\ cm^3s^{-1})$$

$$Ar^+ + H_2 \rightarrow ArH^+ + H \qquad (K\sim10^{-9}\ cm^3s^{-1})$$

In additionally, we found the peaks located at 308.9 nm and 336 nm, which are indentified as an OH and NH emission, respectively [18]. It is supposed that the OH and NH groups were the products of the reaction of H_2, O_2 and N_2 in the impurity of Ar or air [20]

2.3.3 XPS analysis of copper particles

Fig. 2.11 (a) shows the main and the satellite peaks of $Cu2p_{3/2}$ of the samples heat-treated and plasma-treated under various conditions. CuO spectra can be distinguished from the spectra of Cu and Cu_2O, since the peak of CuO is at 933.6 eV and the shake-up satellite peak located between Cu $2p_{1/2}$ and Cu $2p_{3/2}$ are corresponded to CuO [21]. As shown in Fig. 2.11 (a)-⑤, the XPS spectra of the sample only heat-treated shows the Cu $2p_{3/2}$ peak located at 934.02 eV and the satellite, indicating that the surface of the sample without plasma-treatment was covered with CuO. As for the XPS spectra of the sample heat-treated in the atmosphere of Ar/H_2 (flow rate of Ar=20 L/min, H_2=10 mL/min) shown in Fig. 2.11 (a)-④, which was placed under the plasma torch without plasma-treatment at 425 ℃ for 12 minutes, the Cu $2p_{3/2}$ peak located at 933.23 eV and the shake-up satellite peak appeared obviously between the Cu $2p_{3/2}$ peak and the Cu $2p_{1/2}$ peak. There is little change by the heat-treatment in the Ar/H_2 atmosphere, and it indicated that although the treat condition was almost the same, the sample without plasma-treatment could be hardly reduced. From Fig. 2.11 (a)-③, it shows that the Cu $2p_{3/2}$ peak moved to the position of 932.96 eV corresponding to Cu and the shake-up satellite peak disappeared. It is

considered that with the pure Ar plasma treatment, the Cu-O bond in CuO was broken. As for the sample treated at 425 ℃ by Ar/H_2 plasma for 8 minutes shown in Fig. 2.11-②, the shake-up satellite peak also disappeared and the Cu $2p_{3/2}$ peaks located at 932.82 eV, corresponding to Cu. It is considered that the CuO has been reduced with the Ar/H_2 plasma treatment. In order to investigate the reduction ability of the APC plasma jet, a sample was treated by Ar/H_2 plasma at ambient temperature for 1 minute, the XPS spectra of which is shown in Fig. 2.11 (a) - ①. It shows that the Ar/H_2 plasma-treatment within 1 minute at ambient temperature could result in the reduction of the CuO. In the experiment, at ambient temperature it cost more time to reduce the CuO for the pure Ar plasma than Ar/H_2 plasma.

The broad Cu$2p_{3/2}$ of the sample treated by plasma at ambient temperature for 1 minute in air have been deconvoluted into two peaks which are marked as peak A and B, respectively in Fig. 2.11 (b). The peak B appeared at 933.9 eV, which corresponded to CuO. The peak A appeared at 932.9 eV, which is difficult to be distinguished between Cu or Cu_2O by observation, because the bind energy of Cu and Cu_2O are very close to each other [22, 23]. However it is reported that Cu_2O is the product of early stage of oxidation, while the oxide contained in copper is mainly CuO when the treat temperature is higher than 180 ℃ [24]. In addition, Fig. 2.11 (c) shows the XPS spectra of O 1s of the sample heat-treated and the sample treated by plasma at ambient temperature for 1 minute, respectively. In the spectra of the sample without plasma-treatment, the O 1 peak was asymmetric and could be deconvoluted into the speak located at 529.9 eV corresponding to CuO and the peak located at 531.2 eV corresponding to Cu $(OH)_2$ [23]. While the sample treated by plasma for 1 minute shows only one symmetrical O 1s peak located at 530 eV corresponding to Cu $(OH)_2$. Also the intensity of peak of the O 1s decreased after plasma-treatment. So it can be confirmed that the peak A in Fig.6 (b) is Cu, which appears at greatly

higher position than the peak of CuO. Thus, Fig.6 indicated that the sample can be reduced by the treatment with Ar/H_2 plasma for only 1 minute at ambient temperature. As the reaction progressed, the reduction reaction gradually extended to the internal of the film [24, 25].

2.3.4 SEM observation of copper particles

Fig. 2.12 shows the SEM micrographs of the samples untreated and the one heat-treated at 280 ℃ in an oven for 10 minutes, respectively. The nano-particles didn't change with the heat-treatment. In fact, the nano-particles used in this study could be considered as large nano-particles, and the melting point of which is estimated to close to the bulk copper (1083 ℃) [26, 27].

As shown in Fig. 2.13 (a) and (b), the samples plasma-treated at 425 ℃ for 8 minutes and 12 minutes were sintered in various degrees. The RF power was set at 100 W, the Ar flow rate was 20 L/min and H_2 flow rate was 10 mL/min, the treatment position was at 3mm down from the plasma torch head. With increasing the treat time, the nano-particles began to adhere to each other gradually, until all of the particles sintering into a uniform piece of film when the treatment time was increased to 12 minutes. However, on the sample treated by pure Ar plasma at 425 ℃ for 8 minutes shown in Fig. 2.13 (c), the nano-particles sintered at a relatively low degree. It indicates that H_2 plays an important role in the sintering of copper nano-particles in the experiment. As a comparison, a sample was heat-treated at the 425 ℃ in Ar/H_2 atmosphere with the same gas flow rate without plasma-treatment for 12 minutes, the SEM micrograph of which is shown in Fig. 2.13 (d). It shows that the heat-treatment at 425 ℃ without plasma could not lead to the sintering of the copper nano-particles.

It suggests that the sintering of the copper nano-particles didn't result from the increased temperature in this study. We suppose that the plasma-treatment increased the surface energy of the nano-particles leading to the high reactivity [28].

2.3. 5 Electrical resistances

Fig. 2.14 shows the changes of resistance for the printed films of copper nano-paste treated under various conditions. The resistance of the film untreated was as large as more than 3.5×10^7 Ω/cm. As shown in Fig. 8, the resistance of the sample heat-treated obviously decreased to about 2.88×10^5 Ω/cm. What's more, the resistance of the sample treated by plasma at ambient temperature decreased by five orders of magnitude to 1.13 Ω/cm, and that of the sample treated at 425 ℃ decreased to 0.687 Ω/cm. However, the resistance of the sample also treated at 425 ℃ in atmosphere of Ar/H_2 for 12 minutes without plasma-treatment changed little. With the plasma-treatment, the oxide film on the surface of the copper paste was removed, and the resistance greatly decreased. As for the film plasma-treated at 425 ℃, the surface of which was sintered, the electrical conductivity increased to the level of bulk copper. It should be noted in addition, the alumina substrate used in the present experiment kept insulating property after the various treatments.

2.4 Conclusions

In this study, the non-equilibrium atmospheric pressure plasma was used to reduce and sinter the copper nano-particle. From the electrical characterization of the discharge voltage and RF current, it is confirmed that the plasma discharge is a stable α-mode discharge, and the addition of H_2 had little influent on the discharge of Ar plasma. With increasing the flow rate of H_2, the temperature of plasma tended to rise, but remained around 150 - 175 ℃. The copper nano-particles could be reduced by Ar or

Ar/H_2 plasma. Especially, with Ar/H_2 plasma, the sample could be reduced at ambient temperature within 1 minute. At 425 ℃, the nano-particles treated by Ar/H_2 plasma for 8 minutes and 12 minutes had been sintered to reduce the electric resistance to the level of bulk copper. It was strongly suggested that the Ar/H_2 plasma enhanced the reduction and sintering of copper nano-particles at ambient temperature.

References

[1] S. Ono, S. Teii, Y. Suzuki, T. Suganuma: *Thin Solid Films*, **518**, 981(2009)

[2] E. S. Lee, J. H. Choi, H. K. Baik: *Surf. Coat. Technol.*, **201**, 4973 (2007)

[3] M. Jung, H. Choi: *J. Colloid Interface Sci.*, **310**, 550(2007)

[4] A. R. Dayal, D. R. Sadedin: *Plasma Chem Plasma P.*, **23**, 627 (2003)

[5] J. Liu, Z. Shen, M. Nygren, B. Su, T. W. Butten: *J. Am. Ceram. Soc.*, **89**, 2689 (2006)

[6] Y. Iriyama: *J. Photopolym. Sci. Tec.*, **23**, 599 (2010)

[7] J. Laimer, H. Reicher, Qurat-ul-Ain: *28th ICPIG*, Prague, Czech Republic, July 15-20, 10 (2007)

[8] A. Simchi: *Mater. Sci. Eng. A*, **428**, 148 (2006)

[9] M.C. Kim, S.H. Yang, J. H. Boo, J.G. Han: *Surf. Coat. Technol.*, **174 –175** (8392003).

[10] L. N. Ho, H. Nishikawa, T. Takemoto, Y. Kashiwagi, M. Yamamoto, M. Nakamoto: *Microelectron. Packag. Conf., EMPC 2009*, Eur. **1**.

[11] X. Fei, S. Kuroda, Y. Kondo, T. Mori, K. Hosoi: *J. Mat. Life Soc.*, Accepted, 2010.

[12] Y. Sawasa, H. Tamaru, M. Kogoma, M. Kawase, K. Hashimoto: *J. Phys. D: Appl. Phys.*, **29**, 2539 (1996)

[13] J. H. Hsieh, L. H. Fong, S. Yi, G. Metha: *Surf. Coat. Technol.*, **112**, 245 (1999)

[14] X. Fei: *Characterization, Comparison and Application of Two Types of Atmospheric Pressure Cold Argon Plasma Jets*, Doctoral Thesis, Kiryu: Gunma University, 2011.

[15] N. Terada: *JIEP*, **11**, 300 (2008)

[16] J. Laimer, S. Haslinger, W. Meissl, J. Hell, H. Stŏri: *Vacuum*, **79**, 209 (2005)

[17] Y. H. Choi, J. H. Kim, K. H. Paek, W. T. Ju, Y. S. Hwang: *Surf. Coat. Technol.*, **193**, 319 (2005)

[18] Q. S. Yu, H, K, Yasuda: *Plasma Chem. Plasma P.*, **18**, 461 (1998)

[19] B. K. Pawlak, P. Jamroz: *Plasma Chem. Plasma P.*, **30**, 641 (2010)

[20] M. C. Garc á, M. Varo, P. Mart ńez: *Plasma Chem. Plasma P.*, **30**, 241 (2010)

[21] W. Y. Sung, W.J. Kim, S.M. Lee, H.Y. Lee, Y. H. Kim, K.H. Park, S. Lee: *Vacuum*, **81**, 851 (2007)

[22] Terry L. Barr: *J. Phys. Chem.*, **82**, 1801 (1978)

[23] T. Ghodselahi, M.A. Vesaghi, A. Shafiekhani, A. Baghizadeh, M. Lameii: *Appl. Sur. Sci.*, **255**, 2730 (2008)

[24] Y. Sawada, N. Taguchi, K. Tachibana: *Jpn. J. Appl. Phys. Vol.,* **38**, 6506 (1999)

[25] W. K. Han , J. W. Choi, G. H. Hwang, S. J. Hong, J. S. Lee, S. G. Kang: *Appl. Surf. Sci.*, **252**, 2832 (2006)

[26] O. A. Yeshchenko, I. M. Dmitruk, A. A. Alexeenko, A. M. Dmytruk: *Phys. Rev. B*, **75**, 085434(2007)

[27] M. Naito, H. ABE, K. Nogi: *Nanoparticle Processing and Its Application*. SFJ, **56**, 748 (2006)

[28] W. W. Kwan, V. Kripesh, M. K. Iyer, M. Gupta, A. A. O. Tay, R. Tummala: *Electron. Packag. Technol. Conf.*, 551 (2003).

Table 2.1 Most emission lines observed in Ar/H_2 plasma generated by APC plasma torch at the position of 3 mm down from the plasma torch head and 2 mm side from plasma jet end. The integration time was 100 ns [18-20].

Species	Wavelength (nm)	Transition	Threshold energy (eV)
OH	308.9	$A^2\Sigma^+ \rightarrow X^2\Pi$ -	-
NH	336	$A^3\Pi \rightarrow X^3\Sigma^-$	3.7
Ar	696.5	$2p_2$–$1s_5$	13.32
	706.7	$2p_3$–$1s_5$	13.29
	714.7	$2p_4$–$1s_5$	13.28
	728	$2p_2$–$1s_4$	13.33
	738.4	$2p_3$–$1s_4$	13.3
	751.4	$2p_5$–$1s_4$	13.27
	763.5	4p-4s	13.17
	772.4	4p-4s	13.33
	794.8	4p-4s	13.28
	801.5	4p-4s	13.15
	811.5	4p-4s	13.08

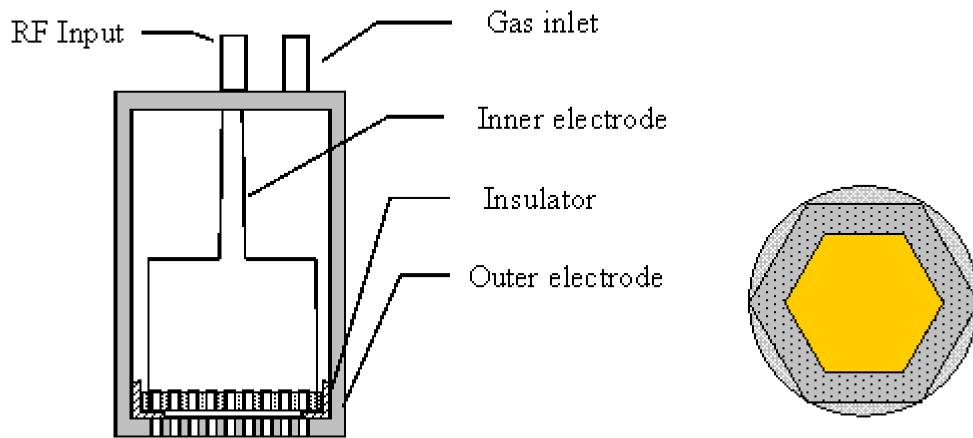

Fig.2.1 Schematic diagram of APC plasma torch.

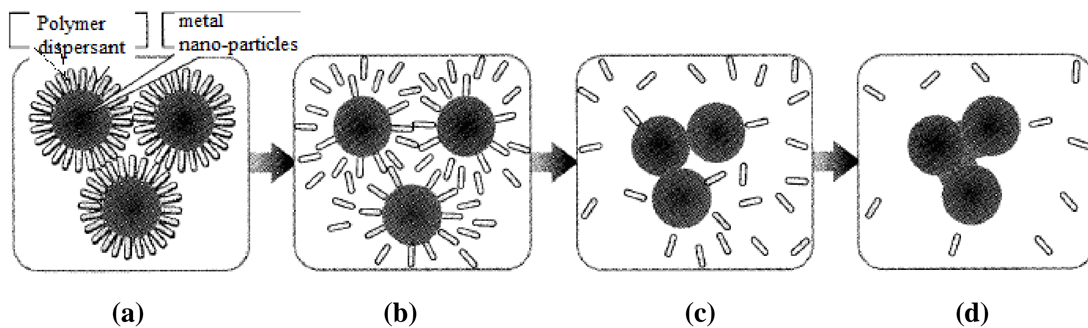

Fig. 2.2 The process of heat-treatment and sintering for metal nano-paste. At ambient temperature without treatment (a), heat-treatment (b), decomposition of the polymer additive (c), sintering of metal nano-particles (d) [15].

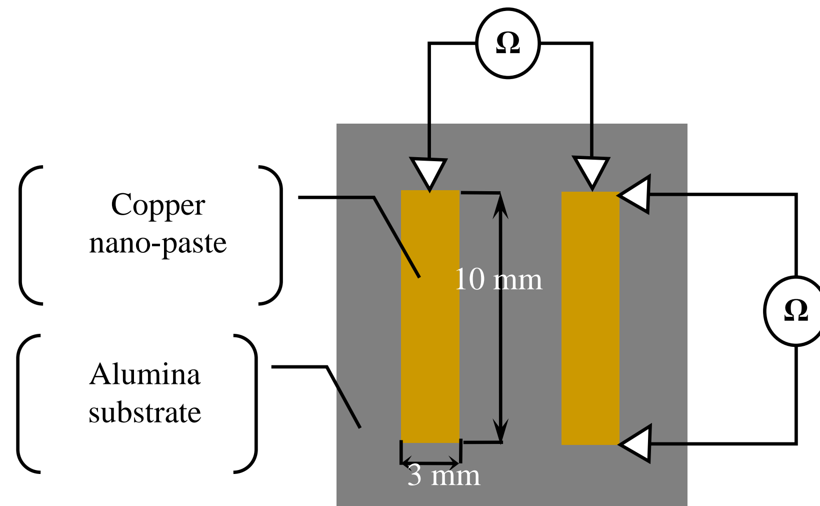

Fig.2.3 Schematic diagram of the sample used in the experiment

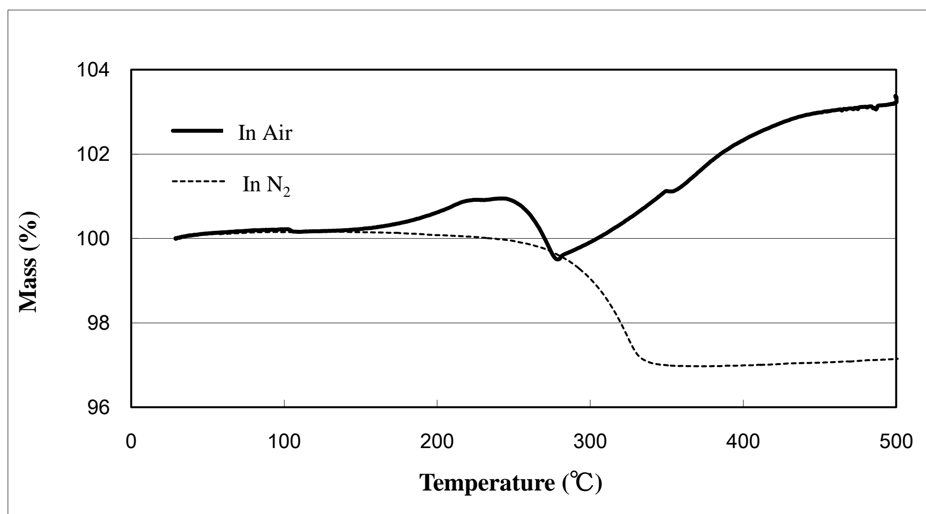

Fig. 2.4 TGA trace obtained from the untreated copper nano-paste heated in air at scan rate of 10 ℃/ min

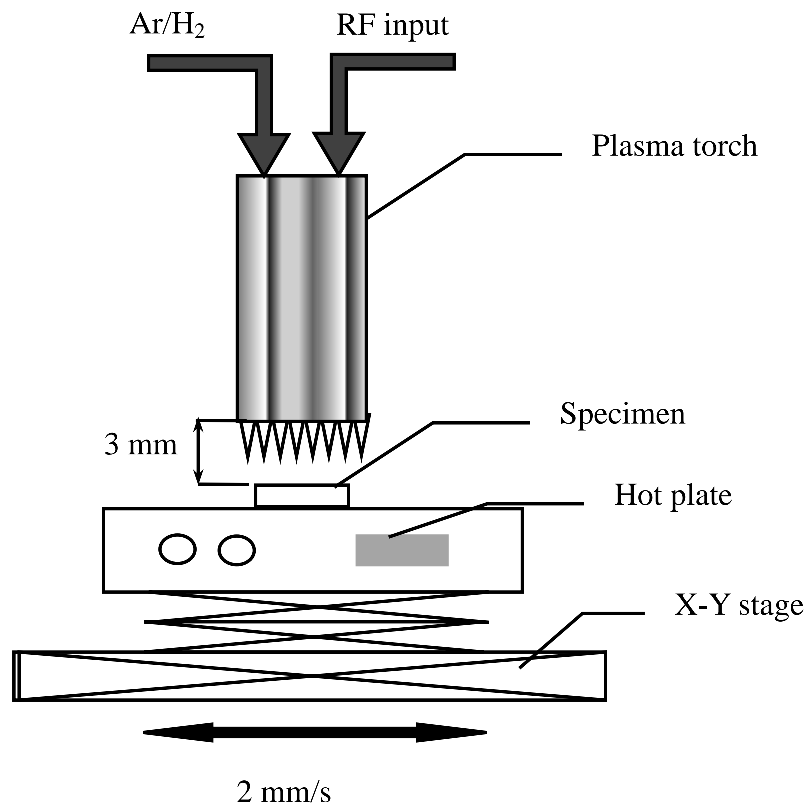

Fig. 2.5 Schematic diagram of the experimental setups for the plasma-treatment of samples

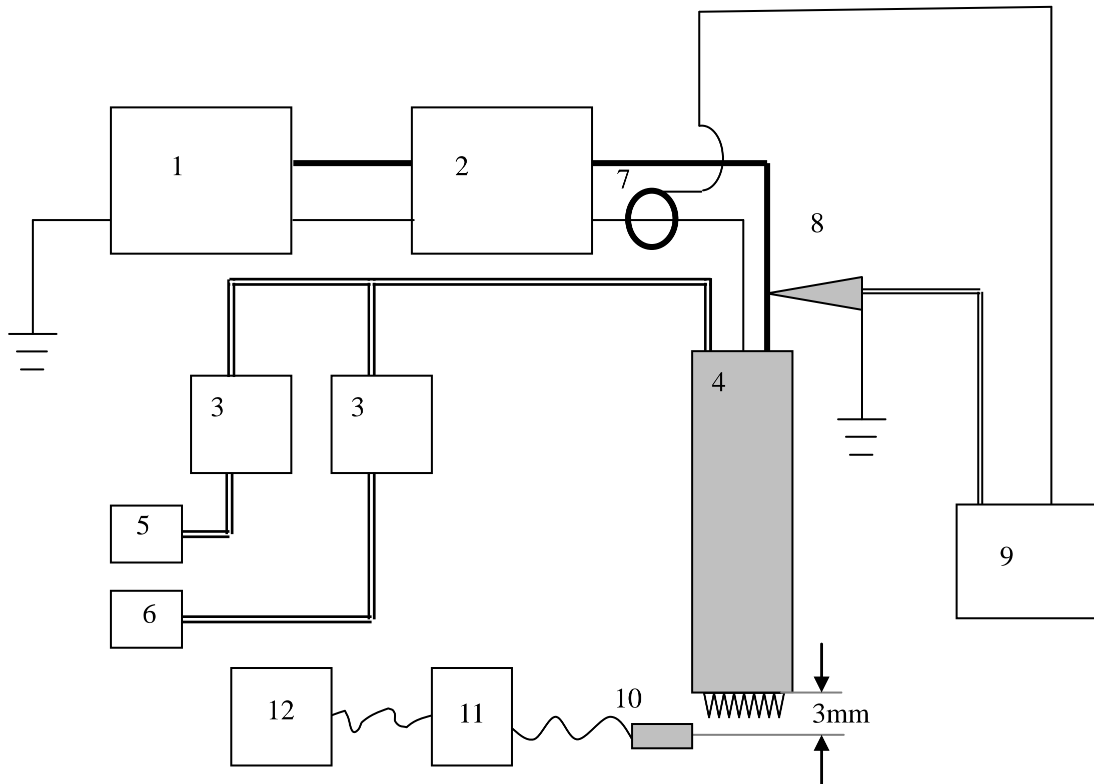

Fig. 2.6 Schematic diagram of the experimental setups for plasma diagnosis. 1, RF power source; 2, Matching box; 3, Mass flow controller; 4, APC plasma torch; 5, Ar gas, 6, Additive gas (H_2); 7, Current probe; 8, High-Voltage probe; 9, Oscilloscope; 10, Optical fiber; 11, Spectrometer; 12, Personal computer.

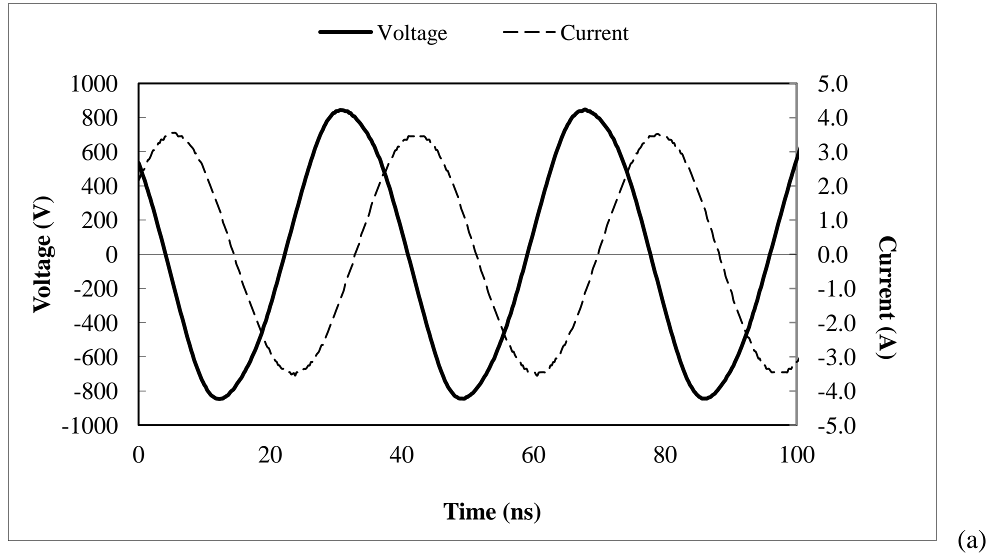

(a)

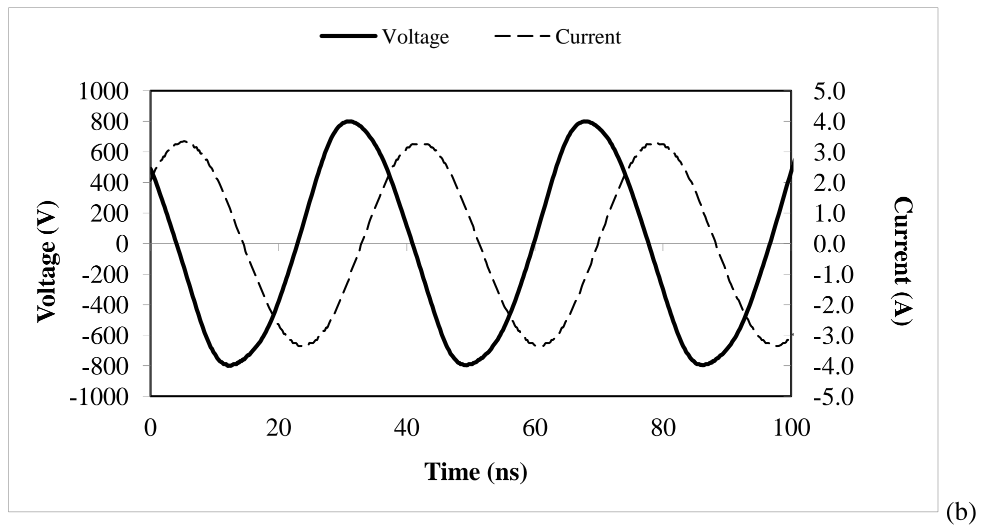

(b)

Fig. 2.7 Waveforms of the discharge voltage and the RF current for Ar/H_2 plasma (RF=100 W); the flow rate of Ar=20 L/min and the flow rate of H_2=0 mL/min (a), the flow rate of Ar=20 L/min and the flow rate of H_2=10 mL/min (b)

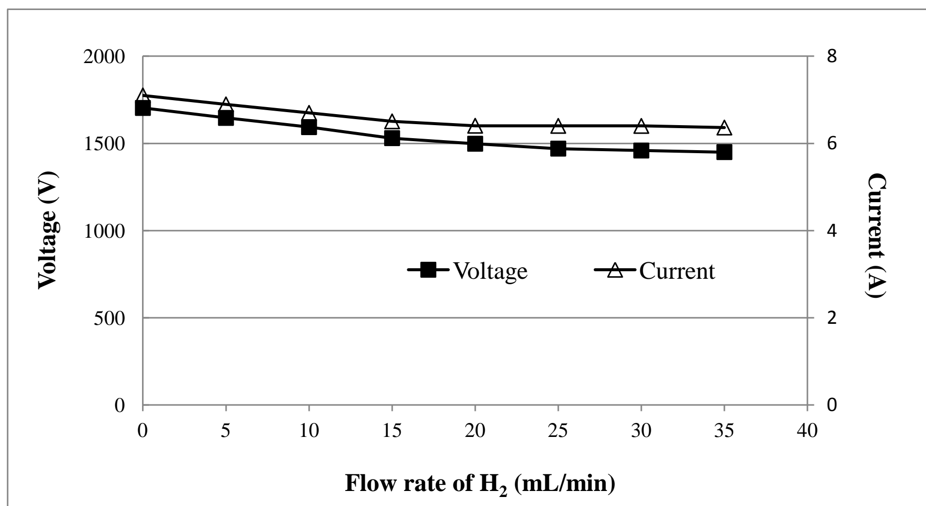

Fig. 2.8 Effect of H_2 flow rate on discharge voltage and RF current as the RF power set at 100W and Ar flow rate set at 20 L/min.

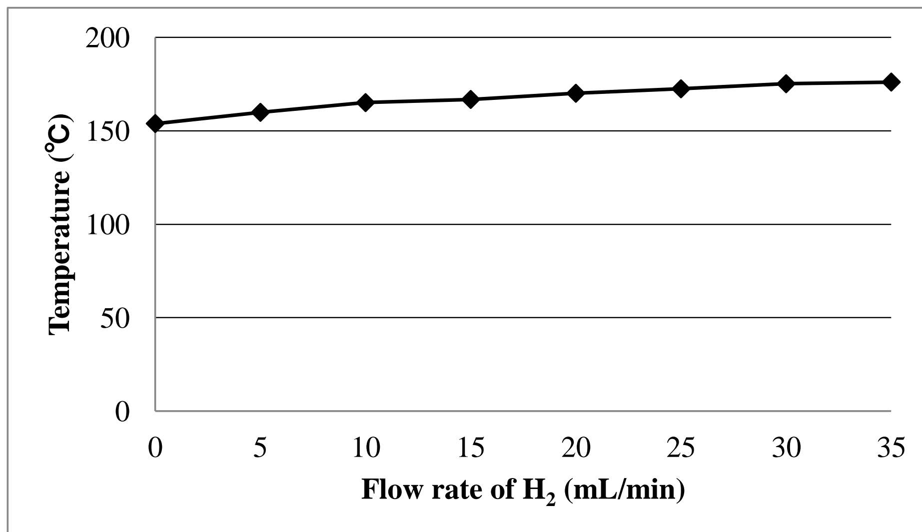

Fig. 2.9 Effect of flow rate of H_2 on the temperature of Ar/H_2 plasma jet as the RF power set at 100 W and Ar flow rate set at 20 L/min.

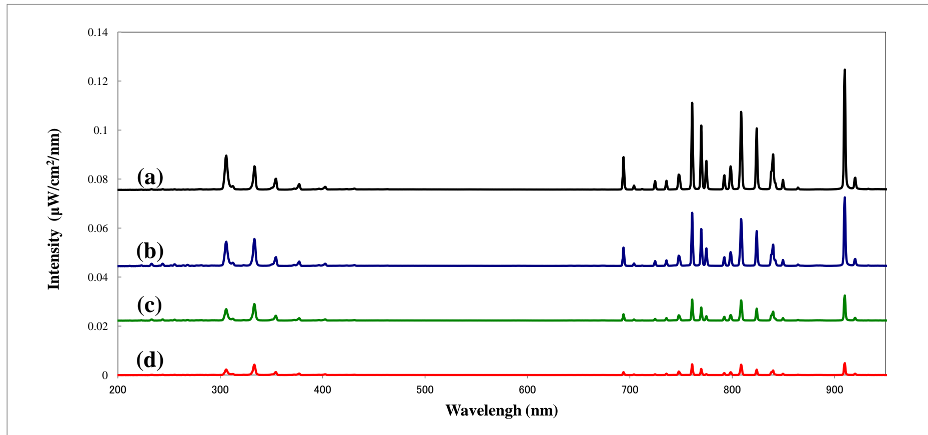

Fig. 2.10 Optical emission spectra from the Ar/H_2 plasma jet with different flow rate of H_2; Ar flow rate =20 L/min and H_2 flow rate=0 mL/min (a), Ar flow rate =20 L/min and H_2 flow rate =5 mL/min (b), Ar flow rate =20 L/min and H_2 flow rate=10 mL/min (c), Ar flow rate =20 L/min and H_2 flow rate=15 mL/min (d)

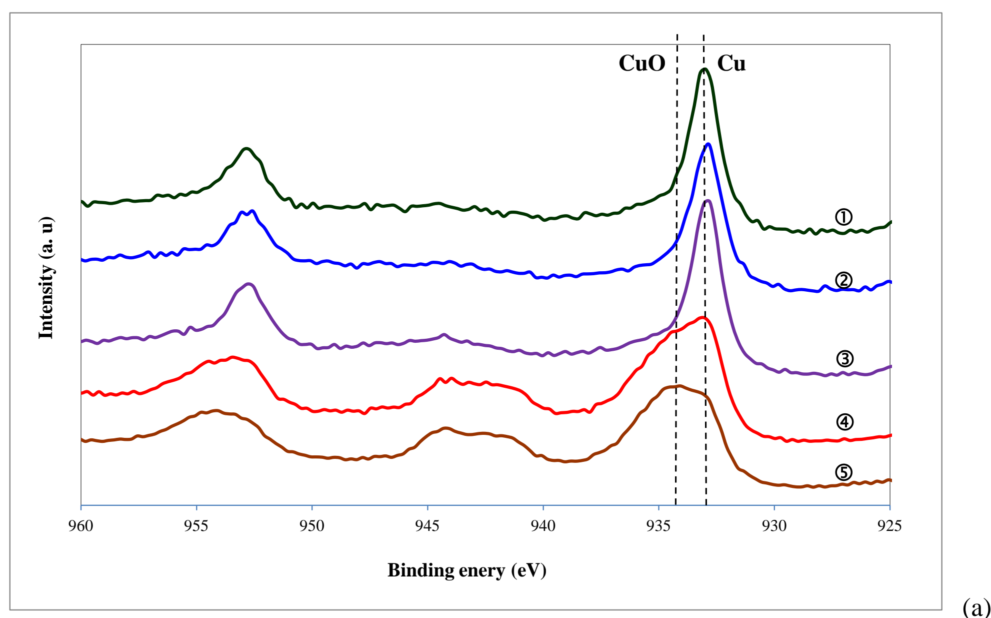

(a)

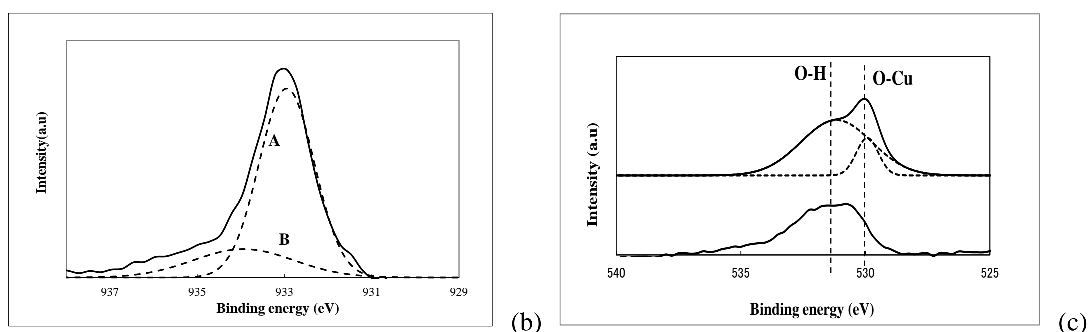

(b) (c)

Fig. 2.11 Main and satellite peaks of Cu $2p_{3/2}$ and Cu $2p_{1/2}$ of the XPS spectra for copper nano-paste (a) treated by Ar/H_2 plasma for 1 minute at ambient temperature ①, treated by Ar/H_2 plasma for 8 minutes at 425 ℃ ②, treated by pure Ar plasma for 8 minutes at 425 ℃ ③, Heat-treated at 425 ℃ in Ar/H_2 atmosphere without plasma for 12 minutes ④, heat-treated at 280 ℃ ⑤; typical deconvolution of Cu $2p_{3/2}$ main peak of the sample treated by plasma for 1 minute at ambient temperature (b); O 1s peak of the XPS spectra for the sample heat-treated (up) and the sample treated by plasma for 1 minute at ambient temperature (down) (c).

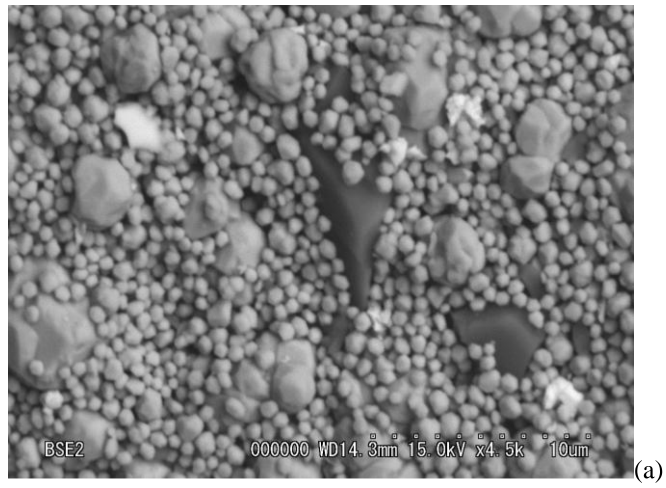

(a)

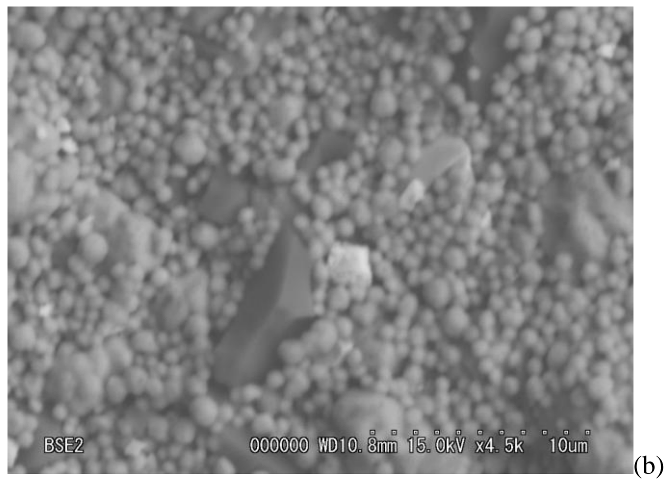

(b)

Fig. 2.12 SEM images of the sample untreated (a), heat-treated at 280 ℃ for 10 minutes (b)

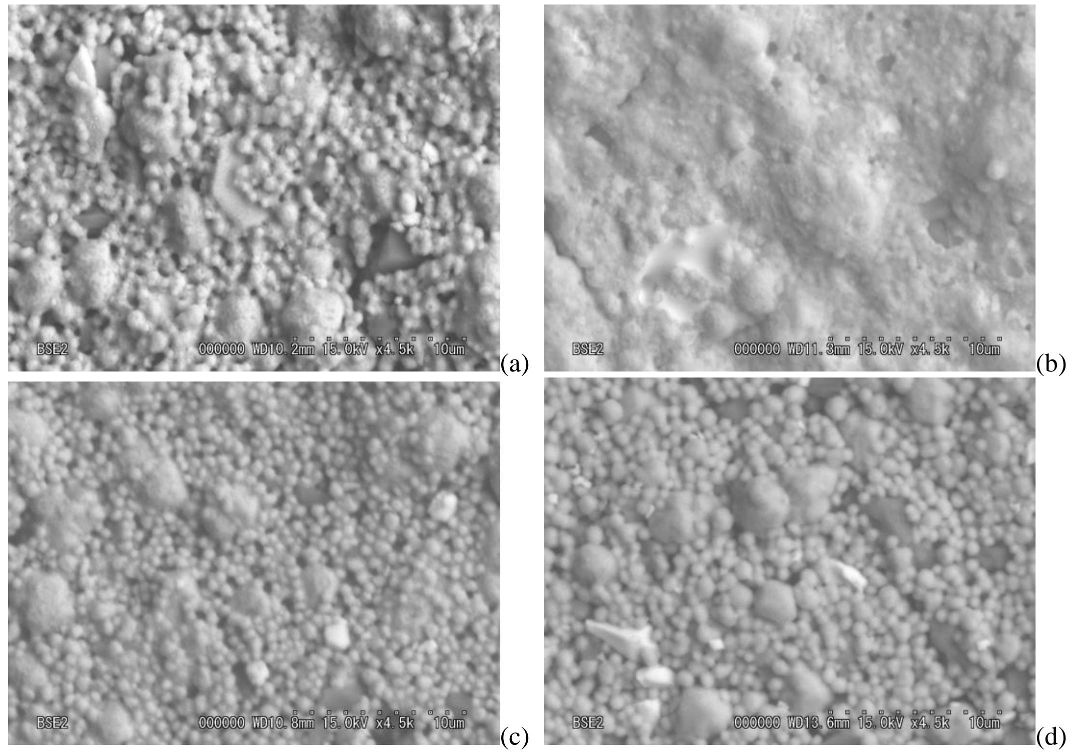

Fig. 2.13 SEM images of the sampe Ar/H_2 plasma-treated for 8 minutes at 425 ℃ (a), Ar/H_2 plasma-treated for 12 minutes at 425 ℃ (b), pure Ar plasma-treated for 8minutes at 425 ℃ (c), heat-treated in the atmosphere of Ar/H_2 for 12 minutes without plasma-treatment at 425 ℃ (d) Flow rate of Ar was 20 L/min and flow rate of H_2 was 10 mL/min as power set at 100W and distance kept as 3 mm down from the head of plasma torch.

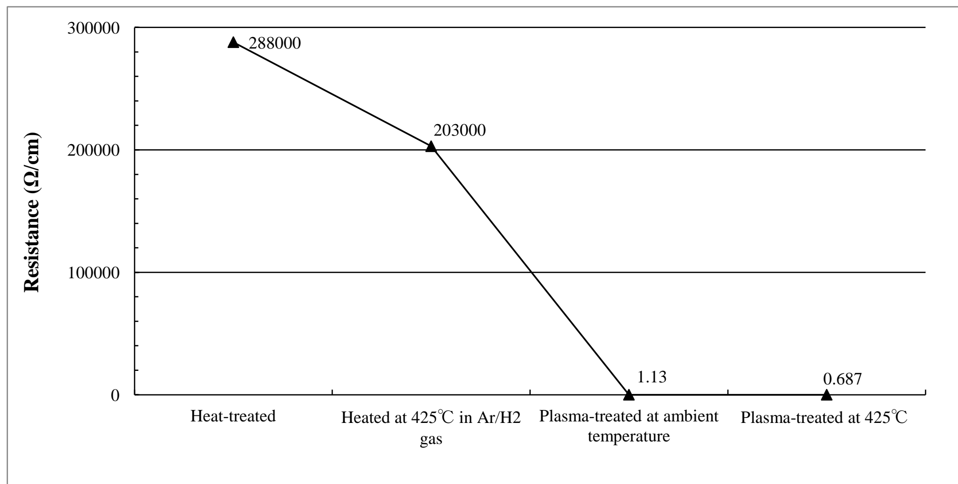

Fig.2.14 Resistance changes of the printed films of copper nano-paste treated under various conditions

Character 3 Reduction and sintering of copper nano-particles by non-equilibrium atmospheric pressure plasma jet generated by “beam plasma torch”

3.1 Introduction

In chapter 2, an APC plasma torch with the electrode diameter of 15 mm was used. At 425 ℃ the Ar/H_2 plasma jet resulted in the sintering of copper nano-particles.

In order to sinter the copper nano-particles at ambient temperature, a plasma torch with stronger emission intensity was desired. In fact, as the one of the most critical plasma parameter, it’s considered as a challenge to sustain a high emission density while maintaining a glow discharge at low temperature [1].

In this chapter, a plasma torch called “beam plasma torch” with the plasma nozzle diameter of φ1 mm generating the stronger emission intensity was used. The electrical property of plasma jet was characterized using a high-voltage probe and a current probe. Optical emission spectra (OES) were collected to identify the active species in generated plasma jet and compare the intensity from spectra under various conditions in experiment.

Scanning electron microscope (SEM) and X-ray photoelectron spectroscopy (XPS) were used to the surface characterization of the treated samples.

3.2 Experimental details

3.2.1 Non-equilibrium atmospheric pressure plasma device and experimental procedures

The schematic diagram of the plasma torch used in the experiment is shown in Fig. 3.1. The beam plasma torch consists of two stainless steel (SUS) co-axial electrodes and the inner electrode with the diameter of 10 mm is connected to a RF power source of frequency of 27.12 MHz through an impedance matching network, while the outer electrode is grounded (o.d.: 20 mm, i.d.: 16 mm). A glass pipe was used as an insulator between the two electrodes and the gap spacing between them is 1 mm. The experimental conditions used were: 25 L/min of Ar and 0-15 mL/min of H_2 with RF power set at 60 W without any reflect power. The distance between the plasma torch head and sample was 3 mm.

In this chapter, two experimental setups were used to treat the samples. One is the same to that used in chapter 2 for the APC plasma torch as shown in Fig.3.2. Because the size of sample was much larger than that of plasma nozzle, in order to treat the surface of the sample uniformly, the sample on the X-Y stage was raster-scanned as shown in Fig. 3.2. The speed was kept at 2 mm/s.

The other one is shown in Fig. 3.3. In order to prevent the sample from being oxidized by oxygen in atmosphere, the experiment was carried out in a 3 L-size sealed glass chamber. Before plasma-treatment, the chamber was evacuated for 1 minute, then was injected N_2 at the flow rate of 3 L/min for 1 minute, the procedures was repeated 3 times to replace the air to N_2 in the chamber.

3.2.2 Sample preparation

The copper nano-paste developed by Mitsuboshi Belting Ltd. consists of copper nano-particles with the diameter of 700-900 nm and the polymer additives as the binder. The copper nano-paste was printed on alumina substrates with the thickness of 30 μm as shown in Fig. 2.2 in Chapter 2, and the printed films were dried at 100 ℃ in an oven for 30 minutes. In order to remove the polymer additives in the paste, the dried films were heat-treated at 280 ℃ for 10 minutes with the heating rate of 5 ℃/min. The treatment temperature was determined through TGA experiment shown in Fig.2.3 in Chapter 2.

3.2.3 Plasma diagnostic*s*

In order to characterize the plasma generated by the beam plasma torch, electrical characterization and optical emission spectrometry (OES) measurements were carried out. The schematic experimental setups were as same as those shown in Fig. 2.6 in Chapter 2.

Electrical characterization was performed by a Tekronix TDS3012C digital phosphor oscilloscope. The waveform of discharge voltage was measured with a 10:1 voltage probe (Tektronix P6139 10X Passive Probe 063-0870-05), and the RF current was measured with a wide band current monitor (PearsonTM current monitor) manufactured by Pearson Electronics Inc., Palo Alto, California, U.S.A..

Optical emission spectra (OES) were collected by an Ocean Optics USB4000 spectrometer at the position of 2 mm side from the plasma end and 3mm down from the plasma torch head, through an optical fiber with a diameter of 100 μm. The integration time was 100 ns.

The temperature of plasma jet was measured by a thermocouple at 3 mm down from the plasma torch head.

3.2.4 Characterization of the copper nano-particles surface

X-ray photoelectron spectroscopy (XPS; AXIS-NOVA) was performed to analyze the surface composition of the copper nano-paste at accelerating voltage of 10 kV.

SEM (Hitachi S-3000N scanning electron microscope) was utilized to observe the microstructures of the nano-particles to distinguish the changing on the surface morphology of the plasma-treated sample.

3.3 Results and discussion

3.3.1 Electrical characterization of plasma

Fig. 3.4 shows the waveform of the discharge voltage (solid line) and RF current (dashed line) of pure Ar plasma generated by the beam plasma torch as RF power of 60W for various Ar flow rate. At the high flow rate of Ar as 25 L/min, both waveforms of voltage and current are smooth and completely sinusoidal, as shown in Fig.3.4 (a). In addition, the capacitive nature of the discharge is clearly observed as the current waveform leads the voltage waveform by about 81°. It indicates it is an α-mode discharge at Ar flow rate of 25 L/min [2-7]. With decreasing Ar flow rate to 15 L/min, both the waveforms of voltage and current were weakened slightly, and the waveform of voltage shows minor deviation, as shown in Fig. 3.4 (b). It indicates that a decreasing of Ar flow rate results in a discharge regime transition from α-mode to γ-mode. Additional decreasing of the

Ar flow rate leads a more serious deformation and reduction of amplitude for the discharge voltage, as shown in Fig. 3.4(c) at Ar flow rate of 5 L/min.

As shown in Fig.3.5, the increasing the Ar flow rate leads to α-mode discharge and both the amplitude of discharge voltage and RF current are greatly enhanced by increasing the Ar flow rate from 5 L/min to 25 L/min. It reveals that with increasing the Ar flow rate, the electron consumption for the generation of plasma jet increased.

Fig. 3.6 shows the effect of Ar flow rate on the temperature of plasma jet for pure Ar plasma. Decrease of Ar flow rate results in a great increase in the temperature of plasma jet. It suggests that with the decreasing of gas flow rate, severe thermal damage to the electrode would be lead by the transition of discharge regime.

As well known, the resident time of the Ar gas in the discharge region would be increased with decreasing the Ar flow rate. It is also reported that the γ-mode is unstable under the atmospheric condition, which might be ascribed to the contamination of working gas by air [5, 7].

Fig.3.7 shows the effect of H_2 flow rate on the discharge voltage and the RF current at the Ar flow rate of 25 L/min. The peak-to-peak amplitude is used in Fig. 3.7. With increasing the flow rate of H_2 from 0 mL/min to 35 mL/min, both the changes of voltage and current are quite slight. It indicates that the electrical characteristics of plasma generated by the beam plasma torch are determined by the main working gas, Ar. As for the slight change in the voltage and current, with the additional H_2, it is assumed to be raised by the disturbance of RF impedance [5].

Fig.3.8 shows changes of the waveforms of the discharge voltage (solid line) and the RF current (dashed line) at H_2 flow rate of 0-15 mL/min with the constant Ar flow rate of 25 L/min, the RF power set at 60 W. With the addition of H_2 to the pure Ar plasma, both the waveforms of discharge

voltage and RF current are almost unchanged. It was reported that the glow discharge in He or Ar gas becomes more stable and more homogenous when trace of N_2 is added [8]. Analogously, we assume that the α-mode discharge became more stable after the addition of H_2 gas.

Fig.3.9 shows the effect of the RF power increasing on both the amplitude of discharge voltage and RF current. With increasing the RF power from 30 W to 90 W, the waveforms of discharge voltage and RF current changed a little. They at 30 W exhibit more ordinary sinusoidal than wave than at 90 W as shown in Fig. 3.9.

As shown in Fig. 3.10, the temperature of plasma jet changes with increasing the RF power under different H_2 flow rate. The increase of RF power resulted in the rise of the temperature for the plasma jet, which is assumed to lead a thermal damage on the electrode of beam plasma torch. It might be the reason that the electrical waveforms were deformed at the higher RF power in Fig. 3.9.

3.3.2 Optical emission spectra of plasma jet generated by beam plasma torch

Fig. 3.11 shows the typical emission spectra from the pure Ar plasma jet with increasing the Ar flow rated at the RF power of 60W. The main emission lines observed in Ar/H_2 plasma generated by beam plasma torch are shown in Table 3.1, the position of the spectra collected at 3 mm down from the plasma torch head and 2 mm side from plasma jet end. The integration time was 100 ns. With increasing the Ar flow rate, the emission intensity from active species are greatly strengthened, meanwhile the discharge regime transits from γ-mode to α-mode when the flow rate of Ar was increased to 25 L/min as shown in Fig. 3.4. It is obvious that the most powerful optical emission

spectra of pure Ar plasma generated by the beam plasma torch could be obtained at the Ar flow rate of 25 L/min.

Changes in emission intensity of active species from Ar/H_2 plasma jet with constant flow rate of Ar and increasing flow rate of H_2 are shown in Fig. 3.12. It has been reported that Ar plasma would be quenched with addition of H_2 [9, 12]. However, in present experiment the phenomenon was not observed. As shown in Fig.3.12 (a) the emission intensity from all active species is greatly enhanced with addition of H_2 at the flow rate of 5 mL/min. Additional increasing the H_2 flow rate will decrease of the emission intensity from Ar/H_2 plasma jet. What is more, the emission spectra from "Balmer" series at 656 nm (Hα, n=3) was detected and enhanced with increasing the flow rate the H_2 as shown in Fig.3 .12(b) [11, 12]. It is supposed that at the constant Ar flow rate of 25 L/min, the most powerful optical emission spectra of Ar/H_2 plasma generated by the beam plasma torch could be obtained at the H_2 flow rate of 5 mL/min owing to the more stable α-mode discharge as discussed at Fig.3.8.

As is expected, both the emission intensity from Ar atoms and H atoms increase with increasing the RF power, as shown in Fig. 3.13.

To explain the interesting results above, chemical reactions in Ar-H_2 plasma jet were proposed. The following reactions show the process of the radiation of argon active species and hydrogen active species.

$$e^* + Ar^0 \rightarrow Ar^m + e \qquad (1)$$

$$e^* + Ar^m \rightarrow Ar^* (4p) + e \qquad (2)$$

$$e^* + Ar^0 \rightarrow Ar^* (4p) + e \qquad (3)$$

$$Ar^* (4p) \rightarrow Ar^* (4s) + h\nu \quad \text{(atomic Ar radiation)} \qquad (4)$$

$$Ar^m + H_2 \rightarrow Ar^0 + H_2^* \rightarrow Ar + 2H \qquad (5)$$

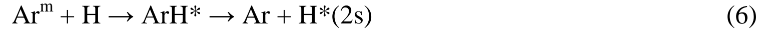

$$Ar^m + H \rightarrow ArH^* \rightarrow Ar + H^*(2s) \qquad (6)$$

$$e^* + H_2 \rightarrow H_2^* + e \rightarrow e + 2H \qquad (7)$$

$$Ar^+ + H_2 \rightarrow ArH^+ + H \qquad (8)$$

$$ArH^+ + e^* \rightarrow Ar + H^*(2s) \qquad (9)$$

$$e^* + H \rightarrow H^*\ (n=3) + e \qquad (10)$$

$$e^* + H_2 \rightarrow H^*\ (n=3) + H + e \qquad (11)$$

$$H^*\ (3s) \rightarrow H^*\ (2s) + 2\ h\nu \quad (H\alpha \text{ radiation}) \qquad (12)$$

Where, X^o indicates ground state of atoms, X^m indicates metastable state of atoms, asterisk mark denotes excited state of molecules, atoms or electrons [9-14].

From reactions (1-4) above, we can see that Ar atoms were excited by energetic electrons. The emission intensity of excited Ar atoms depends on the amount of energetic electrons. From reaction (11), it is seen that the excited hydrogen atoms (H* (n=3)) can be generated through collisions between energetic electrons and ground state hydrogen molecules. However, the required energy is very high (about 19 eV). Therefore, reaction (11) is not the main channel for the creation of excited hydrogen atoms (H* (n=3)), which decides the emission intensity of atomic hydrogen (Hα radiation).On the other hand, the required energy in reaction (10) is lower (about 12.1 eV).It is suggested that most of excited hydrogen atoms (H* (n=3)) were produced through reaction (10). From reaction (10), we can see that ground state hydrogen atoms play an important role in the Hα radiation. When more H_2 gas was added into the Ar plasma jet, more ground state hydrogen atoms were created through reaction (5, 7, 8). Therefore, the emission intensity of Hα increased with the increasing H_2 flow rate (see Fig. 4 (b)). As we mentioned above, the emission intensity of excited argon atoms increased after the addition of trace of H_2 gas and an expected quenching effect was not observed. It has been reported that the electron energy distribution

function (EEDF) expands towards higher energies as H_2 was added into Ar plasma [10]. Therefore, reaction (3) will be enhanced when the electron energy distribution function (EEDF) shifts towards higher energies. Consequently, more excited Ar atoms (4p) were generated through reaction (3) and stronger emission intensities were observed by OES. Once more H_2 was added, a number of Ar metastables were consumed through reaction (5, 6), which results in restraining reaction (2). Therefore, when more H_2 was added, the Ar plasma must be quenched and the quenching effect of H_2 gas will appear. From reaction (9), we can see that a lot of electrons were consumed through this reaction. This reaction can be used to explain why the discharge current decreased after the H_2 gas addition.

3.3.3 Application on surface treatment of copper nano-paste

Fig.3.15 shows XPS spectra of the sample plasma-treated for 12 cycles by beam plasma torch with the RF power of 60 W at 425 ℃, Ar flow rate was 5 L/min and H_2 flow rate was 10 mL/min. As shown in Fig. 3.14 (a), the shake-up satellite peak between the Cu $2p_{3/2}$ peak and Cu $2p_{1/2}$ is very obvious, and it is known to be formed as a result of the electron uncoupling in the 3d or 4f shell of the electron structure [15]. On one hand, the Cu $2p_{3/2}$ peak at 933.8 eV corresponds to CuO [16-19]. On the other hand, the Cu $2p_{3/2}$ peak was deconvoluted into two peaks A and B, respectively, as shown in Fig. 3.14(b). The position of peak B at 933.78eV due to CuO is greatly higher than that of the peak A due to Cu at 932.5 eV. It indicates that the surface of the sample treated by the beam plasma torch in atmosphere at 425 ℃ was oxidized though hydrogen was added to the plasma. It is considered that because the area of the sample used is much larger than the diameter of beam plasma torch nozzle, the plasma-treated part on the sample exposed in atmosphere at high temperature (425 ℃) was oxidized again.

APC plasma torch was used to reduce the oxide on the surface of the sample by the experimental setup shown in Fig. 2.6 in Chapter 2. The Ar flow rate was 20 L/min and H_2 flow rate was 10 mL/min with the RF power set at 100 W, and the sample was treated for 1minute at the position of 3 mm down from the plasma torch head. The XPS spectra of the reduced sample are shown in Fig. 3.15. The shake-up peak between the main peaks Cu $2p_{3/2}$ and Cu $2p_{1/2}$ has been significantly decreased as shown in Fig. 3.15 (a). Fig. 3.15 (b) shows the deconvolution of the main peak Cu $2p_{3/2}$ as peak A and peak B. The position of peak A at 932.9 eV corresponding to Cu is greatly higher than that of peak B at 933.7 due to CuO, indicating that the oxidized surface of the sample has been reduced by the Ar/H_2 plasma-treatment with APC plasma torch.

The photograph and the SEM image of the sample plasma-treated for 12 cycles at 425 ℃ by beam plasma torch and then reduced by APC plasma torch are shown in Fig. 3.16. As the photograph of the sample treated shown in Fig. 3.16 (a), the surface of the sample became pink and the metallic luster is appeared, which is the feature of bulk copper. The corresponding SEM image shown in Fig. 3.16 (b) exhibits that copper nano-particles has been completely sintered.

It is suggested that the copper nano-particles could be sintered by the plasma-treatment with the beam plasma torch. However, the oxidizing of the surface plasma-treated in atmosphere is a critical problem.

In order to prevent the sample being oxidized in atmosphere, on one hand, a sealed glass chamber was used as shown in Fig. 3.3 to treat the sample in an inert atmosphere. In this chamber, the sample was fixed without moving. On the other hand, according to the plasma diagnostics, a relatively powerful experimental condition, the Ar flow rate of 25 L/min and the H_2 flow rate of 5 mL/min was selected.

Fig. 3.17 shows the XPS spectra of the sample treated in the experimental setup shown in Fig. 3.3 at ambient temperature for 1 minute with the RF set at 30 W and the Ar flow rate of 25 L/min and H_2 flow rate of 5 mL/min. As shown in Fig3. 17 (a) the shake-up satellite peak between the Cu $2p_{3/2}$ peak and Cu $2p_{1/2}$ is not obvious and the Cu $2p_{3/2}$ peak at 932.2 eV corresponds to Cu [16-19]. The typical deconvolution of peak Cu $2p_{3/2}$ is shown in Fig. 3.17 (b). The position of peak B at 933.9 eV corresponding to CuO is greatly lower than that of the peak A at 932 eV due to Cu. It indicates that Ar/H_2 plasma-treatment with the Ar flow rate of 25 L/min and H_2 flow rate of 5 mL/min with the RF power set at 30 W within 1 minute can lead the reduction of oxidized copper nano-particles. In order to sinter the copper nano-particles at ambient temperature, a sample was plasma-treated at RF power of 60 W for 5 minutes with the Ar flow rate of 25 L/min and H_2 Flow rate of 5 mL/min at the position of 3 mm down from the plasma torch head in the experimental setup shown in Fig.3.3. The photograph and the SEM image of the sample treated are shown in Fig. 3.18.

As shown in Fig. 3.18 (a), there is metallic luster on the area plasma-treated. The corresponding SEM image is shown in Fig. 3.18 (b). The copper nano-particles have been completely sintered and formed a copper files. The temperature of the sample was measured by thermocouple at the position of 3 mm down from the plasma torch head as 73.2 ℃.

It is suggested that, on one hand, comparing with APC plasma torch in Chapter 2, the smaller plasma nozzle resulted in stronger emission intensity from plasma jet. On the other hand, with the emission intensity of the optical spectra increasing for the Ar/H_2 plasma owing to both increased Ar flow rate and the addition of H_2 into Ar plasma, the copper nano-particles could be sintered at

ambient temperature by the Ar/H_2 plasma-treatment. In additionally, plasma-treatment in the sealed glass chamber shown in Fig. 3.3 prevents the sample from being oxidized again.

3.4 Conclusions

In this chapter, in order to reduce the sintering temperature, a beam plasma torch was introduced. It was investigated the characteristics of non-equilibrium atmospheric pressure plasma generated by the beam plasma torch. On one hand, in the case of pure Ar plasma, with increasing Ar flow rate from 5 L/min to 25 L/min, it could result in the transition of the discharge regime from γ-mode to α-mode. In addition, the amplitude of the waveform of discharge voltage and RF current was also greatly enhanced, while the temperature of pure Ar plasma jet was deeply decreased. On the other hand, in the case of Ar/H_2 plasma, with increasing the H_2 flow rate, it has little effect on the discharge regime or the amplitude of both the discharge voltage and RF curre. Increasing the RF power would lead a slight distortion for the waveform of discharge voltage, but kept an α-mode discharge.

Similar to the electrical characteristics, in the case of pure Ar plasma, the emission intensity from the Ar plasma jet was greatly enhanced with increasing the Ar flow rate, and a powerful pure Ar plasma jet could be obtained at the Ar flow rate of 25 L/min. In the case of Ar/H_2 plasma, it lead to an increase of emission intensity from plasma jet and slightly decreased with increasing flow rate of H_2 while the temperature of plasma jet was also increased. It is suggest that a powerful Ar/H_2 plasma jet could be generated by the beam plasma torch at the Ar flow rate of 25 L/min and the H_2 flow rate of 5 mL/min. Increasing the RF power lead to a increase of the emission intensity from both the excited Ar atoms and H atoms.

At the Ar flow rate of 5 L/min and H_2 flow rate of 10 mL/min, the copper nano-particles could be sintered by Ar/H_2 plasma with the RF power set at 60 W at 425 ℃ and exhibited the feature of bulk copper. However, the critical problem was the plasma-treatment by the beam plasma torch at 425 ℃ in atmosphere leading to the re-oxidization of the sample. A glass sealed chamber was used to treat the sample in an inert atmosphere. The oxidized copper nano-particles could be reduced in the chamber by Ar/H_2 plasma in 1 minute with the RF power set at 30 W and the flow rate of Ar and H_2 at 25 L/min and 5 mL/min, respectively. With increasing the RF power to 60 W, the copper nano-particles could be sintered by Ar/H_2 plasma jet at ambient temperature. The powerful plasma generated by beam plasma torch with large Ar flow rate and the addition of H_2 greatly improved the reduction and sintering abilities of Ar/H_2 plasma jet for the copper nano-particles.

References

[1] M. C. García, M. Varo, P. Martínez: *Plasma Chem. Plasma P.*, **30**, 241(2010)

[2] Y. H. Choi, J. H. Kim, K. H. Paek, W. T. Ju, Y. S. Hwang: *Surf. Coat. Technol.*, **193**, 319 (2005)

[3] S. Y. Moon, J. K. Rhee, D. B. Kim, W. Choe: *Phys. Plasmas*, **13**, 033502 (2006)

[4] X. Yang, M. Moravej, G. R. Nowling, S. E. Babayan, J. Panelon: J. P. Chang, R. F. Hicks: *Plasma Sources Sci. Technol.*, **14**, 314 (2005)

[5] J. Laimer, S. Haslinger, W. Meissl, J. Hell, H. Stǒri: *Vacuum*, **79**, 209 (2005).

[6] J. Laimer, H. Reicher, Qurat-ul-Ain: *28th ICPIG*, Prague, Czech Republic 10 (2007)

[7] J. Park, I. Henins, H. W. Herrmann, G.S. Selwyn: *J. Appl. Phys.*, **89**, 20(2001)

[8] S. Ono, S. Teii, Y. Suzuki, T. Suganuma: Thin Solid Films 2009, **518**, 981.

[9] E. S. Lee, J. H. Choi, H. K. Baik: *Surf. Coat. Technol.*, **201**, 4973 (2007)

[10] Barbara, K.P.P J. : *Plasma Chem Plasma Process*, **30**, 641 (2010)

[11] Altenberend J, Majchrzak M, Delannoy Y, Chichignoud G: *J. Phys: Conf. Series,* **275**, 012001 (2001）

[12] Y. H. Choi, J. H. Kim, K. H. Paek, W. T. Ju, Y. S. Hwang: *Surf. Coat. Technol.*, **193**, 319 (2005)

[13] V. Monna, A. Ricard: *Vacuum*, **61**, 409 (2001)

[14] J. Laimer, S. Haslinger, W. Meissl, J. Hell, H. Stŏri: *Vacuum*, **79**, 209 (2005)

[15] W. Y. Sung, W.J. Kim, S.M. Lee, H.Y. Lee, Y. H. Kim, K.H. Park, S. Lee: *Vacuum*, **81**, 851 (2007)

[16] Terry L. Barr. : *J, Phys. Chem.*, **82**, 1801 (1978)

[17] T. Ghodselahi, M.A. Vesaghi, A. Shafiekhani, A. Baghizadeh, M. Lameii: *Appl. Sur. Sci.*, **255**, 2730 (2008)

[18] Y. Sawada, N. Taguchi, K. Tachibana: *Jpn. J. Appl. Phys.*, **38**, 6506 (1999)

[19] W. K. Han, J. W. Choi, G. H. Hwang, S. J. Hong, J. S. Lee, S. G. Kang: *Appl. Surf. Sci.*, **252**, 2832 (2006)

[20] Q. S. Yu, H, K, Yasuda: *Plasma Chem. Plasma P.*, **18**, 461 (1998)

[21] B. K. Pawlak, P. Jamroz: *Plasma Chem. Plasma P.*, **30**, 641 (2010)

[22] U. Lommatzsch, D. Pasedag, A. Baalmann, G. Ellinghorst, H.-E. Wagner: *Plasma Process. Polym.*, **4**, S1041 (2007)

[23] M. Jung, H. Choi: *J. Colloid Interface Sci.*, **310**, 550 (2007)

[24] A. R. Dayal, D. R. Sadedin: *Plasma Chem. Plasma P*., **23**, 627 (2003)

[25] J. Liu, Z. Shen, M. Nygren, B. Su, T.W. Button: *J. Am. Ceram. Soc.*, **89**, 2689 (2006)

[26] K. TakedaP, H. InuiP, H. KondoP, K. Ishikawa, M. Sekine, M. Hori: *30th ICPIG*, Belfast, Northern Ireland, UK 2011, D14.

[27] J. Ryu, H. Kim, H. THOMAS HAHN: *J. Electron Mater*, **40**, 42 (2011)

[28] O. A. Yeshchenko, I. M. Dmitruk, A. A. Alexeenko, A. M. Dmytruk: *Phys. Rev. B*, **75**, 085434 (2007)

[29] M. Naito, H. ABE, K. Nogi: *SFJ*, **56**, 748 (2006)

Table 3.1 Most emission lines observed in Ar/H_2 plasma generated by beam plasma torch at the position of 3 mm down from the plasma torch head and 2 mm side from plasma jet end. The integration time was 100 ns [20, 21].

Species	Wavelength (nm)	Transition	Threshold energy (eV)
H	656.3	3d-2p	12.09
Ar	696.5	4p-4s	13.32
	706.7		13.29
	714.7		13.28
	728		13.33
	738.4		13.3
	751.4		13.27
	763.5		13.17
	772.4		13.33
	794.8		13.28
	801.5		13.15
	811.5		13.08

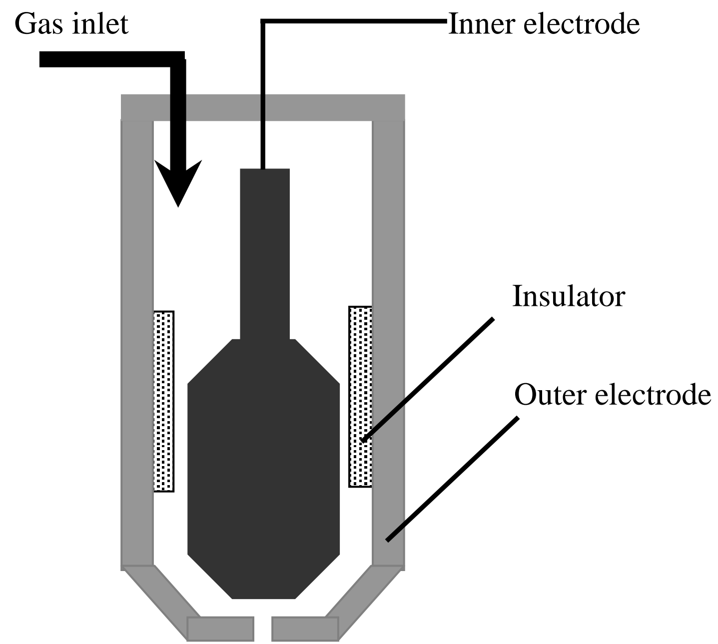

Fig.3.1 Schematic diagram of the beam plasma torch

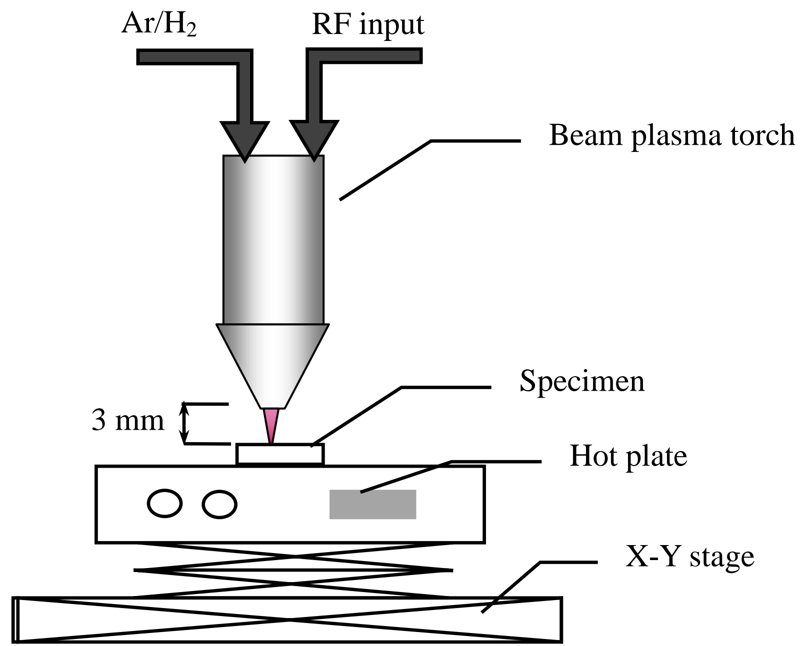

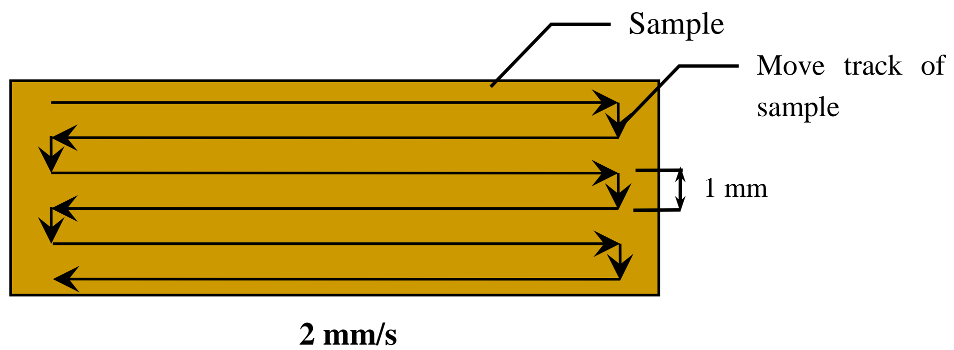

2 mm/s

Fig.3.2 Schematic diagrams of the experimental setup used to treat the sample at 425 ℃ (up) and the raster scan for the plasma-treatment on the X-Y stage (down).

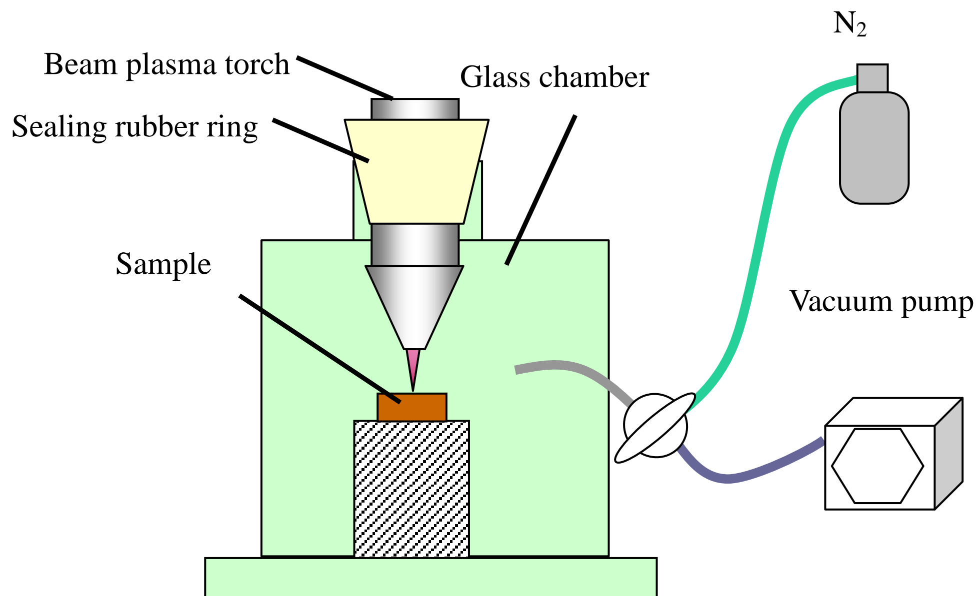

Fig. 3.3 Schematic diagram of the experimental setup used to treat the sample at ambient temperature in inert atmosphere.

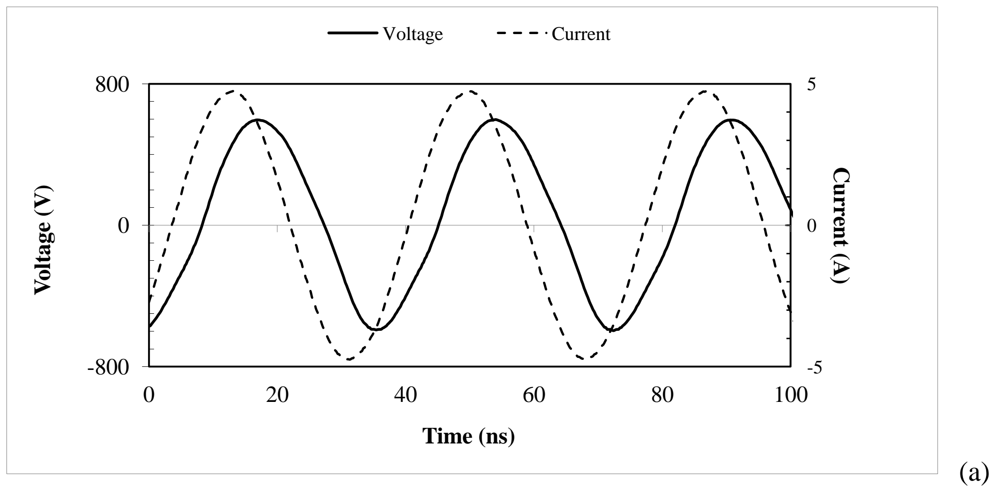

(a)

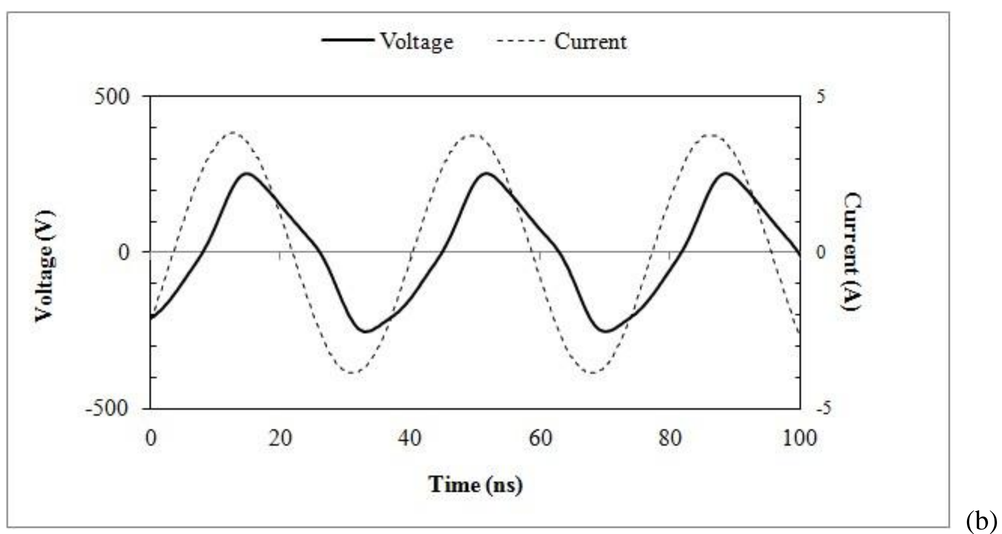

(b)

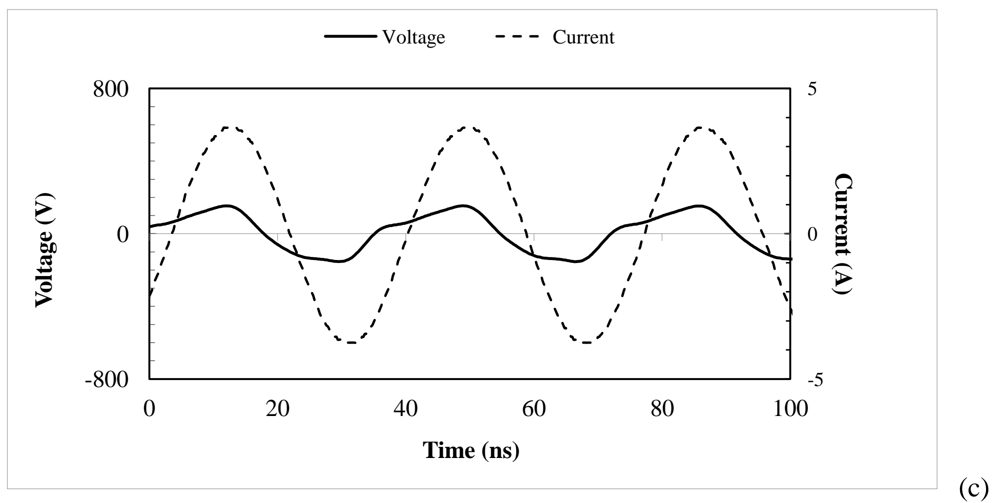

(c)

Fig. 3.4 Waveforms of discharge voltage and RF current of pure Ar plasma at RF power of 60W, Ar flow rate was 25 L/min (a); Ar flow rate was 15 L/min (b); Ar flow rate was 5 L/min (c)

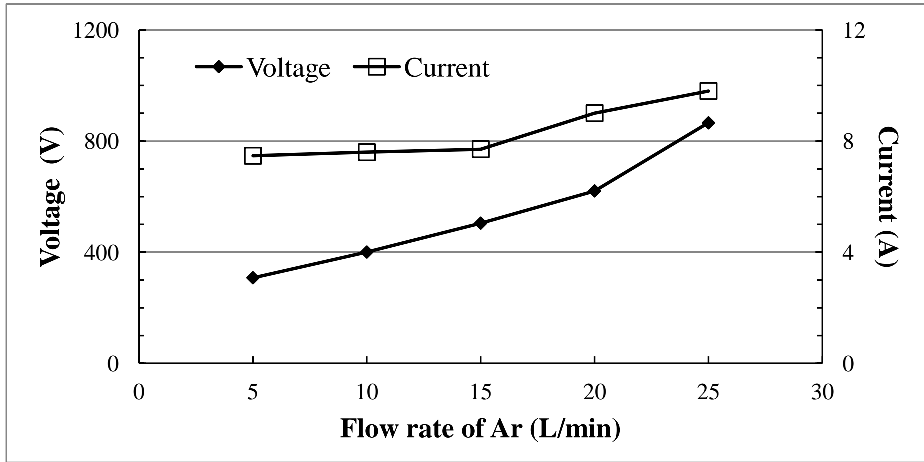

Fig. 3.5 Effect of Ar gas flow rate on the discharge voltage and RF current for pure Ar plasma at RF power of 60W

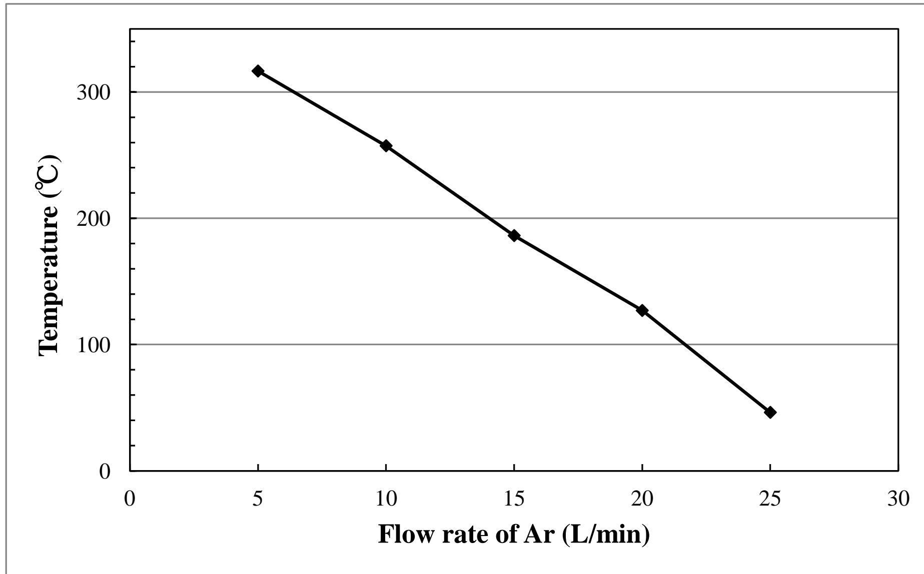

Fig.3.6 Effect of Ar gas flow rate on the temperature of pure Ar plasma jet at the RF power of 60W.

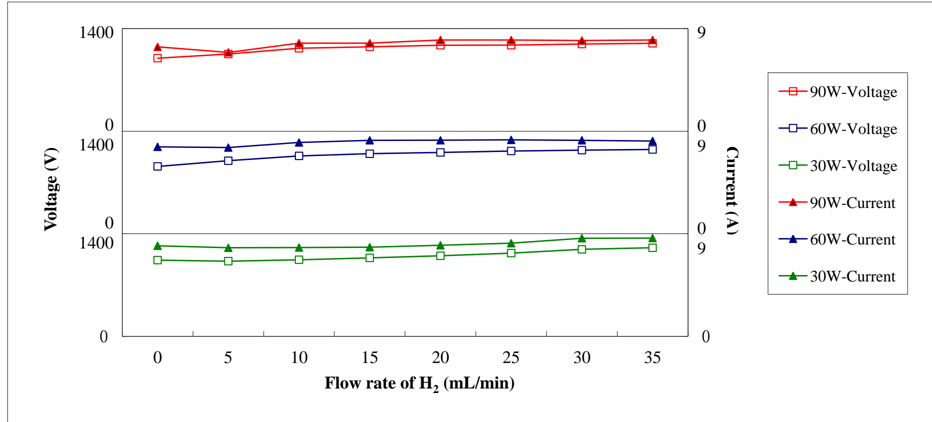

Fig. 3.7 Effect of H_2 flow rate on the discharge voltage and RF current for Ar/H_2 plasma at Ar flow rate of 25 L/min.

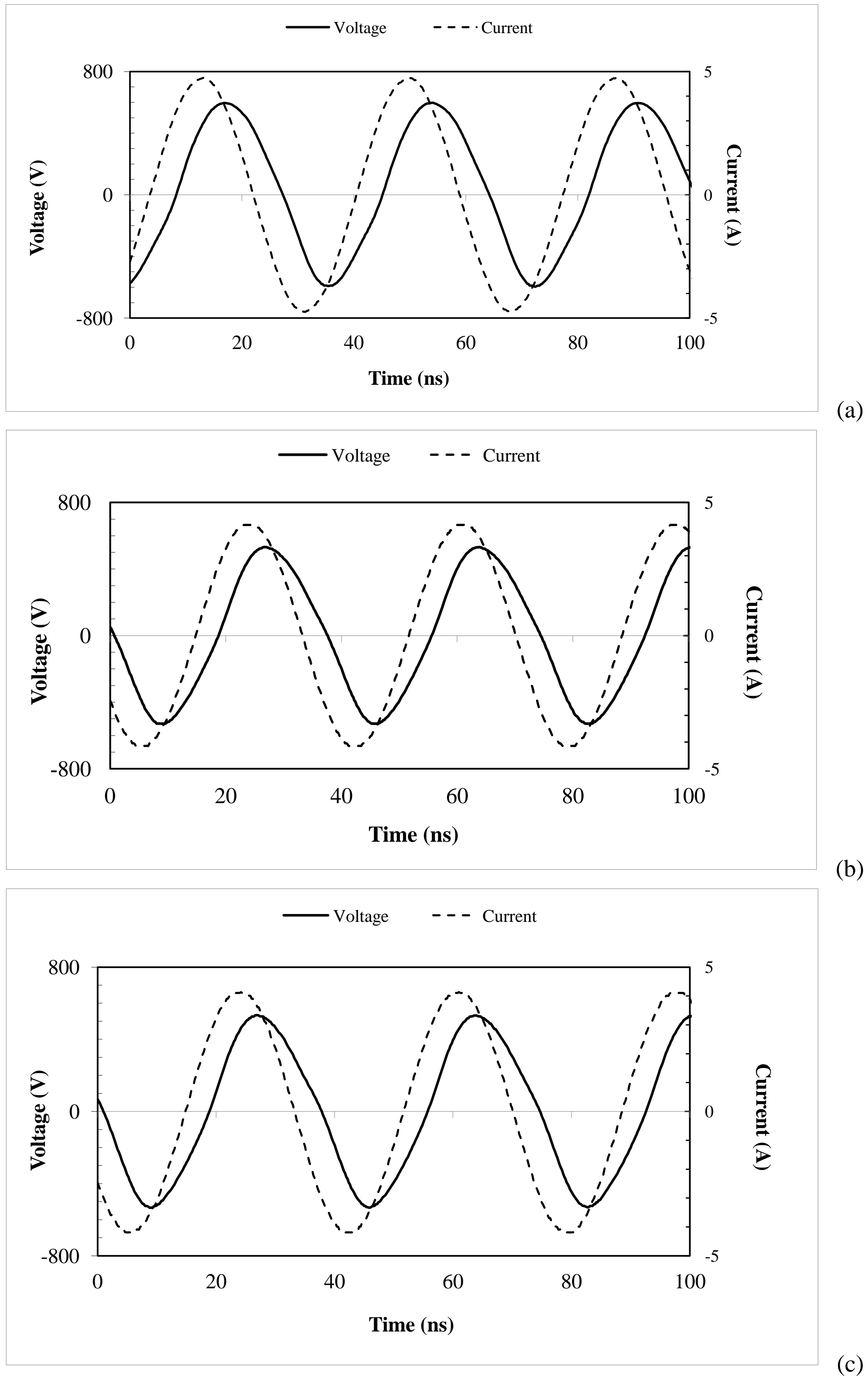

Fig.3.8 Waveforms of the discharge voltage and the current of RF for Ar/H_2 plasma at the RF power of 60 W, the flow rate of Ar=25 L/min and the flow rate of H_2=0 mL/min (a), the flow rate of Ar=25 L/min and the flow rate of H_2=5 mL/min (b), the flow rate of Ar=25 L/min and the flow rate of H_2=15 mL/min (c)

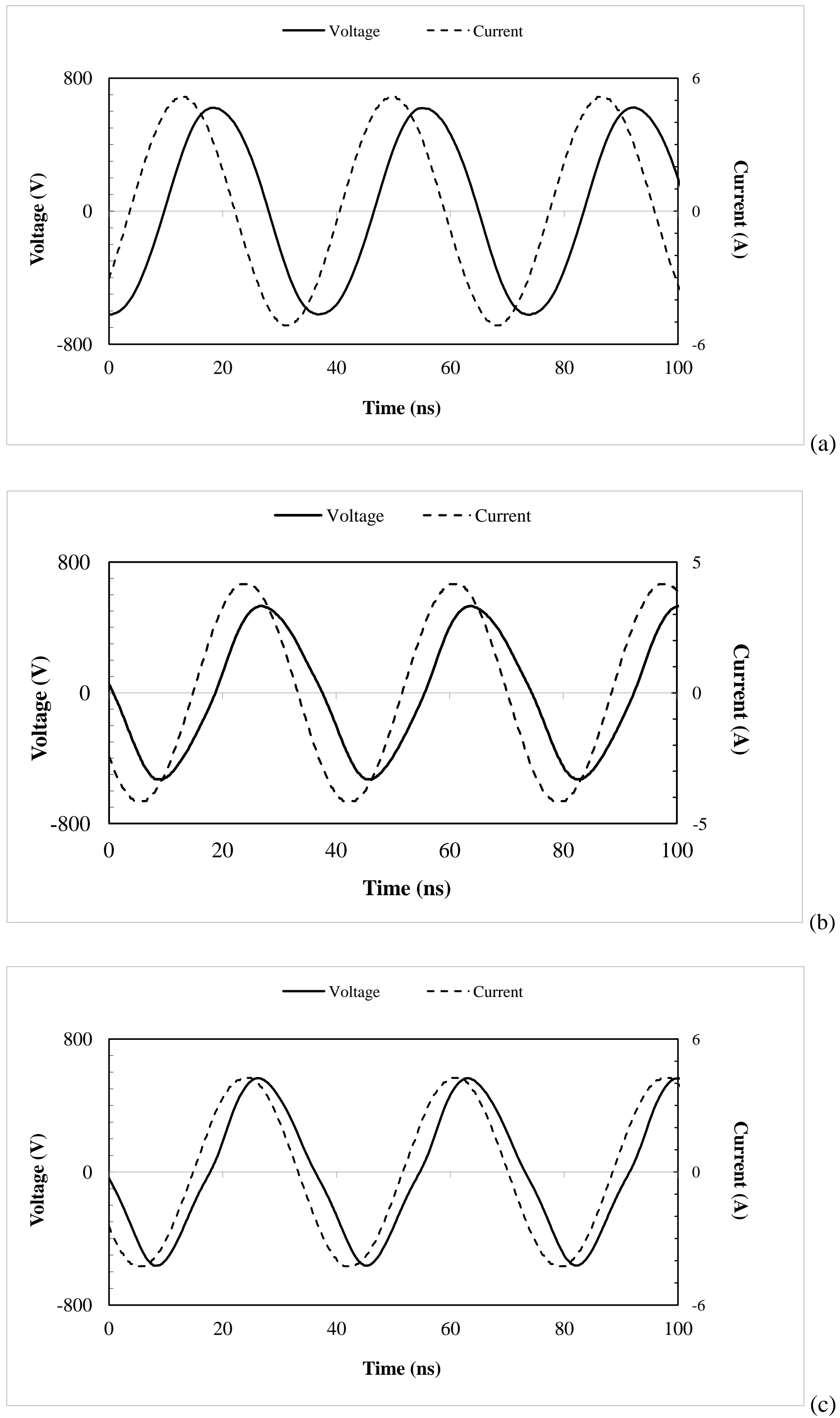

Fig.3.9 Waveforms of discharge voltage and RF current for Ar/H_2 plasma as the Ar flow rate of 25 L/min and H_2 flow rate of 5 mL/min, RF power was 30 W (a); RF power was 60W (b); RF power was 90 W (c)

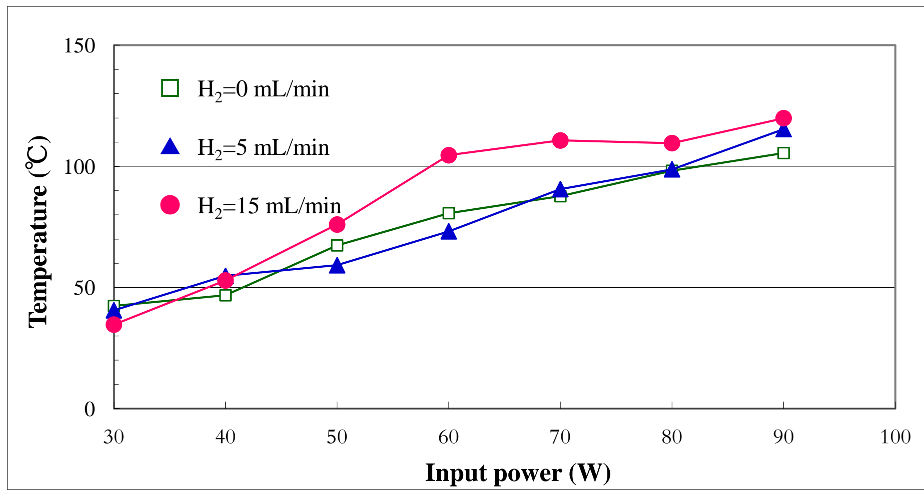

Fig. 3.10 Effects of RF power and H_2 flow rate on the temperature of plasma jet. Ar Flow rate was 25 L/min and the measure distance was 3 mm down from the plasma torch head.

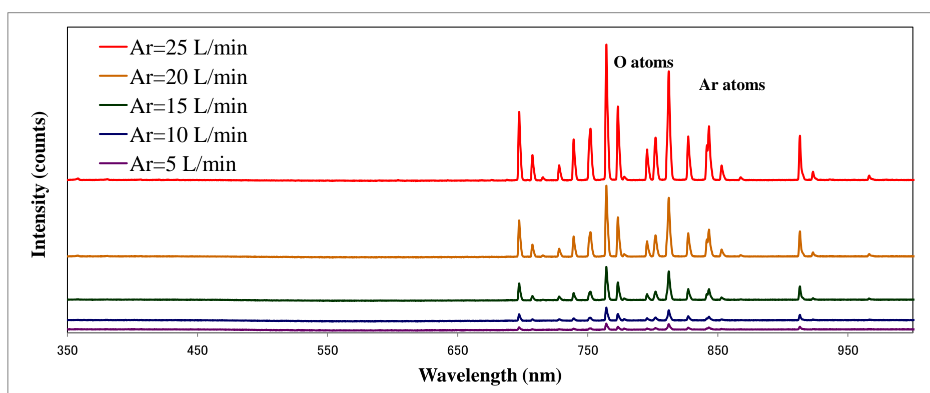

Fig.3.11 Emission spectra from the pure Ar plasma in the 350-1000 nm wavelength region at the flow rate of Ar of 5-25 L/min at the position of 3 mm down from the plasma torch head and 2 mm side from the plasma jet end. The integration time was 100 ns.

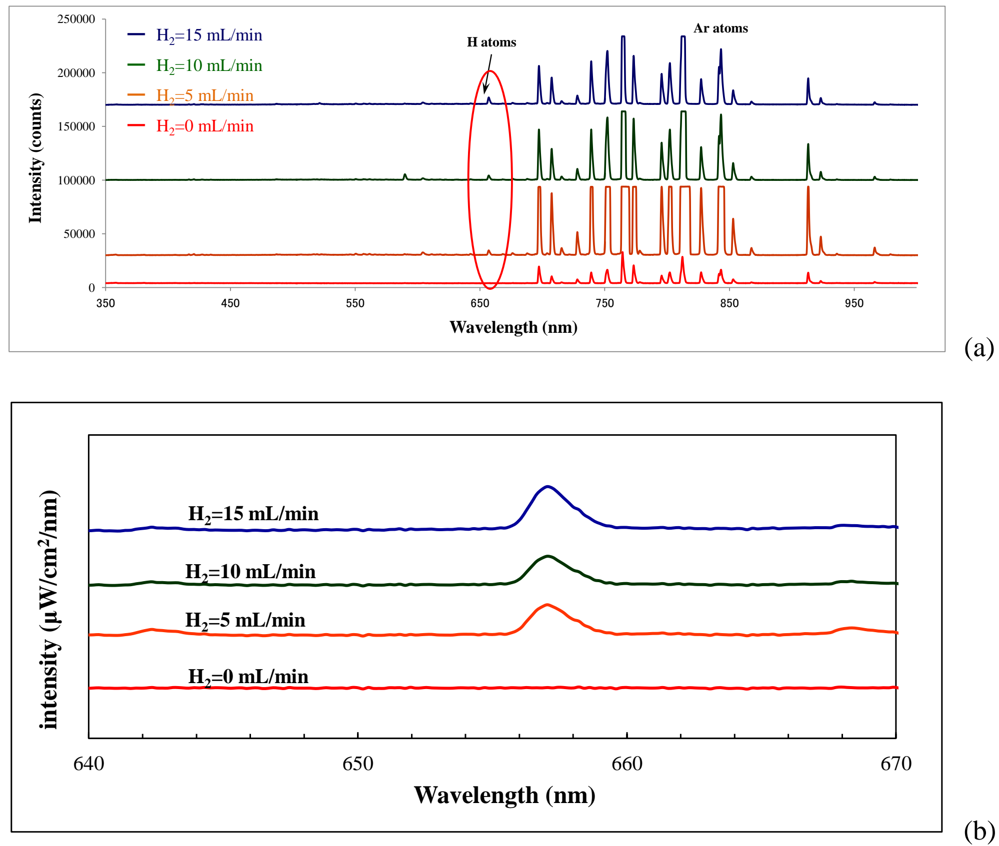

Fig. 3.12 Typical optical spectra emitted by Ar/H_2 plasma generated by beam plasma torch as RF power of 60 W with the constant flow rate of Ar as 25 L/min and increasing the H_2 flow rate 0-15 mL/min (a); changes of the peak at 656.28 nm corresponding to Hα with increasing the H_2 flow rate marked in red oval (b). The position of the collect emission spectra was at 3 mm down from the plasma torch head and 2 mm side from plasma jet end, and the integration time was 100 nm

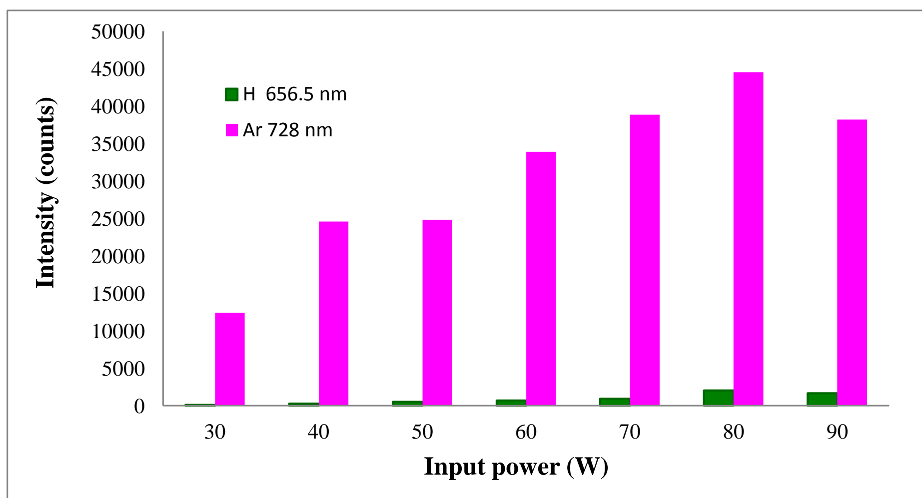

Fig.3.13 Effect of RF power on the emission intensity from active species in Ar/H_2 plasma jet generated by beam plasma torch at the position of 2 mm side from the plasma end and 3 mm down from the plasma torch head. Ar flow rate was 25 L/min and H_2 flow rate was 5 mL/min. The integration time was 100 ns.

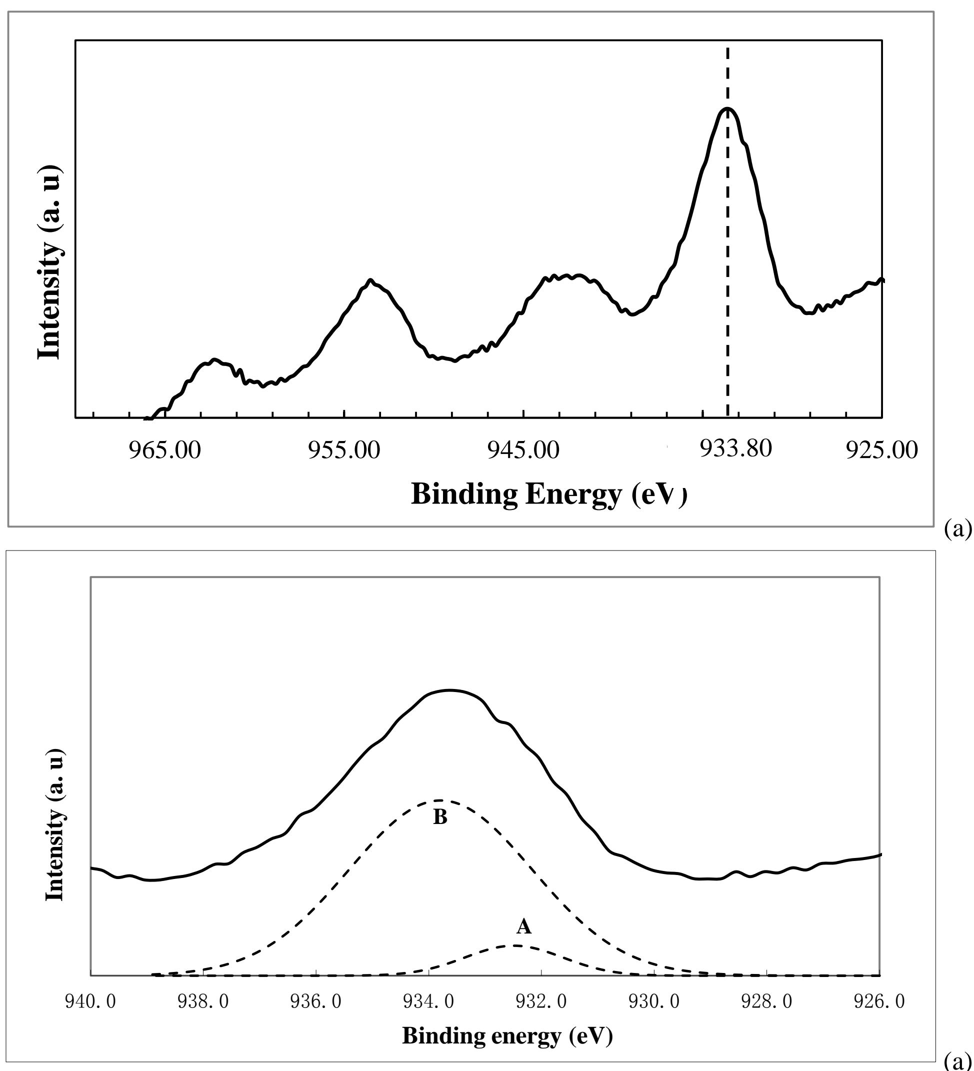

Fig. 3.14 Main and satellite peaks of Cu $2p_{3/2}$ and Cu $2p_{1/2}$ of the XPS spectra for copper nano-particles treated by the beam plasma torch for 12 cycles at 425 ℃ at the Ar flow rate of 5 L/min and H_2 flow rate of 10 mL/min and RF power set at 60 W at the position of 3 mm down from the plasma torch head (a); Typical deconvolution of Cu $2p_{3/2}$ main peak (b).

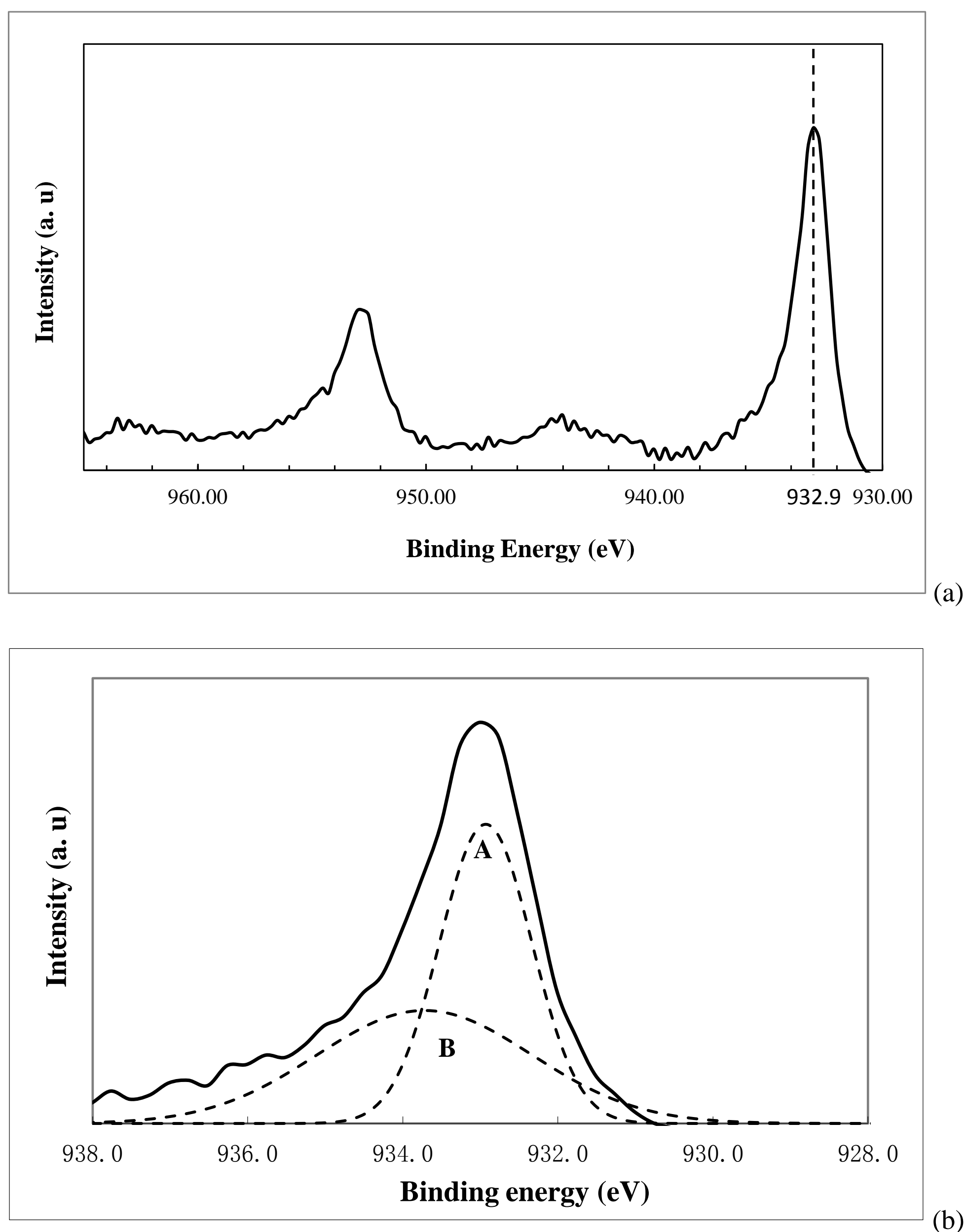

Fig. 3.15 Main and satellite peaks of Cu $2p_{3/2}$ and Cu $2p_{1/2}$ of the XPS spectra for copper nano-particles treated by the beam plasma torch for 12 cycles at 425 ℃ as the Ar flow rate of 5 L/min and H_2 flow rate of 10 mL/min and RF power set at 60 W, and then reduced by APC plasma torch for 1 minute at the Ar flow rate of 20 L/min and H_2 flow rate of 10 mL/min and RF power set at 100W with the experimental setup shown in Fig. 2.6 in Chapter 2 (a) Typical deconvolution of Cu $2p_{3/2}$ main peak (b);

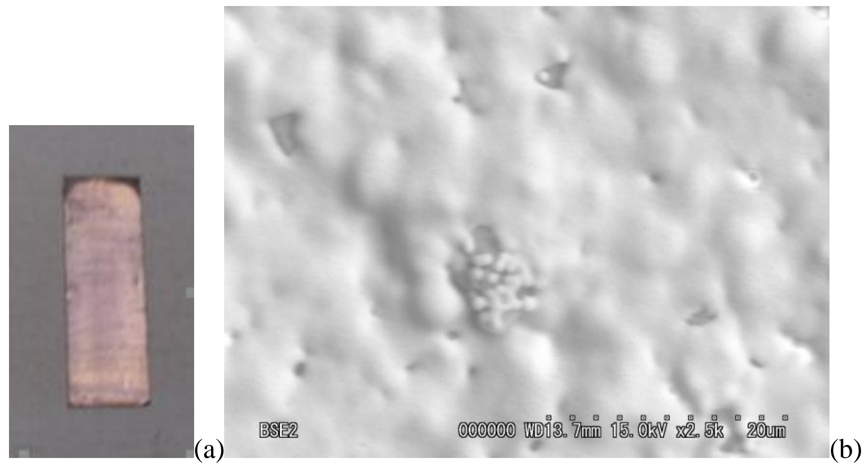

Fig.3.16 Photograph of the sample plasma-treated by the beam plasma torch for 12 cycles at 425 ℃ under the condition that Ar flow rate was 5 L/min, H_2 flow rate was 10 mL/min, and the RF power was 60 W at the position of 3 mm down from the beam plasma torch head and then reduced by APC plasma torch under the condition of Ar flow rate at 20 L/min and the H_2 flow rate was 10 mL/min for 1 minute with the experimental setup shown in Fig. 2.6 in Chapter 2 (a); SEM image of the same sample (b).

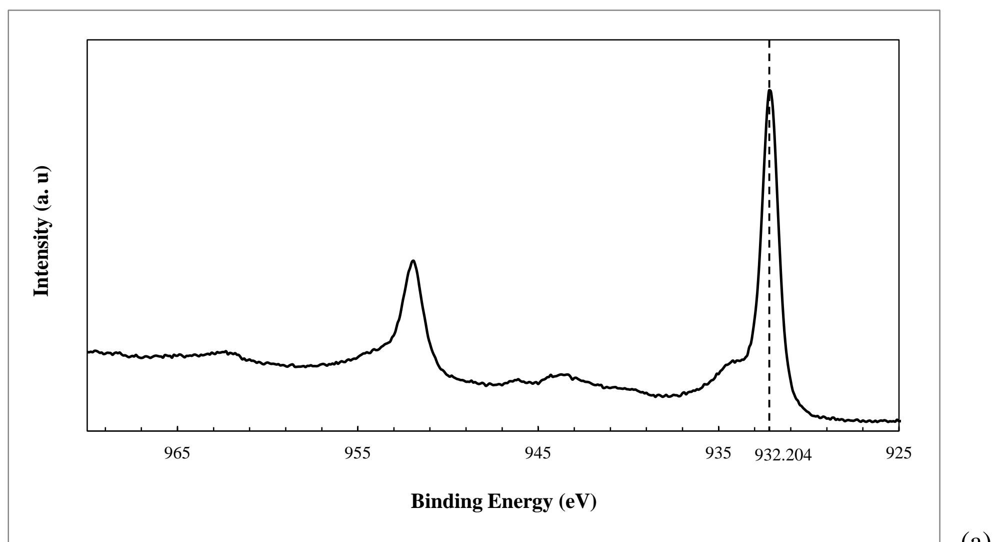

(a)

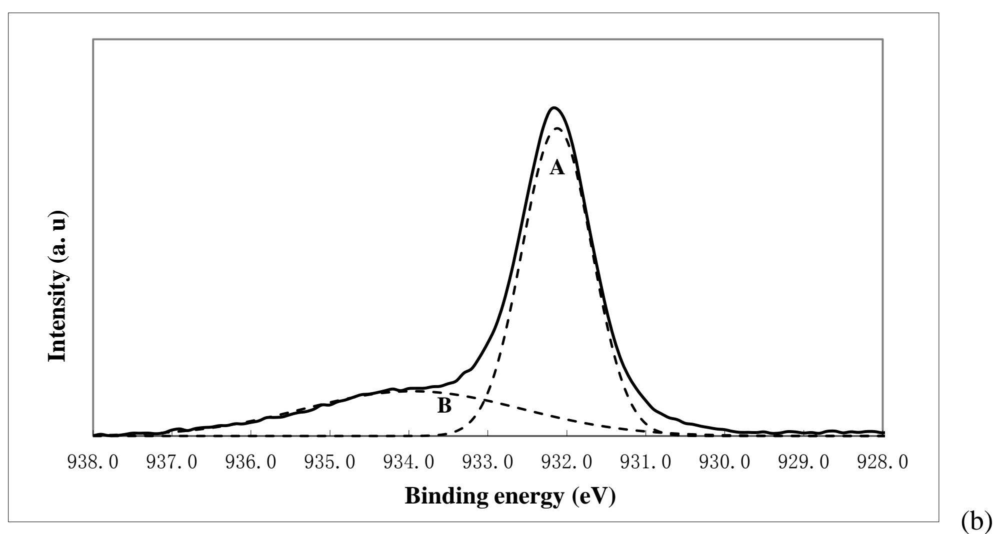

(b)

Fig.3.17 Main and satellite peaks of Cu $2p_{3/2}$ and Cu $2p_{1/2}$ of the XPS spectra for copper nano-paste plasma-treated for 1 minute at the RF power of 30 W, the flow rate of Ar at 25 L/min and H_2 flow rate at 5 mL/min in inert atmosphere (a); Typical deconvolution of Cu $2p_{3/2}$ main peak (b).

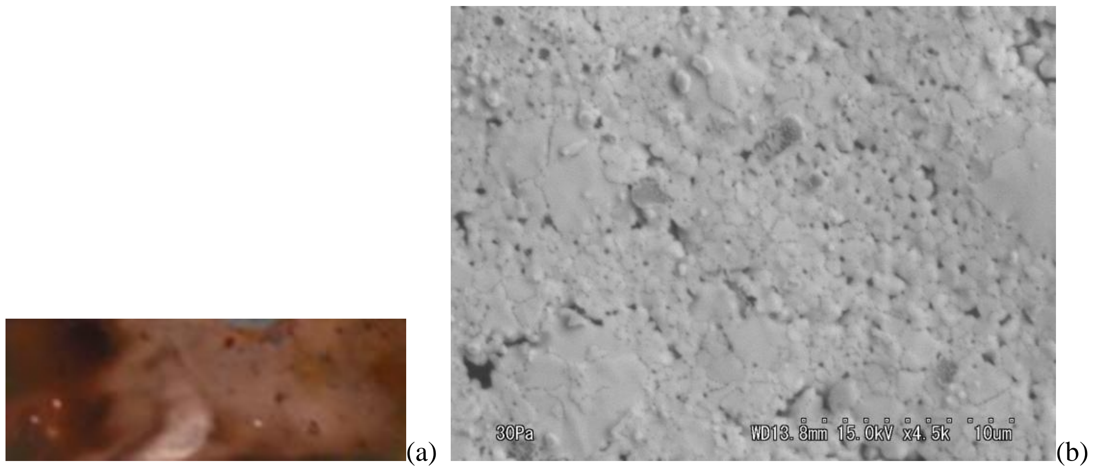

Fig.3.18 Photograph of the sample plasma-treated for 5 minutes at ambient temperature by the beam plasma torch with the Ar flow rate of 25 L/min and H_2 flow rate of 5 mL/min at the RF power set at 60 W in inert atmosphere (a); Micrograph by SEM image of the same sample (b).

Chapter 4 Reduction and sintering of copper nano-particles by atmospheric pressure plasma generated by beam plasma torch with air-cooling

4.1 Introduction

In Chapter 3, it is suggested that the addition of H_2 as the additive gas to pure Ar plasma lead to an increase of emission intensity for Ar/H_2 plasma generated by the beam plasma torch. What is more, the reduction and sintering of copper nano-particles could be achieved at ambient temperature, and the metallic luster appeared on the surface of the sample plasma-treated. However, as for electrical characteristic, at low Ar flow rate (lower than 25 L/min), it showed a failure discharge regime γ-discharge, while with increasing the flow rate of Ar gas, the waveforms of discharge voltage and RF current became smooth and completely sinusoidal. It indicated that under the high flow rate of Ar as the working gas, it exhibited typical α-discharge characteristic and low temperature of the plasma jet.

It was assumed the thermal influence to the electrode was ascribed to a transition of the discharge regime. The high flow rate of Ar gas was assumed to play a role in reducing the temperature of the electrode for beam plasma torch used in Chapter 3. In order to investigate the effect of electrode cooling on the properties of the plasma generated by the beam plasma torch, a new beam plasma torch with an air-cooling system on electrode was developed.

The purposes in this study are to investigate the effect of electrode air-cooling of beam plasma torch on the plasma characteristic and verify its effect on the sintering of copper nano-particles.

4.2 Experimental details

4.2.1 Non-equilibrium atmospheric pressure plasma device and experimental procedures

The schematic diagram of the plasma torch used in the experiment is shown in Fig. 1. The beam plasma torch consists of two stainless steel (SUS) co-axial electrodes and the inner electrode as the diameter of 10 mm is connected to a RF power source with frequency of 27.12 MHz through an impedance matching network, while the outer electrode is grounded. A glass pipe was used as an insulator between the two electrodes and the gap spacing between them is 1 mm. The difference between the air-cooling beam plasma torch and the beam plasma torch mentioned in Chapter 3 is the air-cooling system of the inner electrode. Cool air was pumped from the inlet into the interior of the inner electrode and flows through the surface of the electrode to remove the heat. The cooling route of the cooling air is shown in blue line in Fig. 4.1.

Fig. 4.2 shows the experimental setups used in this study. In order to prevent the sample from being oxidized by oxygen in air, the experiment was carried out in a 3 L-size sealed glass chamber. Before the plasma-treatment, the chamber was pumped to vacuum for 1 minute, then N_2 was injected at the flow rate of 3 L/min for 1 minute, and repeated the procedures 3 times to replace the air to N_2 in the chamber. In the case of the plasma-treatment by the beam plasma torch with air-cooling, it is necessary to continuously inject the cooling air to the electrode during the plasma-treatment, while, as a comparison, in the case of plasma-treatment without air-cooling, the same beam plasma torch was used without injecting the cooling air into the inner electrode.

4.2.2 Sample preparation

The copper nano-paste developed by Mitsuboshi Belting Ltd. consists of copper nano-particles with the diameter of 700-900 nm and the polymer additives as the binder. The copper nano-paste was printed on alumina substrates with the thickness of 30 μm as shown in Fig. 2.2 in Chapter 2, and the printed films were dried at 100 ℃ in an oven for 30 minutes. In order to remove the polymer additives in the paste, the dried films were heat-treated at 280 ℃ for 10 minutes with the heating rate of 5 ℃/min. The treatment temperature was determined through TG-DTA experiment shown in Fig.2.3 in Chapter 2.

4.2.3 Plasma diagnostic*s*

In order to characterize the plasma generated by the beam plasma torch, electrical characterization and optical emission spectrometry (OES) measurements were carried out. The schematic experimental setups were as same as those shown in Fig. 2.6 in Chapter 2.

Electrical characterization was performed by a Tekronix TDS3012C digital phosphor oscilloscope. The waveform of discharge voltage was measured with a 10:1 voltage probe (Tektronix P6139 10X Passive Probe 063-0870-05), and the RF current was measured with a wide band current monitor (PearsonTM current monitor) manufactured by Pearson Electronics Inc., Palo Alto, California, U.S.A..

Optical emission spectra (OES) were collected by an Ocean Optics USB4000 spectrometer at the position of 2 mm side from the plasma end and 3mm down from the plasma torch head, through an optical fiber with a diameter of 100 μm. The integration time was 100ns.

The temperature of plasma jet was measured by a thermocouple at 3 mm down from the plasma torch head.

4.2.4 Characterization of the copper nano-particles surface

X-ray photoelectron spectroscopy (XPS; AXIS-NOVA) was performed to analyze the surface composition of the copper nano-paste at accelerating voltage of 10 kV.

SEM (Hitachi S-3000N scanning electron microscope) was utilized to observe the microstructures of the nano-particles to distinguish the changing on the surface morphology of the plasma-treated sample

4.3 results and discussion

4.3.1 Effect of air-cooling system of electrode on the electrical characterization of plasma jet

Fig. 4.3 shows the waveform of the discharge voltage (solid line) and RF current (dashed line) of pure Ar plasma jet generated by beam plasma torch with air-cooling (green line) and without air-cooling (red line) as RF power set at 30 W (see in Fig.4.3 (a)) and 60W (see in Fig. 4.3(b)), respectively, with the constant Ar flow rate of 25 L/min. With increasing the RF power from 30 W to 60 W, both the waveforms of the RF current are standard sinusoidal, while the waveforms of the discharge are slightly distorted. When the RF power was set at 60 W, it is considered as γ-mode discharge for the pure Ar plasma jet because of the waveforms deformation and the small phase between the voltage and current [1-13]. With air-cooling of electrode (shown in green lines), both the amplitude of the discharge voltage and RF current was increased, especially when the RF

power set at 30 W, suggesting that the air-cooling of electrode improved the discharge properties to a certain extent.

Fig. 4.4 show the effect of electrode air-cooling of beam plasma torch on the discharge voltage and the RF current of Ar/H_2 plasma with the Ar flow rate maintained at 25 L/min and the H_2 flow rate maintained at 30 mL/min, the RF power set at 30 W and 60 W, respectively. The amplitude of discharge voltage generated by the beam plasma torch with air-cooling (green line) is higher than that without air-cooling (red line), while the amplitude of RF current generated by the beam plasma torch without air-cooling is slightly higher than that with air-cooling when the RF power was set at 30 W. The differences are not obvious when the RF power was set at 60 W. The addition of H_2 to pure Ar plasma lead the waveforms of discharge voltage generated by beam plasma torch with and without air-cooling became smoother, suggesting the transition of discharge regime from γ-mode to α-mode could be resulted from the addition of H_2.

Fig.4.5 shows the effect of Ar flow rate on the peak-to-peak amplitude of discharge voltage (square) and RF current (triangle) in pure Ar plasma generated by the beam plasma torch with air-cooling (green line) and without air-cooling (red line) at the constant RF power of 30 W and 60 W, respectively. As is expected, with increasing the Ar flow rate, both the discharge voltage and RF current were increased, which is similar with the conclusion in Chapter 3. In addition, both the discharge voltage and RF current generated by the beam plasma torch with air-cooling are quite higher than that without air-cooling.

The effect of H_2 flow rate on the amplitudes of discharge voltage and RF current at the RF power of 30 W and 60 W is shown in Fig. 4.6, constant Ar flow rate was 25 L/min. There is almost

no change in these curves, but when the flow rate of H_2 increased to 20 mL/min at the RF power of 60 W, the RF current generated by the beam plasma torch with air-cooling was enhanced.

Based on the facts mentioned above, it is indicated that with air-cooling of electrode, the amplitudes of both discharge voltage and RF current in pure Ar plasma were increased. With the addition of H_2 to Ar plasma, the discharge regime was improves as the waveform of the discharge voltage and RF current became smoother. However, the changes in the amplitude of the discharge voltage and RF current between the beam plasma torch with and without air-cooling with increasing the H_2 flow rate are not obvious.

4.3.2 Effect of air-cooling of electrode on the OES characteristics of plasma jet

Fig. 4.7 shows the typical optical emission spectra of pure Ar plasma at the Ar flow rate of 25 L/min and RF power set at 30 W generated by the beam plasma torch with air-cooling (green line) and without air-cooling (red line). In this study, the position of all the optical emission spectra collected was at 3 mm down from the plasma torch head and 2 mm side from the plasma jet end, and the integration was 20 ns. The emission intensity from the Ar plasma generated by the air-cooling beam plasma torch is twice as powerful as that generated by the non-air-cooling beam plasma torch.

With increasing the Ar flow rate from 5 L/min to 25 L/min, the emission intensity from excited Ar atoms at 696.5 nm increased as shown in Fig. 4.8. Also, the emission intensity from plasma generated by air-cooling beam plasma torch (green square) is greatly higher than that generated by the non-air-cooling beam plasma torch (red square).

It is suggested that with air-cooling of electrode, the emission intensity from pure Ar plasma jet was deeply enhance.

Fig.4.9 shows the effect of H_2 flow rate on the emission intensity from the active species in Ar/H_2 plasma generated by beam plasma torch with air-cooling (green line) and beam plasma torch without air-cooling (red line) at the RF power of 30 W and the constant Ar flow rate of 25 L/min. The effect of H_2 flow rate on the emission intensity from the active species in Ar/H_2 plasma generated by the non-air-cooling beam plasma torch is similar to the one generated by the air-cooling beam plasma torch. There is a peak on the curve of the emission intensity from excited Ar atoms at 728 nm with increasing the flow rate of H_2, subsequently decreased slightly. The emission intensity from excited Ar atoms for the air-cooling plasma torch is much higher than that for the non-air-cooling beam plasma torch. In additionally, by the air-cooling beam plasma torch and the non-air-cooling beam plasma torch, in both the emission intensity of Hα at 656.3 nm was enhanced with increasing the H_2 flow rate in the Ar/H_2 plasma generated, however, the intensity generated by former is higher than that generated by latter.

Fig. 4.10 shows the comparison of the effect of H_2 flow rate on the emission intensity from the active species in Ar/H_2 plasma generated by the beam plasma torch with and without air-cooling at the power of 60 W and the constant Ar flow rated of 25 L/min. The trend of Ar emission intensity changes is similar with that generated at the RF power of 30 W, which is first increased with the increasing the H_2 flow rate and then slightly decrease with additional increasing of the H_2 flow rate. Comparing with the data shown in Fig. 4.9 at the RF power set at 30 W, the emission intensity from the active species in Ar/H_2 plasma was greatly increased with RF power increasing.

Base on the fact mentioned above, air-cooling of electrode could lead to a great increase of emission intensity from both pure Ar plasma and Ar/H_2 plasma jet. In addition, with the addition H_2 to Ar plasma, both the air-cooling beam plasma torch and non-air-cooling beam plasma torch have similar change trends for the active species, which is the emission intensity from excited Ar atoms increased firstly, and then slightly decreased, meanwhile the emission intensity from Hα increased with increasing the H_2 flow rate.

4.3.3 Effect of air-cooling of electrode on the temperate of Ar/H_2 plasma jet

In Fig.4.11, the temperature of plasma jet was measured at a position of 3 mm down from the plasma torch head under polyimide tape with the thickness of 35 μm and the Ar flow rate was 25 L/min. As the RF power set at 30 W shown in Fig. 4.11 (a), the temperature of the plasma jet generated by the non-air-cooling beam plasma torch (red line) is lower than that generated by the air-cooling plasma torch (green line). With addition of H_2 to Ar plasma, the temperature of the Ar/H_2 jet decreased little.

Fig. 4.11 (b) shows the temperature of the plasma jet at the RF power of 60 W and the flow rate of Ar was 25 L/min generated by the beam plasma torch with air-cooling (green line) and without air-cooling (red line). The temperature of the former is lower than that of the latte, and decreased with the H_2 flow rate increasing.

In this chapter, the temperature of plasma jet generated by the air-cooling beam plasma torch was lower than that generated by the the non-air-cooling beam plasma torch at RF power of 60W, while at 30W, relatively low RF power, the temperature of Ar/H_2 plasma jet generated by

air-cooling beam plasma torch is higher than that generated by non-air-cooling beam plasma torch. It is considered that at low RF power, the temperature of electrode is low because of the large flow rate of Ar, which played a role in cooling the electrode. So the effect of air-cooling system on the temperature of plasma jet is not obvious [4-6]. In addition, in this chapter, the temperature of plasma jet was not higher than 200 ℃

4.3.4 The OES characteristics of beam plasma torch with air-cooling system

Fig. 4.12 shows the effect of H_2 flow rate increasing on the emission intensity from active species in Ar/H_2 plasma generated by beam plasma torch with air-cooling at RF power of 30 W with the constant Ar flow rate of 25 L/min. The main emission lines observed in Ar/H_2 plasma generated by beam plasma torch with air-cooling and without air-cooling are shown in Table 4.1 [7, 8], the position of the spectra collected at 3 mm down from the plasma torch head and 2 mm side from plasma jet end. The integration time was 20 ns. The emission of excited Ar atoms is still predominant. With addition of H_2 to Ar plasma, the emission intensity was enhanced. When the H_2 flow rate was more than 15 mL/min, the Hα emission at 656.3 nm could be obviously observed. Fig. 4.12 (b) shows the changes in the intensity of the excited Ar atoms at 728 nm and Hα at 656.3 nm in Ar plasma with increasing the H_2 flow rate as mentioned above, the changes trend is clearly exhibited.

Fig.4.13 shows the effect of H_2 flow rate on the emission intensity from the active species in Ar/H_2 plasma at RF power of 60 W with the constant Ar flow rate at 25 L/min. With addition of H_2 to Ar plasma, the emission intensity was enhanced. As the H_2 flow rate got close to 15 mL/min, the emission intensity from Ar/H_2 plasma jet was greatly enhanced. Also, both the peak of excited Ar atom at 728

and the Hα peak deeply increased when the H_2 flow rate reached to 15 mL/min. The emission intensity from the active species in Ar/H_2 plasma jet slightly decreased with additional increasing the H_2 flow rate from 15 mL/min to 30 mL/min. In this chapter, H_2 flow rate of 15 mL/min was selected as a powerful experimental condition for the plasma-treatment.

The effect of RF power on the emission intensity from Ar/H_2 plasma generated by the air-cooling beam plasma torch is shown in Fig. 4.14, the Ar flow rate of Ar was 25 L/min and the H_2 flow rate was 15 mL/min. With increasing the RF power, the emission intensity from both Ar and H active species in plasma was strengthened as expected, and then decreased at the high power. It is assumed that with increasing the RF power, the temperature of electrode was raised, resulting in a decrease of electron emission efficiency of the electrode. As a powerful and stable experimental condition, RF power of 60 W was selected for plasma-treatment.

4.4 Application on reduction and sintering of copper nano-particles

Fig. 4.15 shows the optical emission spectra of Ar/H_2 plasma with Ar flow rate of 25 L/min and H_2 flow rate of 15 mL/min at 60 W without air-cooling (red line), Ar flow rate of 25 L/min and H_2 flow rate of 15 mL/min at 90 W with air-cooling (blue line), and Ar flow rate of 25 L/min and H_2 flow rate of 15 mL/min at 60 W with air-cooling (green line), respectively. Without air-cooling at 60 W (red line), the emission intensity was very weak, and similarly, the emission intensity of plasma jet at RF power of 90 W (blue line) with air-cooling on the electrode was also lower than that at RF power of 60 W (green line). As shown in Fig. 4.11, the temperature of plasma jet at 60 W without air-cooling is higher than that generated with air-cooling. And the temperature of Ar/H_2

plasma jet was around 180 ℃ at RF power of 90 W. The emission intensity from the Ar/H_2 plasma jet generated by the air-cooling beam plasma torch at RF power of 60 W is the most powerful, but with the lowest temperature of plasma jet.

In order to investigate the effect of emission intensity and temperature on the sintering of copper nano-particles, three samples were plasma-treated under the same experimental conduction for 10 minutes at the distance of 3 mm down from the plasma torch head under the plasma conditions mentioned above.

In order to investigate the reduction ability of the Ar/H_2 plasma, XPS measurement was carried out for the sample plasma-treated by the beam plasma torch with air-cooling for 1 minute at a position of 3 mm down from the plasma torch. The Ar flow rate was 25 L/min and H_2 flow rate was 15 mL/min at RF power of 30 W.

4.4.1 XPS analysis

Fig. 4.16 (a) shows the main and satellite peaks of Cu $2p_{3/2}$ in XPS spectra of the sample, and the shake-up satellite peak between the Cu $2p_{3/2}$ peak and Cu $2p_{1/2}$ is not obvious and the Cu $2p_{3/2}$ peak at 932.3 eV corresponds to Cu. On the other hand, the deconvolution of the Cu $2p_{3/2}$ as peak A and peak B is shown in Fig. 4.16 (b). The position of peak A at 932.28 eV corresponding to Cu is greatly higher than that of peak B at 934.02 eV corresponding to CuO, indicating the oxidized copper nano-particles have been reduced by plasma-treatment. We considered it could result in the reduction of oxidized copper nano-particles by Ar/H_2 plasma generated by air-cooling beam plasma torch as the RF power of 30 W within 1 minute. Therefore, the other samples

plasma-treated in this study with stronger emission intensity from plasma and longer treatment time are believed to be reduced [9].

4.4.2 Observation by SEM

The SEM images are shown in Fig. 4.17 (a), (b), (c) corresponding to Fig. 4.15, respectively, that is the SEM image of the sample plasma-treated at the RF power of 60 W by the non-air-cooling beam plasma torch shown in Fig. 4.17 (a), the SEM image of the sample plasma-treated as the RF power of 90 W by the air-cooling beam plasma torch shown in Fig. 4.17 (b) and the SEM image of the sample plasma-treated as the RF power of 60 W by the air-cooling plasma torch shown in Fig. 4.17 (c). It is considered that the samples plasma-treated for 10 minutes at ambient temperature sintered at various degrees, and the sintering degree of the samples increased with increasing the emission intensity. As shown in Fig. 4.17 (c), almost all the copper nano-particles on the surface of the sample are sintered, forming a copper film on the surface of the sample. In fact, the metallic luster was appeared on the area plasma-treated, which is considered as the bulk copper characteristic. However, copper nano-particles on the samples shown in Fig.4.17 (b) sintered at a low degree compared with the sample shown in Fig. 4.17 (c). As for the Fig. 4.17 (a), it is not considered to be sintered. It is indicated that the emission intensity from active species in plasma jet played an important role in sintering the copper nano-particles, but not the temperature of plasma jet, in this experiment.

Fig. 4.18 shows the SEM images of the sample plasma-treated for 5 minutes at ambient temperature under the same experimental conditions at that in Fig. 4.15 and Fig.4.16. All of the sample did not sinter, indicating that as for the emission intensity shown in Fig. 4.15 (green line),

10 minutes as the treatment time is necessary for sintering copper nano-particles by Ar/H_2 plasma jet at ambient temperature.

4.4 Conclusions

In this chapter, a beam plasma torch with air-cooling system was developed. By comparing with the case without air-cooling, the characteristics of plasma jet generated by beam plasma torch with air-cooling were investigated, and applied in reduction and sintering of copper nano-particles.

On one hand, with air-cooling on the electrode, both the discharge voltage and RF current were enhanced. The addition of H_2 to Ar plasma, the discharge regime was improved. On the other hand, adding H_2 to Ar plasma generated by the beam plasma torch with air-cooling, the emission intensity from the active species was greatly increased. The emission intensity from the excited Ar atoms increased and slightly decreased with additional increasing the H_2 flow rate, while the emission intensity from Hα increased. Increasing RF power results in an increasing the emission intensity from plasma jet and slight decrease. H_2 flow rate of 15 mL/min and RF power of 60 W was selected as powerful experimental condition to treat copper nano-particles.

With air-cooling of electrode, the temperature of plasma jet was decreased at 60 W, while the changes on the temperate of plasma jet as low RF power of 30 W was not obvious.

It could result in reduction of the oxidized copper nano-particles even under a weak experimental condition within 1 minute, and sintering the copper nano-particles at ambient temperature. As for the mechanism of sintering of copper nano-particles by Ar/H_2 plasma, the emission intensity is assumed to play an important role as well as the treatment time.

References

[1] Y. H. Choi, J. H. Kim, K. H. Paek, W. T. Ju, Y. S. Hwang: *Surf. Coat. Technol.*, **93**, 319 (2005)

[2] S. Youn Moon, J. K. Rhee, D. B. Kim, W. Choe: *Phys. Plasmas*, **13**, 033502 (2006)

[3] X. Yang, M. Moravej, G. R. Nowling, S. E. Babayan, J. Panelon, J. P. Chang, R. F. Hicks: *Plasma Sources Sci. Technol.*, **14**, 314 (2005)

[4] J. Laimer, S. Haslinger, W. Meissl, J. Hell, H. Stŏri: *Vacuum*, **79**, 209 (2005)

[5] J. Laimer, H. Reicher, Qurat-ul-Ain: *28th ICPIG*, Prague, Czech Republic 10 (2007)

[6] J. Park, I. Henins, H. W. Herrmann, G.S. Selwyn: *J. Appl. Phys.*, **89**, 20 (2001)

[7] Q. S. Yu, H, K, Yasuda: *Plasma Chem. Plasma P.*, **18**, 461 (1998)

[8] B. K. Pawlak, P. Jamroz: *Plasma Chem. Plasma P.*, **30**, 641 (2010)

[9] T. Ghodselahi, M.A. Vesaghi, A. Shafiekhani, A. Baghizadeh, M. Lameii. : *Appl. Sur. Sci.*, **255**, 2730 (2008)

[10] K. TakedaP, H. InuiP, H. KondoP, K. Ishikawa, M. Sekine, M. Hori: *30th ICPIG*, Belfast, Northern Ireland, UK 2011.

[11] J. Laimer, H. Störi: *Plasma Process. Polym.*, **4**, 266 (2007)

[12] I. Stefanović, C. Scharwitz, E. Kovačević, J. Berndt and J. Winter: *New Journal of Physics*, **5**, 391 (2003)

[13] J. Laimer, H. Störi: *Plasma Process. Polym.*, **3**, 573 (2007)

[14] J. J. Shi, M. G. Kong: *IEEE. Trans. Plasma Sci.*, **33**, 624 (2005)

[15] A. Schütze, J. Y. Jeong, S. E. Babayan, J. Park, G. S. Selwyn, R. F. Hicks: *IEEE Trans. Plasma Sci.*, **26**, 1685 (1998)

[16] X. Fei: *Characterization, Comparison and Application of Two Types of Atmospheric Pressure Cold Argon Plasma Jets*, Doctoral Thesis, Kiryu: Gunma University, 2011.

Table 4.1 Most emission lines observed in Ar/H_2 plasma generated by beam plasma torch at the position of 3 mm down from the plasma torch head and 2 mm side from plasma jet end. The integration time was 20 ns [7, 8].

Species	Wavelength (nm)	Transition	Threshold energy (eV)
H	656.3	3d-2p	12.09
Ar	696.5	4p-4s	13.32
	706.7		13.29
	714.7		13.28
	728		13.33
	738.4		13.3
	751.4		13.27
	763.5		13.17
	772.4		13.33
	794.8		13.28
	801.5		13.15
	811.5		13.08

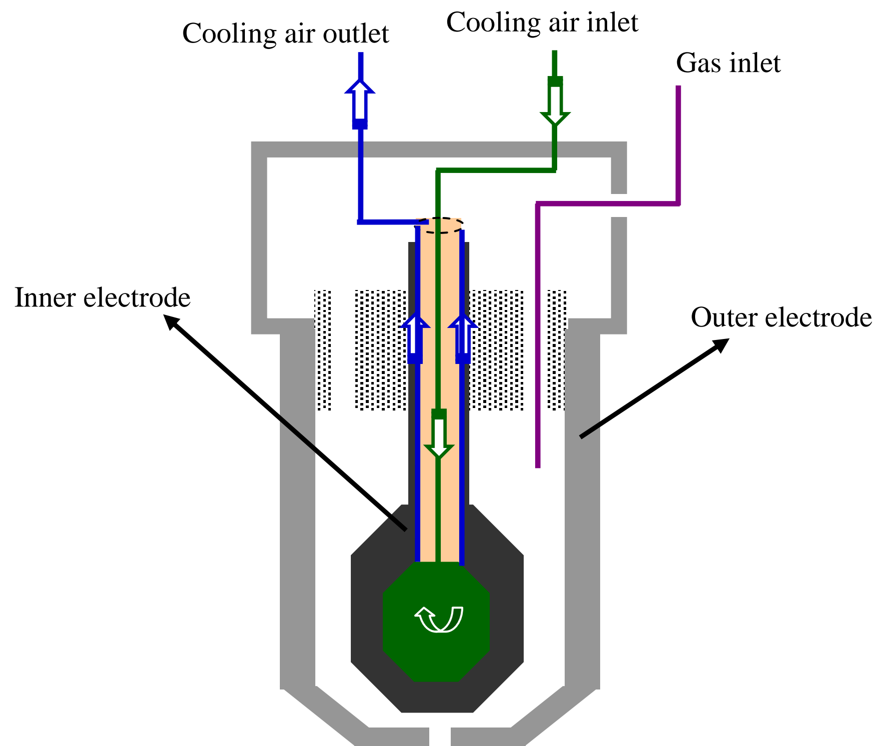

Fig. 4.1 Schematic diagram of the beam plasma torch with air-cooling system on inner electrode used in the experiment.

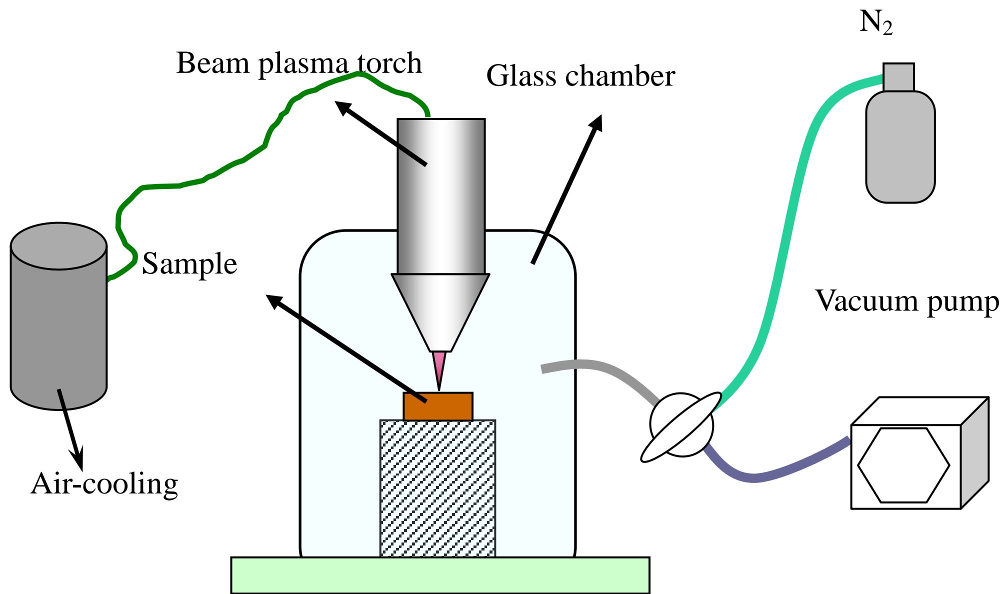

Fig. 4.2 Schematic diagram of experimental setup used in this experiment to treat sample.

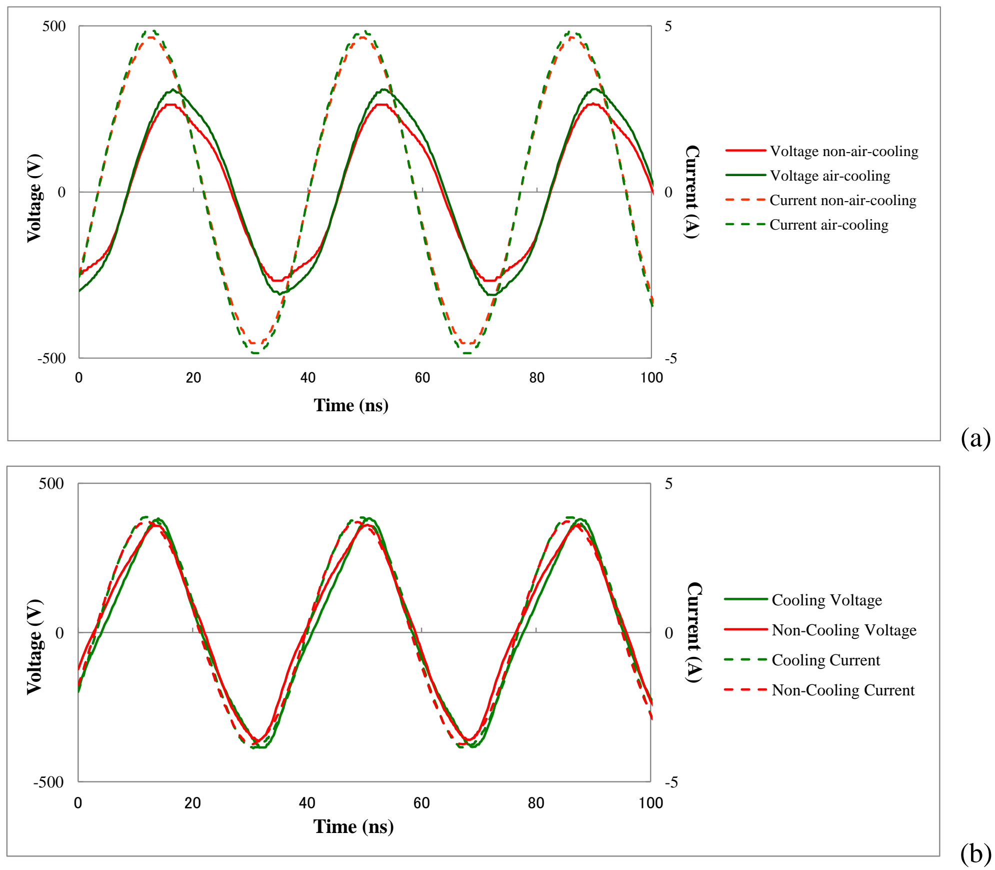

Fig. 4.3 Effect of air-cooling of electrode for beam plasma torch on the discharge voltage and RF current of pure Ar plasma with Ar flow rate maintained at 25 L/min. RF power was 30 W (a), RF power was 60 W (b).

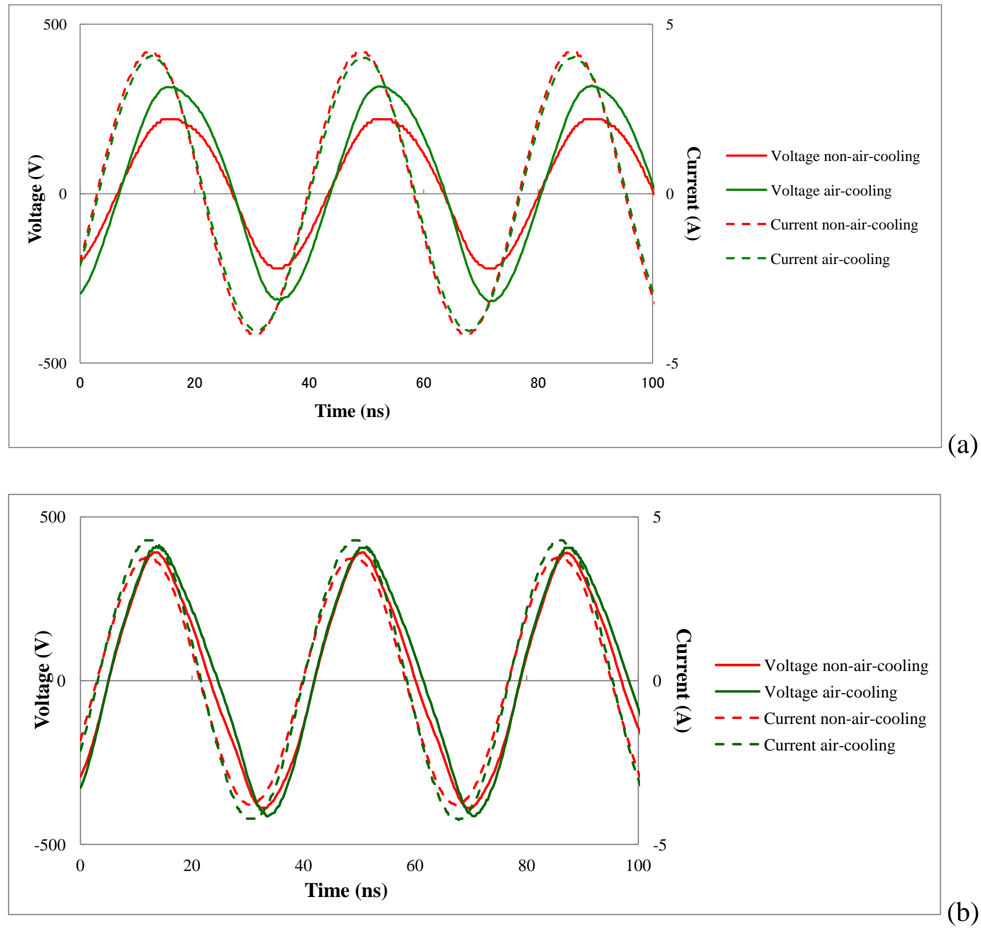

Fig. 4.4 Effect of electrode air-cooling for the beam plasma torch on the discharge voltage and RF current of Ar/H_2 plasma with Ar flow rate maintained at 25 L/min and H_2 flow rate maintained at 30 mL/min. RF power was 30 W (a), RF power was 60 W (b).

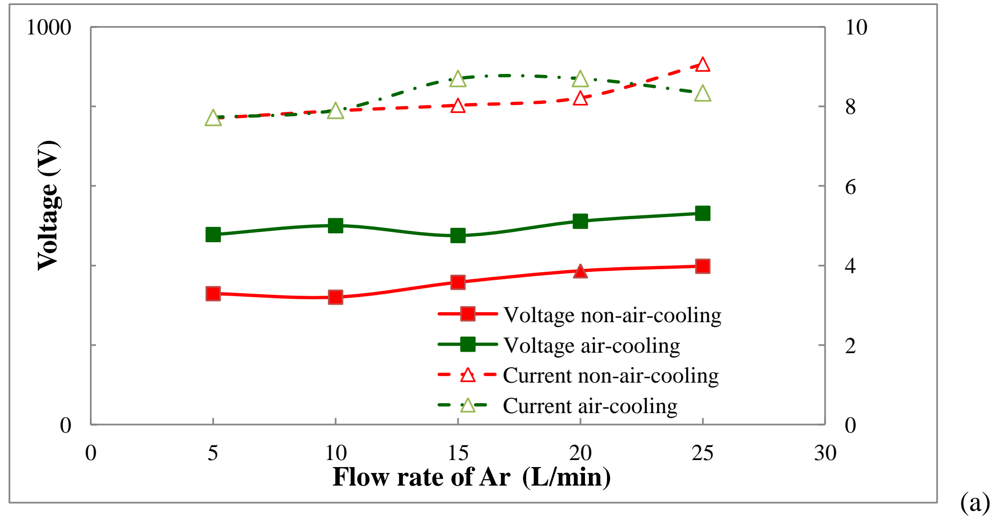

(a)

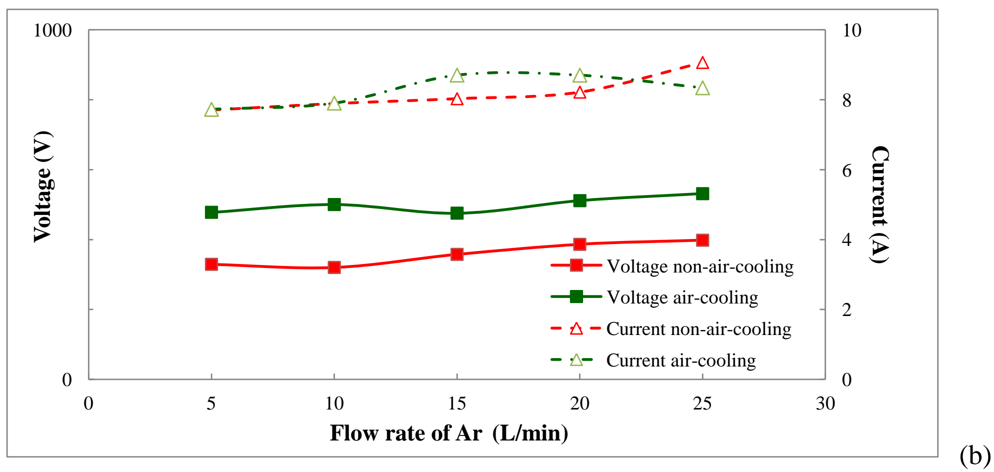

(b)

Fig.4.5 Effect of electrode air cooling for the beam plasma torch on the discharge voltage and RF current of pure Ar plasma with increasing the Ar flow rate at 25 L/min. RF power is 30W (a), RF power is 60 W (b).

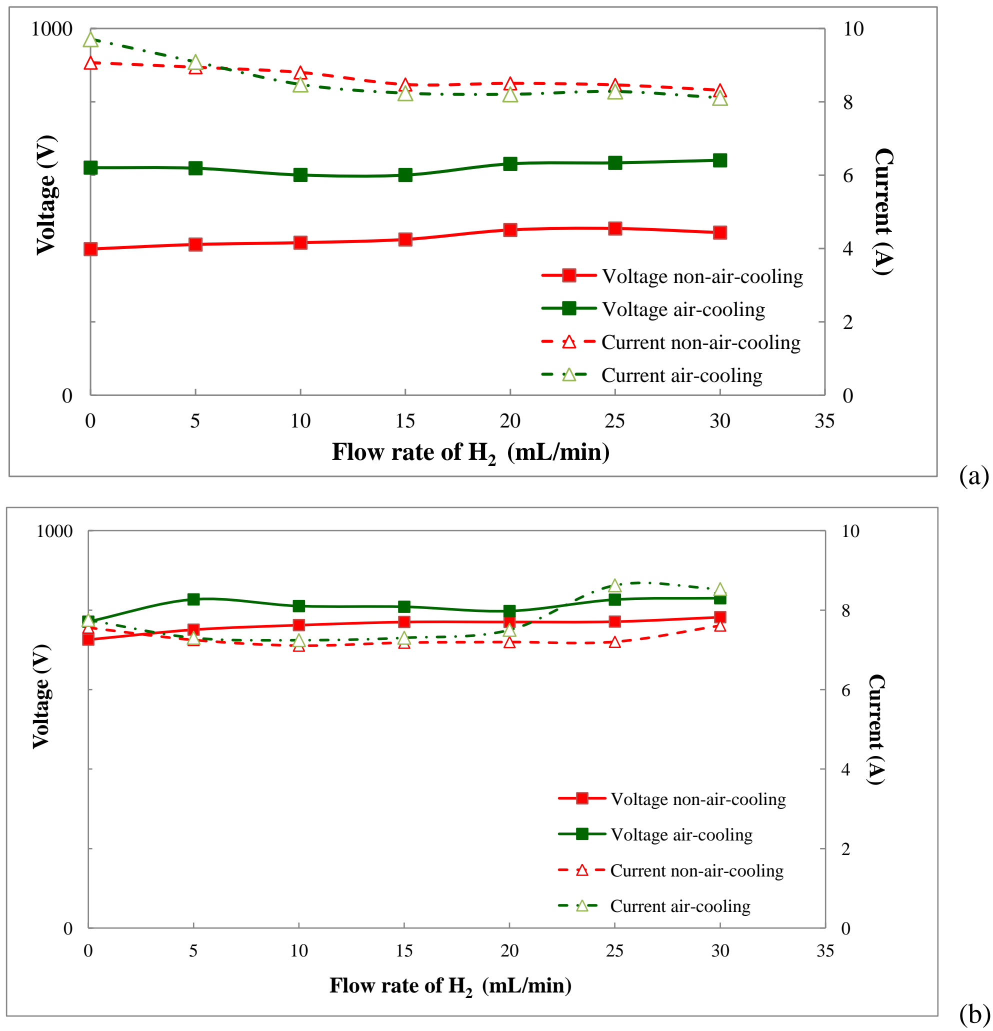

Fig, 4.6 Effect of electrode air cooling for the beam plasma torch on the discharge voltage and RF current of Ar/H_2 plasma with increasing the H_2 flow rate at the constant Ar flow rate of 25 L/min. RF power is 30 W (a), RF power is 60 W (b).

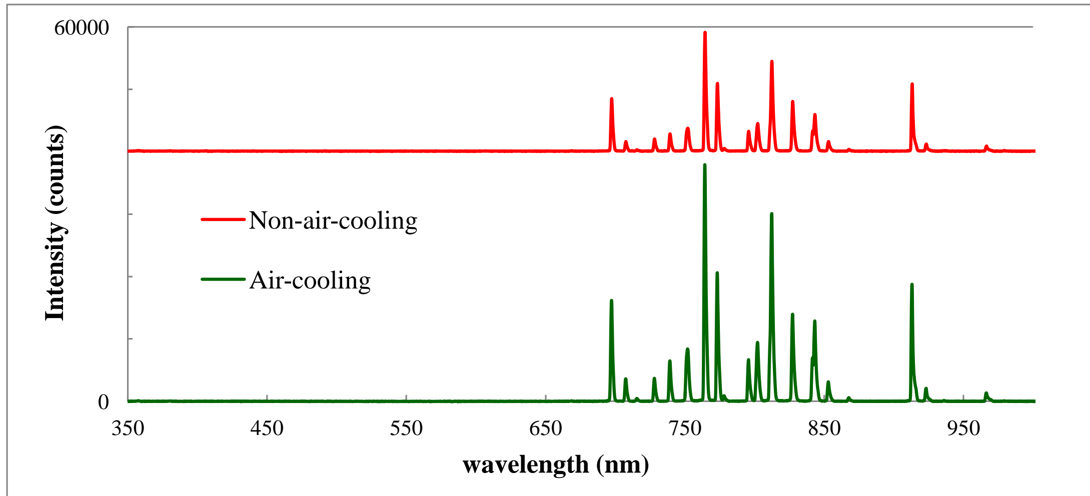

Fig.4.7 Comparison of optical emission spectra of pure Ar plasma generated by the beam plasma torch with air-cooling (green line) and without air-cooling (red line) at RF power of 30 W and with the constant Ar flow rate of 25 L/min at the position of 3 mm down from the plasma torch head and 2 mm side from plasma jet end. The integration time was 20 ns.

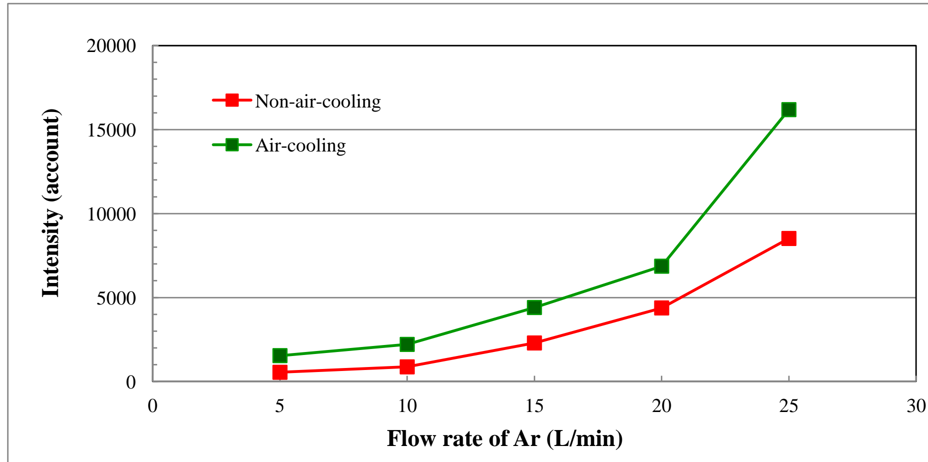

Fig. 4.8 Comparison of the emission intensity from excited Ar atoms at 696.5 nm in pure Ar plasma generated by the beam plasma torch with air-cooling (green line) and without air-cooling (red line) with increasing the Ar flow rate from 5 L/min to 25 L/min at RF power of 30 W at the position of 3 mm down from the plasma torch head and 2 mm side from the plasma jet end. The integration time was 20 ns.

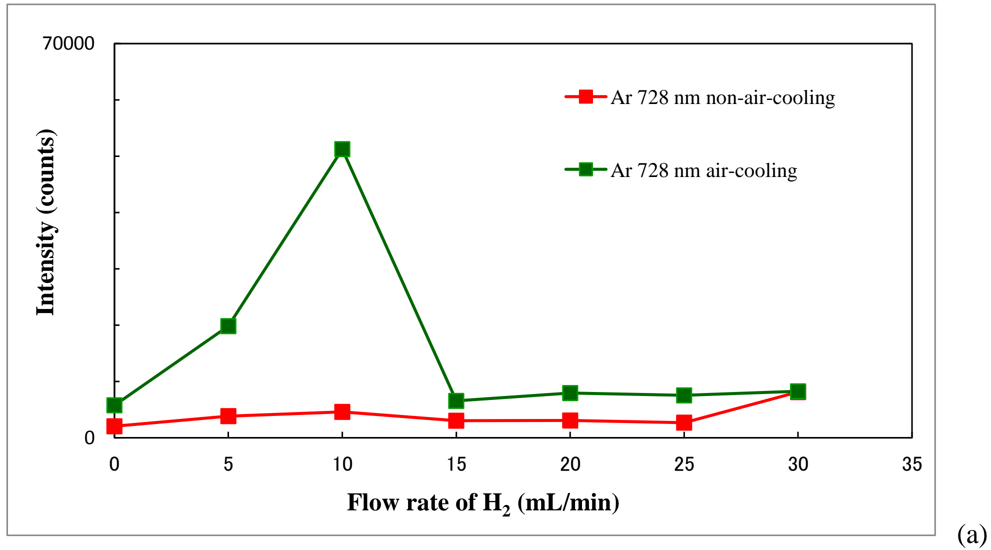

(a)

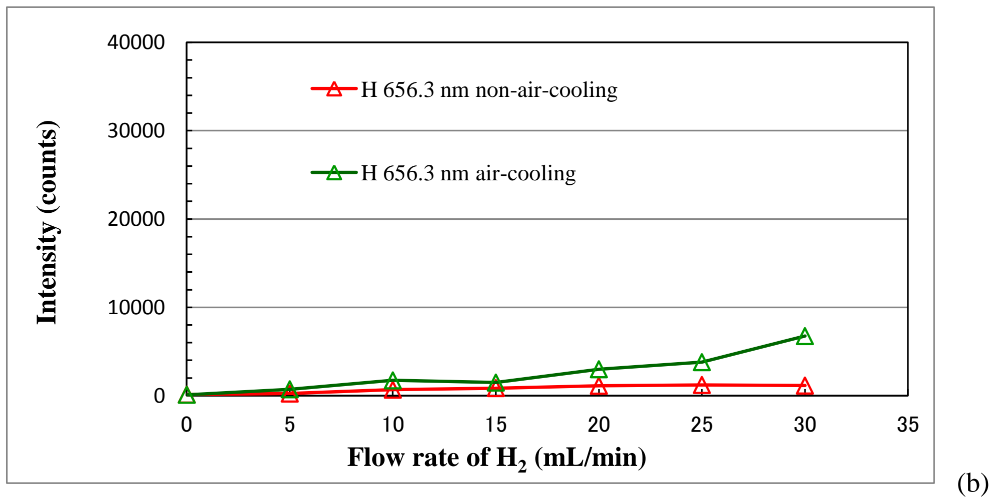

(b)

Fig. 4.9 Comparison of the emission intensity from the excited Ar atoms at 728 nm (a) and H atoms at 656.3 nm (b) in Ar/H_2 plasma generated by the beam plasma torch with air-cooling (green line) and without air-cooling (red line) with increasing the H_2 flow rate from 0 mL/min to 30 mL/min and the constant Ar flow rate of 25 L/min at RF power of 30 W. The optical emission spectra were collected at the position of 3 mm down from the plasma torch head and 2 mm side from theplasma jet end. The integration time was 20 ns.

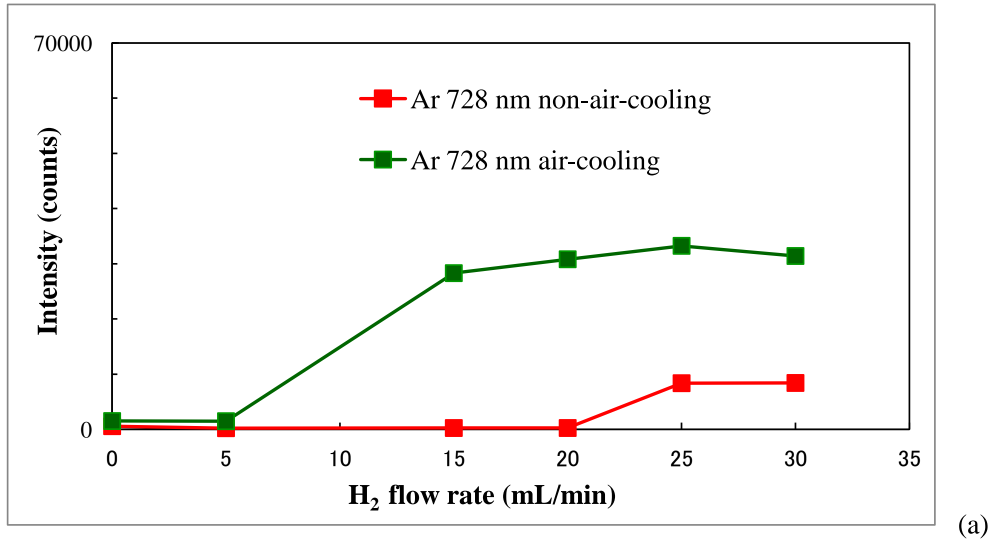

(a)

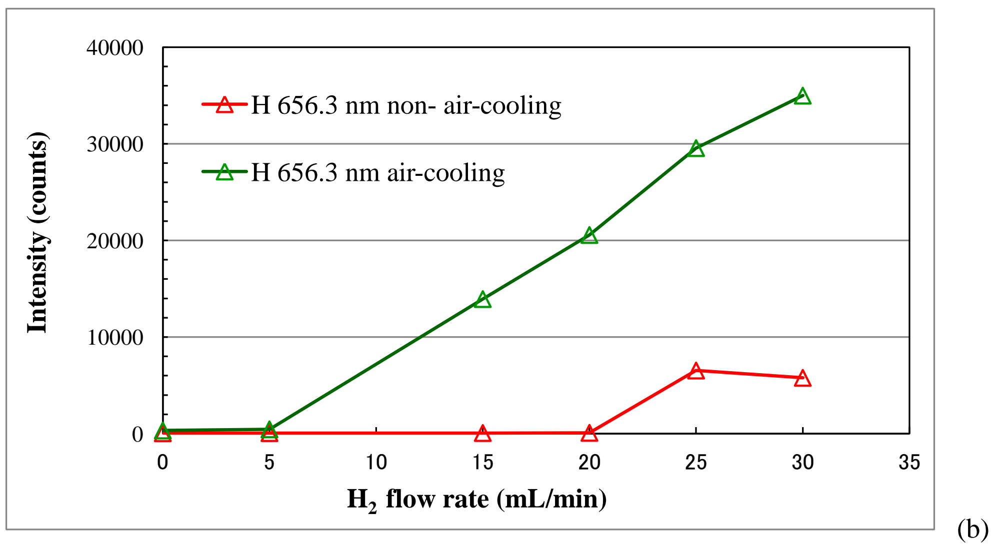

(b)

fig. 4.10 Comparison of the emission intensity from the excited Ar atoms at 728 nm (a) and H atoms at 656.3 nm (b) in Ar/H_2 plasma generated by the beam plasma torch with air-cooling (green line) and without air-cooling (red line) with increasing the H_2 flow rate from 0 mL/min to 30 mL/min and the constant Ar flow rate of 25 L/min at RF power of 60 W at the position of 3 mm down from the plasma torch head and 2 mm side from the plasma jet end. The integration time was 20 ns.

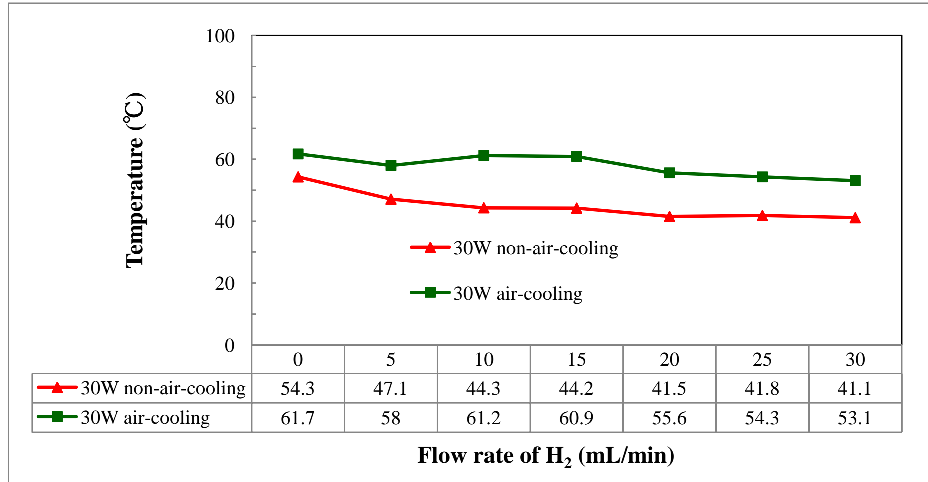

	0	5	10	15	20	25	30
30W non-air-cooling	54.3	47.1	44.3	44.2	41.5	41.8	41.1
30W air-cooling	61.7	58	61.2	60.9	55.6	54.3	53.1

(a)

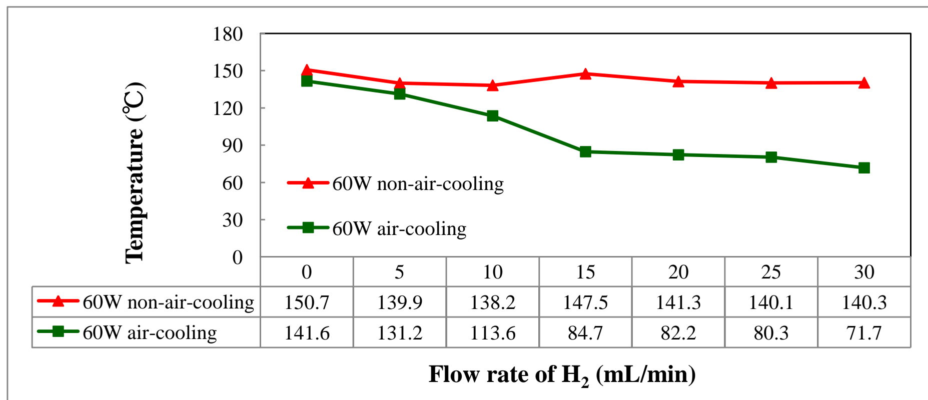

	0	5	10	15	20	25	30
60W non-air-cooling	150.7	139.9	138.2	147.5	141.3	140.1	140.3
60W air-cooling	141.6	131.2	113.6	84.7	82.2	80.3	71.7

(b)

Fig. 4.11 Effect of H_2 flow rate on the temperate of plasma jet at a position of 3 mm down from the plasma torch head. The Ar flow rate was 25 L/min. RF power is 30 W (a), RF power is 60 W (b).

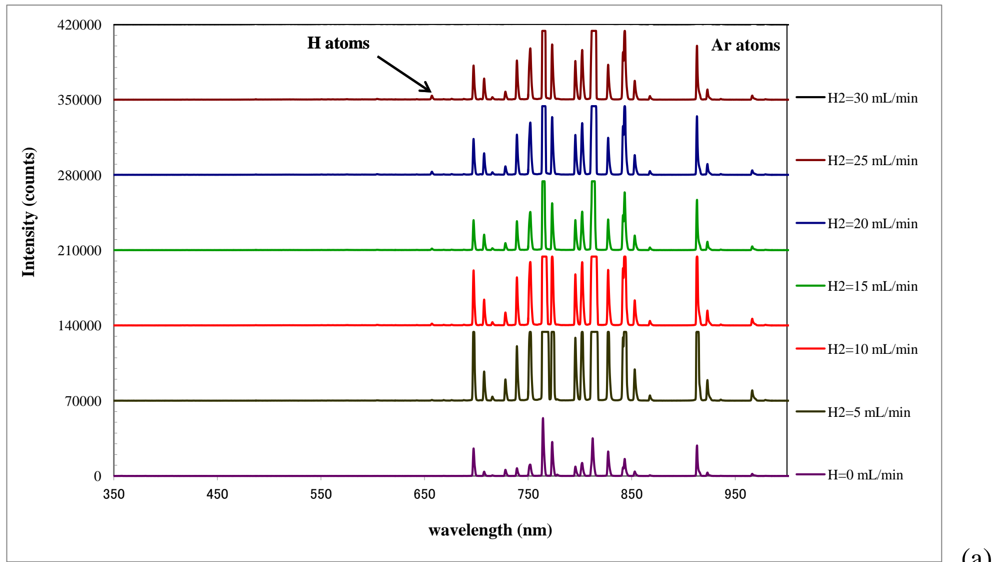

(a)

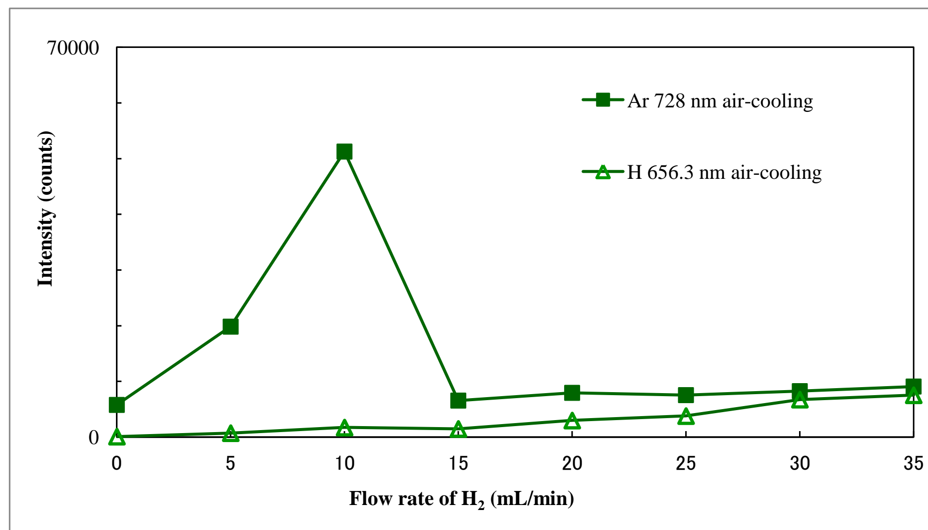

(b)

Fig. 4.12 Comparison of optical emission spectra of Ar/H_2 plasma jet generated by the beam plasma torch with air-cooling with the constant Ar flow rate of 25 L/min and increasing H_2 flow rate from 0 mL/min to 30 mL/min at RF power of 30 W (a); Comparison of the emission intensity from the excited Ar atoms at 728 nm and the excited H atoms at 656.3 nm in the optical emission spectra shown in (a) (b). The optical emission spectra were collected at the position of 3 mm down from the plasma torch head and 2 mm side from the plasma jet end, the integration time was 20 ns.

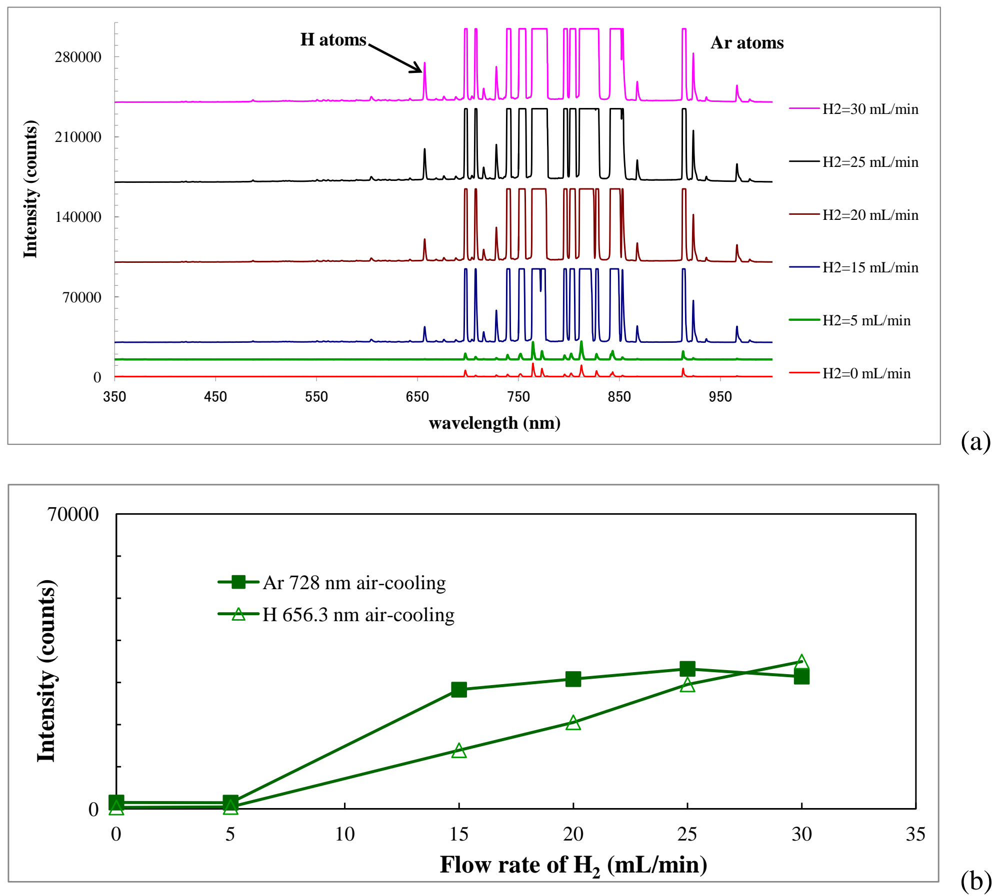

Fig. 4.13 Comparison of optical emission spectra of Ar/H_2 plasma jet generated by the beam plasma torch at air-cooling with the constant Ar flow rate of 25 L/min and increasing H_2 flow rate from 0 mL/min to 30 mL/min at RF power of 60 W (a); Comparison of the emission intensity from the excited Ar atoms at 728 nm and the excited H atoms at 656.3 nm in the optical emission spectra shown in (a) (b). The optical emission spectra were collected at the position of 3 mm down from the plasma torch head and 2 mm side from the plasma jet end, the integration time was 20 ns.

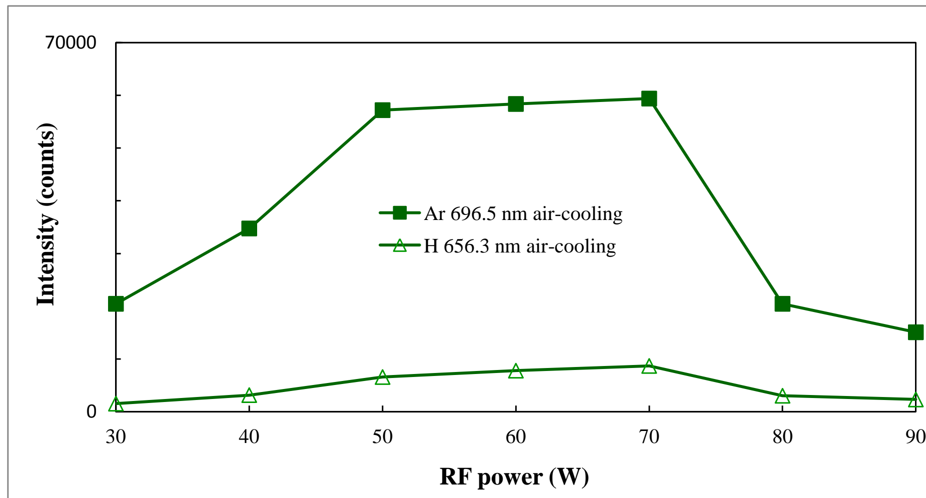

Fig. 4.14 Comparison of the emission intensity from the excited Ar atoms at 696.5 nm and H atoms at 656.3 nm in Ar/H_2 plasma generated by the beam plasma torch with air-cooling with increasing RF power from 30 W to 90 W at the constant Ar flow rate of 25 L/min and H_2 flow rate of 15 mL/min. The optical emission spectra were collected at the position of 3 mm down from the plasma torch head and 2 mm side from the plasma jet end. The integration time was 20 ns

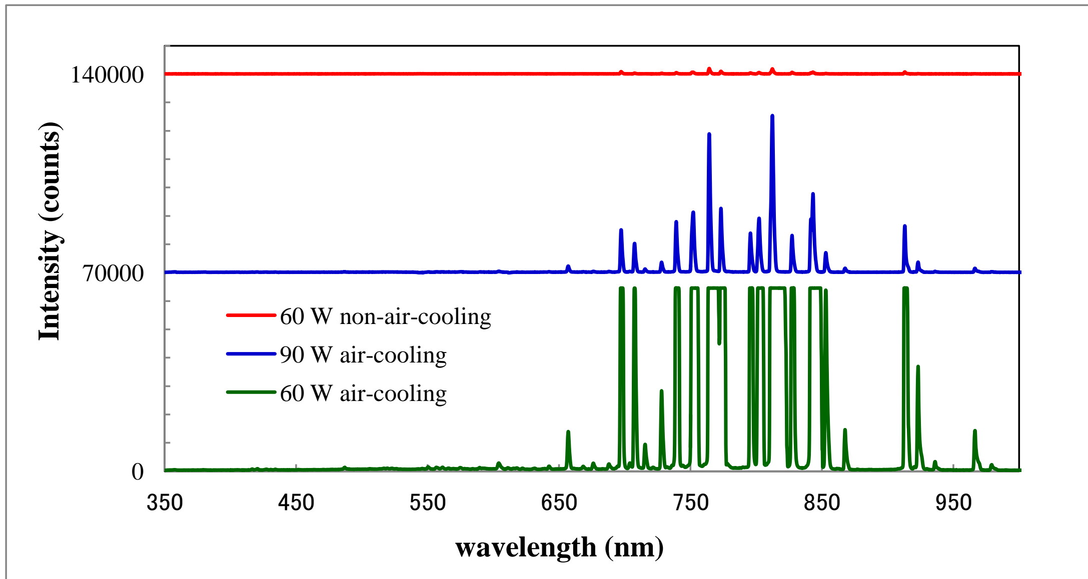

Fig. 4.15 Comparison of optical emission spectra of Ar/H_2 plasma generated by the beam plasma torch without air-cooling at the RF power of 60 W (red line), by the beam plasma torch with air-cooling at RF power of 90 W (blue line) and 60 W (green line) at the Ar flow rate of 25 L/min and H_2 flow rate of 15 mL/min. The optical emission spectra were collected at the position of 3 mm down from the plasma torch head and 2 mm side from the plasma jet end. The integration time was 20 nm.

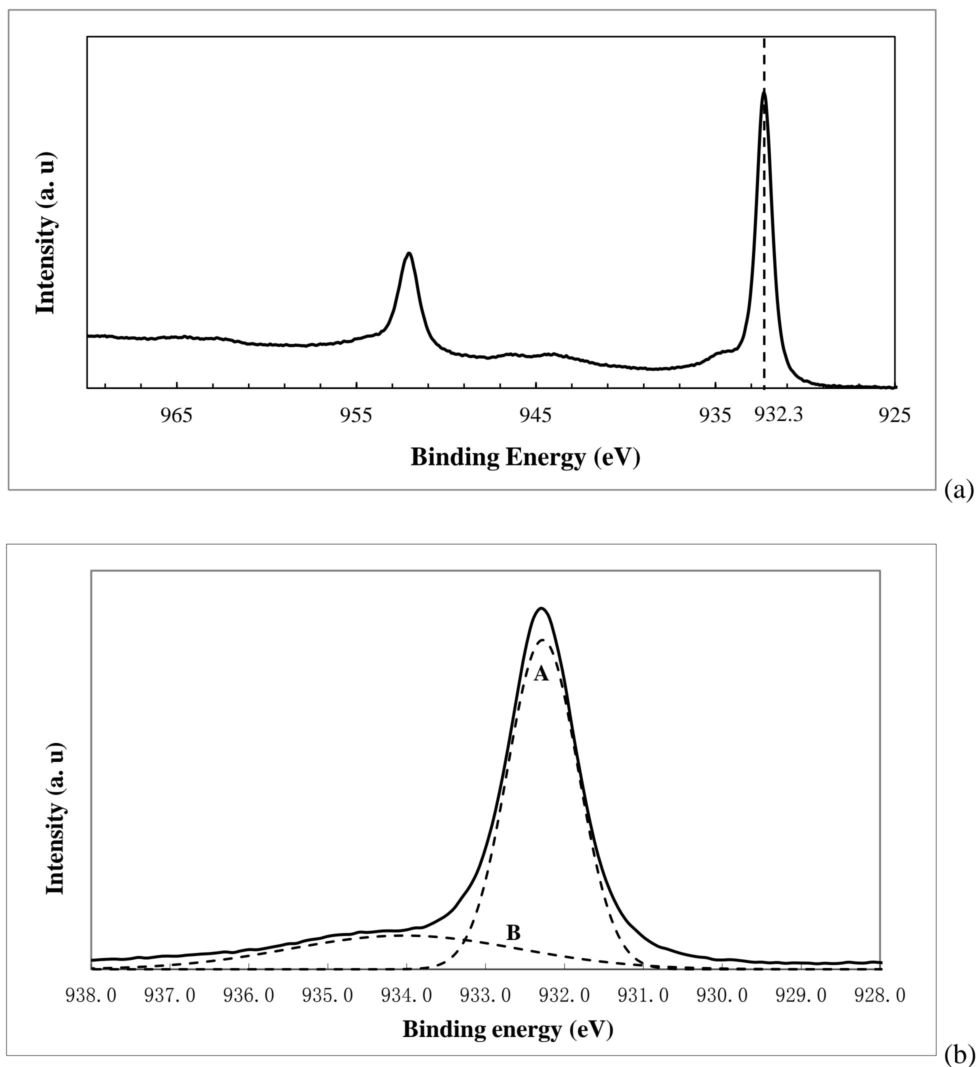

Fig. 4.16 Main and satellite peaks of Cu $2p_{3/2}$ and Cu $2p_{1/2/}$ of the XPS spectra for the sample plasma-treated by the beam plasma torch with air-cooling for 1 minute at RF power of 30 W with the Ar flow rate of 25 L/min and H_2 flow rate of 15 mL/min at the distance of 3 mm down from the plasma torch head (a) the typical deconvolution of Cu $2p_{3/2}$ main peak (b)

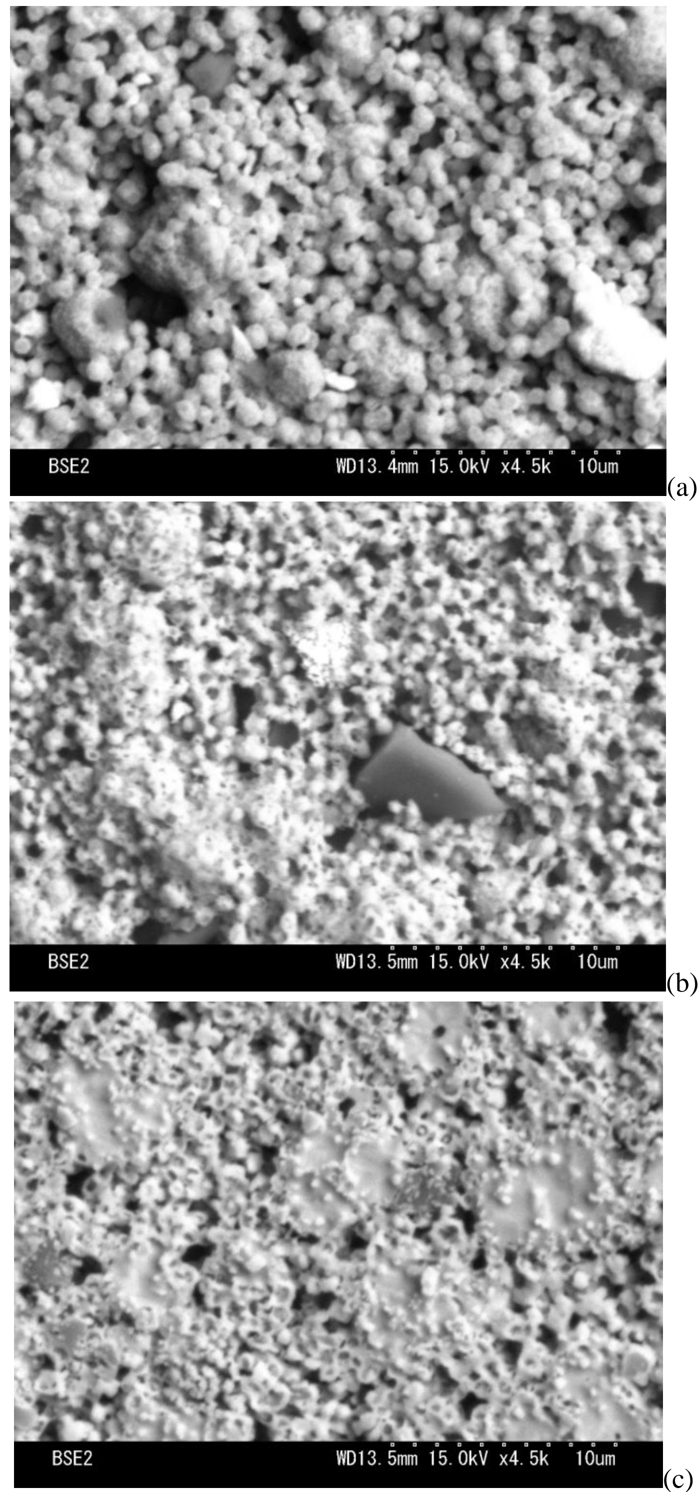

Fig. 4.17 SEM images showing the surface morphologies of the copper nano-particles on the samples treated at ambient temperature for 10 minutes at the constant Ar flow rate of 25 L/min and H_2 flow rate of 15 mL/min. RF power was set at 60 W by the beam plasma torch without air-cooling (a); RF power was set at 90 W by the beam plasma torch with air-cooling (b); RF power was set at 60 W by the beam plasma torch with air-cooling

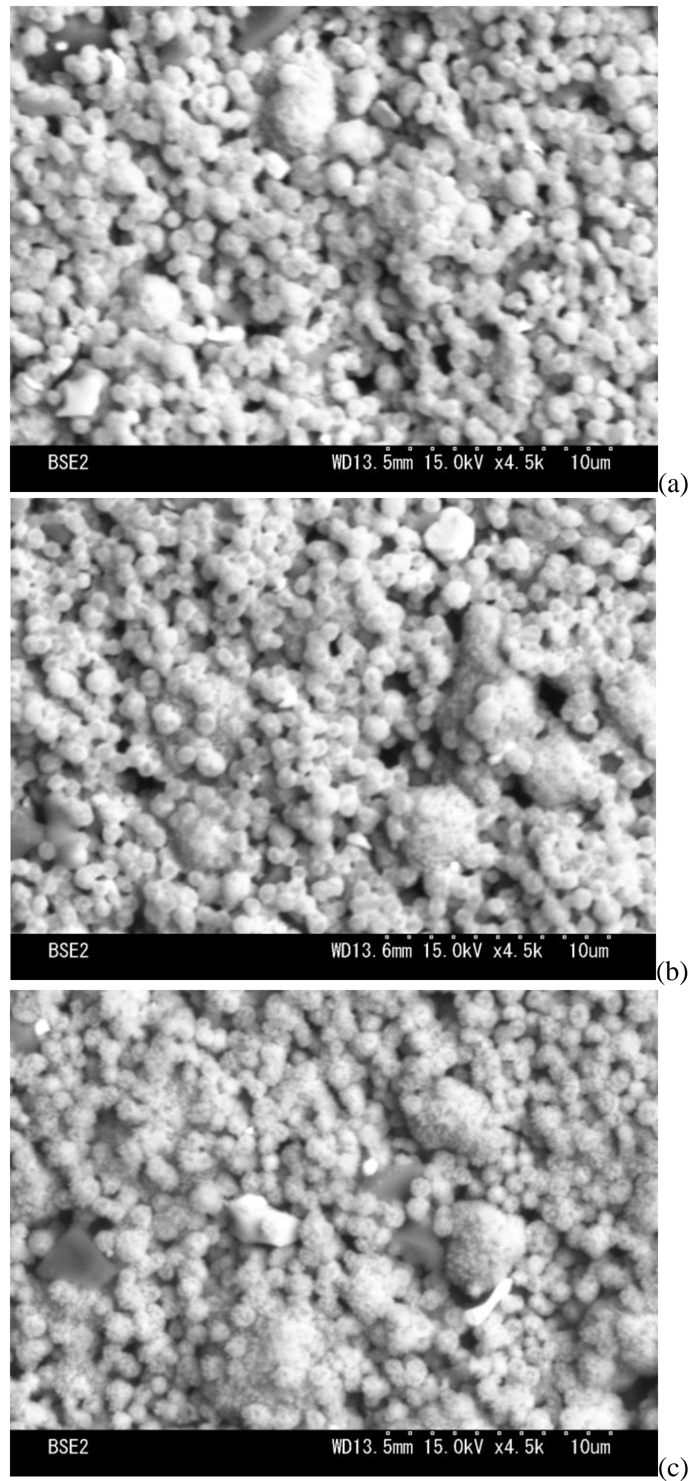

Fig. 4.18 SEM images showing the surface morphologies of the copper nano-particles on the samples treated at ambient temperature for 5 minutes at the constant Ar flow rate of 25 L/min and H_2 flow rate of 15 mL/min. RF power was set at 60 W by the beam plasma torch without air-cooling (a); RF power was set at 90 W by the beam plasma torch with air-cooling (b); RF power was set at 60 W by the beam plasma torch with air-cooling (c)

Chapter 5 Important factors affecting the reduction and sintering of copper nano-particles through plasma-treatment

5.1 Introduction

In Chapter 2 - Chapter 4, the copper nano-particles with the diameter of 700-900 nm, the melting point of which was considered to be close to that of bulk copper (1083 ℃), were reduced and sintered by non-equilibrium atmospheric pressure plasma with the APC plasma torch, common beam plasma torch and modified beam plasma torch with air-cooling system of electrode, respectively. Because the temperature of the three plasma jet used in this study was not higher than 200 ℃, it is considered that the sintering of copper nano-particles did not result from the thermal motion lead by high temperature.

In this chapter, the objective is to investigate the important factors affecting the reduction and sintering of the copper nano-particles.

The treatment distance and time, the emission intensity from plasma jet, which is one of the most important parameters characterizing the energy of plasma jet, and the concentration of H_2 as an additive gas, deeply affected the emission intensity from plasma jet, will be discussed in detail.

In order to investigate the role of H_2 in Ar/H_2 plasma in reduction and sintering copper nano-particles, the emission intensity ratio from the excited H atoms at 656.3 nm (Hα) and the excited Ar atoms at 696.5 nm in Hα/Ar plasma generated by the electrode-air-cooling beam plasma torch is shown in Fig. 5.1. The main emission lines observed in Ar/H_2 plasma generated by

beam plasma torch with air-cooling and without air-cooling are shown in Table 4.1 in Chapter 4, the position of the spectra collected at 3 mm down from the plasma torch head and 2 mm side from plasma jet end. The integration time was 20 ns. With maintaining the Ar flow rate at 25 L/min, increasing RF power and changing the H_2 flow rate, both the emission intensity from excited Ar atoms and excited H atoms were changed. Samples were plasma-treated under the conditions as various the emission intensity ratio of Hα/Ar. According comparison of the sintering result, the role of H_2 in Ar/H_2 plasma will be investigated.

In this chapter, all of the samples were treated in the experimental setup shown in Fig. 4.2 in Chapter 4, which is in an inert atmosphere in a sealed glass chamber. While the optical emission spectra were collected in atmosphere with USB 4000. The schematic diagram of the experimental setup is shown in Fig. 2.6 in Chapter 2. The optical emission spectra were collected at the position of 3 mm down from the plasma torch head and 2 mm side from the plasma jet end. The integration time was 20 ns.

5.2 The effect of treatment distance down from the plasma torch on the sintering of copper nano-particles

Under the experimental condition of the distance of 3 mm down from the plasma torch head and the Ar flow rate of 25 L/min, the H_2 flow rate of 15 mL/min at RF power of 60 W, it was required 10 minutes for sintering copper nano-particles by the plasma-treatment with the air-cooling beam plasma torch, while the sample treated at RF power of 90 W has relatively lower sintering degree, the optical emission spectra of the two plasma jet are shown in Fig. 4.15, in Chapter 4. In order to investigate the effect of treatment distance on the sintering of copper nano-particles, two samples

were treated by beam plasma torch with air-cooling under the same conditions but for 7 minutes at a distance of 1.5 mm down from the plasma torch head. The Ar flow rate was 25 L/min and H_2 flow rate was 15 mL/min. The SEM images are shown in Fig. 5.2. Fig. 5.2 (a) shows the surface morphology of the sample plasma-treated for 7 minutes at RF power of 90 W. Copper nano-particles adhered with each other and show the early sintering state. Fig. 5.2 (b) shows the sample plasma-treated for 7 minutes at RF power of 60 W and the copper nano-particles have completely sintered and formed copper film, exhibiting the bulk copper property. With a shorter distance of 1.5 mm, the copper nano-particles could be sintered within shorter treatment time of 7 minutes.

It is indicated that with reducing the treatment distance, the more powerful emission intensity from Ar/H_2 plasma jet could result in a better ability for sintering the copper nano-particles. It is believed that the emission intensity from plasma jet would be more powerful at the close position from the torch head, because the decay of the active species in plasma jet is very quick. Additionally, as shown in Fig. 5.1, the emission intensity ratio Hα/Ar at RF power of 90 W is higher than that at 60 W when the Ar flow rate was 25 L/min and H_2 flow rate was 15 mL/min, and the temperature of the Ar/H_2 plasma jet generated by the beam plasma torch at 90 W is also higher than that at 60 W. However, the powerful emission intensity from plasma is considered to deeply affect the sintering of copper nano-particles rather than the concentrate of H_2 and the temperature of plasma jet.

5.3 The decisive gas emission intensity for sintering of copper nano-particles

As shown in Fig. 5.3 (a), the emission intensity from Ar/H_2 plasma at Ar flow rate of 25 L/min and H_2 flow rate of 20 mL/min with RF power set at 60 W generated by the beam plasma torch without air-cooling (red line) was compared with that from Ar/H_2 plasma at Ar flow rate of 25 L/min and H_2 flow rated of 15 MLPM with RF power set at 50 W generated by the beam plasma torch with air-cooling (green line). The emission intensity from the Hα at 656.3 nm is almost the same to each other as shown in Fig. 5.2 (b), while the intensity from the excited Ar atoms at 696.5 nm of the former (red bar) is lower than that of the latter (green bar). Two samples were plasma-treated by the both kinds of plasma jet for 10 minutes under the same conditions at the distance of 1.5 mm down from plasma torch head. The SEM images of the samples treated are shown in Fig. 5.4. Fig. 5.4 (a) shows the sample treated by the non-air-cooling beam plasma torch with RF power set at 60 W, and Ar flow rate of 25 L/min and H_2 flow rate of 20 mL/min, its OES shown in Fig. 5.3 (b) as red bar. The copper nano-particles have been stick to each other, exhibiting the early state of sintering. As for the sample plasma-treated by the air-cooling beam plasma torch at RF power set at 50 W, and Ar flow rate of 25 L/min and H_2 flow rate of 15 mL/min, its OES shown in Fig. 5.3 (b) as green bar, the copper nano-particles on the surface of the sample have completely sintered and formed copper film, indicating that the higher emission intensity from excited Ar atoms would result in a better sintering degree in the case of the same H atoms emission intensity. Therefore, Ar is considered as a decisive gas in sintering copper nano-particles.

5.4 Relationship between treatment time and the emission intensity from the Ar/H_2 plasma generated by the beam plasma torch with air-cooling

Fig.5.5(a) shows the Ar/H_2 plasma generated by the beam plasma torch with air-cooling at the Ar flow rate of 25 L/min and H_2 flow rate of 15 mL/min at RF power of 30 W (blue line) and 60 W (green line), respectively. As shown in Fig. 5.5 (b), the emission intensity from the excited Ar atoms at 696.5 nm in the plasma as the RF power of 30 W is about one third of that in the plasma at RF power of 60 W, and the emission intensity from the Hα at 656.3 nm in the plasma as the RF power of 30 W is much weaker than that in the plasma at the RF power of 60 W. Two samples plasma-treated at the distance of 1.5 mm down the from plasma torch head at RF power of 30 W for 10 minutes and 20 minutes, respectively, were used to compare with the one plasma-treated at the distance of 1.5 mm down form plasma torch head at RF power of 60 W for 7 minutes, as discussed in section 5.2.

The SEM image of the sample plasma-treated for 10 minutes at RF power of 30 W and its photograph is shown in Fig. 5.6 (a) and Fig. 5.6 (b), respectively. The copper nano-particles adhered with each other and exhibit the early state of sintering and from the photograph, the metallic luster did not appeared, indicating that the treatment time of 10 minutes was not enough for the sintering of copper nano-particles by beam plasma torch with air-cooling at RF power of 30 W. Fig. 5.6 (c) and Fig. 5.6 (d) show the SEM image of the sample plasma-treated for 20 minutes at ambient temperature at the distance of 1.5 mm down from the plasma torch head at RF power of 30 W and its photograph, respectively. As shown in Fig. 5.6 (c), the copper nano-particles have completely sintered to copper film, showing the property of bulk copper. In Fig. 5.6(d), the

metallic luster appeared on the area plasma-treated. The SEM image of the sample treated at a disposition of 1.5 mm down from the plasma torch head at RF power of 60 W and its photograph as discussed in section 5.2 is shown in Fig. 5.6 (e) and Fig. 5.6 (f). The copper nano-particles are sintered and the metallic luster appeared. It indicates that in order to sintering the copper nano-particles by non-equilibrium atmospheric pressure plasma as the power of 30 W of which emission intensity is shown in Fig. 5.5 (a) (blue line) at ambient temperature, 20 minutes was required as the treatment time is required. The treatment time for sintering copper nano-particles as the RF power of 30 W is almost three times of that as the RF power of 60 W, while the emission intensity of the former is about one-third of the latter.

It indicates that both the emission intensity from plasma and treatment time are necessary for sintering the copper nano-particles. In addition, as shown in Fig. 5.1, the emission intensity ratio Hα/Ar at RF power of 30 W is lower than that at 60 W, It is assumed that the smaller emission intensity ratio would be hinder the sintering of copper nano-particles.

5.5 The effect of H_2 flow rate on the sintering of copper nano-particles through plasma-treatment by beam plasma torch with air-cooling

In order to investigate the role of H_2 playing in reduction and sintering of copper nano-particles, a sample was plasma-treated for 20 minutes at a position of 1.5 mm down from plasma torch head by the beam plasma torch with air-cooling at RF power of 30 W and the flow rate of Ar was 25 L/min without H_2 to compare with the one treated under almost the same experimental condition just with addition of H_2 at 15 mL/min mentioned in section 5.4. The emission from Hα at 656.3

nm could not be observed. The optical emission spectra are shown in Fig. 5.7 (a) (blue line). The optical emission spectra of the Ar/H_2 plasma generated by the beam plasma torch with air-cooling is shown in Fig.5.7 (a) (green line), the peak of Hα at 656.3 nm was observed. Fig. 5.7 (b) shows the comparison of the emission intensity from excited Ar atoms at 696.5 nm and Hα at 656.3 nm in the pure Ar plasma and the Ar/H_2 plasma, the optical emission spectra of which are shown in Fig. 5.7 (a). The emission intensity from excited Ar atoms is almost the same, while in the pure Ar plasma, but the emission intensity from excited H atoms is negligible.

Fig. 5.8 shows the SEM image of the samples plasma-treated by pure Ar plasma and Ar/H_2 plasma, at RF power of 30 W and Ar flow rate of 25 L/min at the distance of 1.5 mm down from the plasma torch head. The copper nano-particles on the sample treated by pure Ar plasma adhered together with each other and exhibit the state of early stage of sintering. However the copper nano-particles treated by Ar/H_2 plasma completely sintered, as mentioned in 5.4.

It is suggested that addition of H_2 to Ar plasma would prove the ability for sintering of copper nano-particles of plasma jet. In reduction and sintering of copper nano-particles, H_2 is considered to play an important role in the Ar/H_2 plasma. In addition, as shown in Fig, 5.1, the emission intensity ratio of Hα/Ar with the H_2 flow rate of 0 mL/min is lower than that with the H_2 flow rate of 15 mL/min. It is also indicated that the small emission intensity ratio Hα/Ar would hider the sintering of copper nano-particles by plasma-treatment.

Based on the facts mentioned above, it is very interesting to confirm whether the greater optical emission intensity from H active species in Ar/H_2 plasma could result in a better ability of sintering copper nano-particles.

Fig. 5.9 (a) shows the optical emission spectra of the Ar/H_2 plasma generated by the beam plasma torch with air-cooling at RF power of 60 W, the Ar flow rate of 25 L/min, the H_2 flow rate of 30 mL/min (blue line) and 15 mL/min (green line), respectively. The emission intensity from excited Ar atoms at 696.5 nm under the both experimental conditions was so strong as to exceed the measure range. Relatively weak emission from Ar active atoms at 728 nm and Hα at 656.3 nm were shown Fig.5.9 (b). In the both case, the emission intensity from the excited Ar atoms in the Ar/H_2 plasma are almost the same, but the emission intensity from Hα atoms in Ar/H_2 plasma at the H_2 flow rate of 30 mL/min is higher than that in the Ar/H_2 plasma at the H_2 flow rate of 15 mL/min.

The SEM image in Fig. 5. 10 (a) shows the sample plasma-treated by Ar/H_2 at a position of 1.5 mm down from the plasma torch head for 20 minutes at RF power of 30 W and Ar flow rate was 25 L/min and H_2 flow rate was 30 mL/min. Comparing with the one plasma-treated as the H_2 flow rate of 15 mL/min shown in Fig. 5.10 (b), the copper nano-particles are considered to have been sintered. However, it is different from the sample treated at the H_2 flow rate of 15 mL/min, there is not metallic luster on the surface plasma-treated. In addition, there are many honeycomb damages on the surface of the sintered copper nano-particles, which is considered to be the reason that the metallic luster did not appear.

We assumed that the excess addition of H_2 to Ar plasma maybe result in the damages on the surface of sintered copper nano-particles. As shown in Fig. 5.1, the emission intensity ratio of Hα/Ar with the H_2 flow rate of 30 mL/min is higher than that with H_2 flow rate of 15 mL/min, indicating that an too high emission intensity ratio of Hα/Ar would be ascribe to lead surface damage.

5.6 Discussion

The temperature of the sample plasma-treated was not higher than 200 ℃ as shown in Fig. 4.11, indicating the sintering of copper nano-particles did not occur thermally.

The changes in atomic orbital of copper due to the copper transfer from the excited state of Ar should be taken into consideration [1]. In the case of the simplest molecule, H_2, the electron wave function changes from the ground state to the excited stage, as shown in Fig. 5.12. The wave function of atom A and B is ψ_A and ψ_B, respectively. With the atoms closing to each other, the wave function would be piled up as $\psi_A + \psi_B$ to form a molecule as shown in Fig. 5.12 (b). When the atoms achieve to the excited state with obtaining energy, the wave function will be piled as an unstable state $\psi_A - \psi_B$ as shown in Fig. 5.12 (c), which is in an excited state. Similarly, the metal bond would be weakened by the excitation of the metal orbital resulting in the atomic diffusion even at ambient temperature.

As for the copper oxide, it would weaken the metal bounding and make it easier to move for the metal atoms, it was observed that there are about three types of structure in the CuO_x species [2]; as (1) the oxides, CuO, OCuO, $OCuO_2$; (2) Cu/O_2 complexes, $Cu(O_2)$, Cu $(O_2)_2$, $Cu(O_2)_3$; and (3) O_2-solvated oxides, $(OCuO)(O_2)$, $(OCuO)(O_2)_2$, $(OCuO_2)(O_2)$, as reported by H. Wu *et al.* [2]. But the CuO_3^- is shown to have an $OCuO_2$ structure that could dissociate and form an internally hot CuO^- plus O_2. Therefore, the structure of CuO_3^- could be considered as CuO perturbed by an O_2. And the CuO_5^- is considered to have the similar structure with CuO_3^-. As for the CuO_4^- and CuO_6^-, they also show as two isomers of each other, and are the isomer of a Cu/O_2 complex. In our study, with the Ar/H_2 plasma-treatment, O_2 would join to the hydrogen-oxygen reaction. Also, the excited states of the anion for CuO^- were observed. It has been reported that the transitions from to $Cu^{2+}O^{2-}$

excited states of CuO, which shows significant geometry changes from the anion ground state, which is assumed to be contributed to the combination of two copper atoms [3, 4].

5.7 Conclusions

In this chapter, the important factors affecting the reduction and sintering of copper nano-particles by plasma-treatment were investigated. Reducing the treatment distance could result in shortening the treatment time for sintering of copper nano-particles and an increase of emission intensity from Ar/H_2 plasma jet. The RF power and treatment time is assumed as an inverse proportional relationship for the copper nano-particles sintering. For the similar emission intensity from Hα, the emission intensity from excited Ar atoms is considered to be decisive on sintering the copper nano-particles. However, nether the flow rate of H_2 too little nor too much could get a good sintering result by plasma-treatment. The obtained results strongly suggested that the emission intensity ratio Hα/Ar played an important role in the sintering of copper nano-particle by Ar/H_2 plasma-treatment at ambient temperature.

The changes in atomic orbital of copper due to the energy transfer from the excited state of Ar should be considered to understand the reactions at ambient temperature induced by the plasma jet.

References

[1] Charles Kittel: *Introduction to Solid State Physics*, New York. John Wjley &Sons, Inc. 1956.

[2] H. Wu, S. R. Desai, L. S. Wang: *J. Phys. Chem. A*, **101**, 2103 (1997)

[3] M. Anpo, T. Nomura, T. Kitao, E. Giamello, D. Murphy, M. Che, M. A. Fox: *Res. Chem. Intermediat.*, **15**, 225 (1991)

[4] H. H. Kart, G. Wang, I. Karaman, T Çağin: *Int. J. Mod. Phys. C*, **20**, 179 (2009)

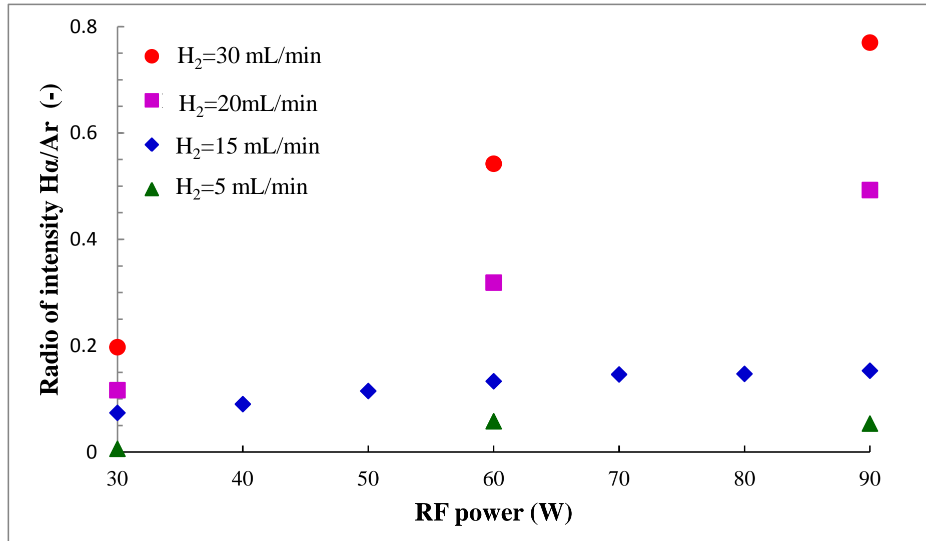

Fig. 5.1 Changes in the ratio of emission intensity Hα/Ar in Ar/H_2 plasma generated by the beam plasma torch with air-cooling depending on the RF power at the constant Ar flow rate of 25 L/min.

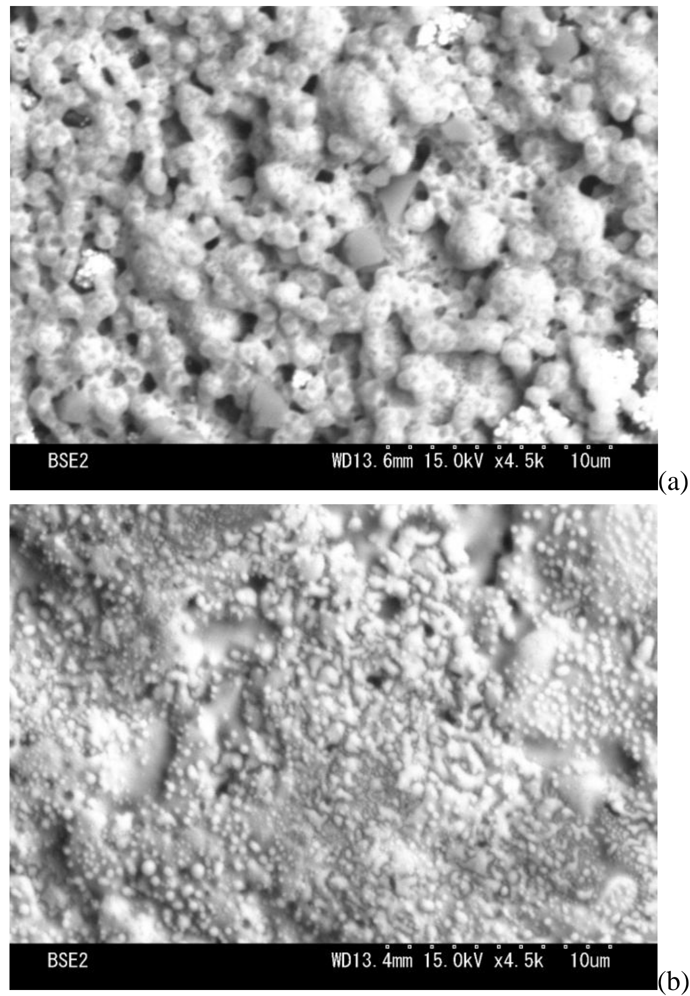

Fig. 5.2 SEM images showing the surface morphologies of the copper nano-particles on the surface of the samples treated for 7 minutes at ambient temperature with the distance of 1.5 mm down from the plasma torch head at the constant Ar flow rate of 25 L/min and H_2 flow rate of 15 mL/min. The RF power was set at 90 W for the beam plasma torch with air-cooling (a); RF power was set at 60 W for the beam plasma torch with air-cooling (b)

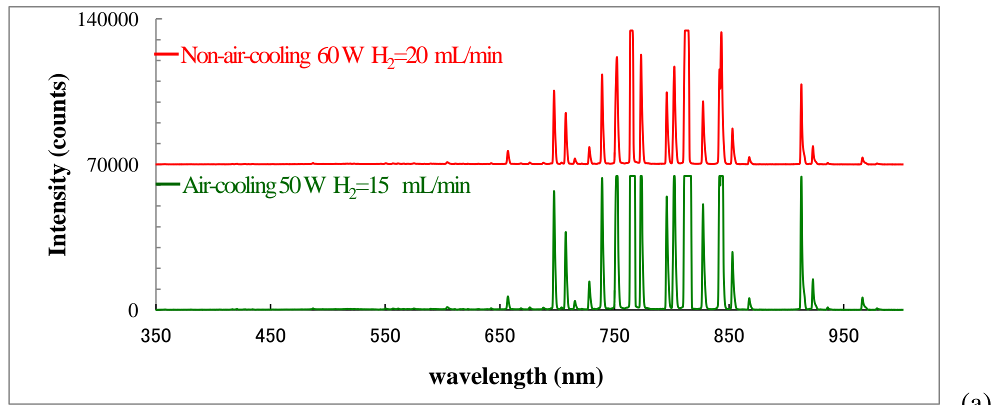

(a)

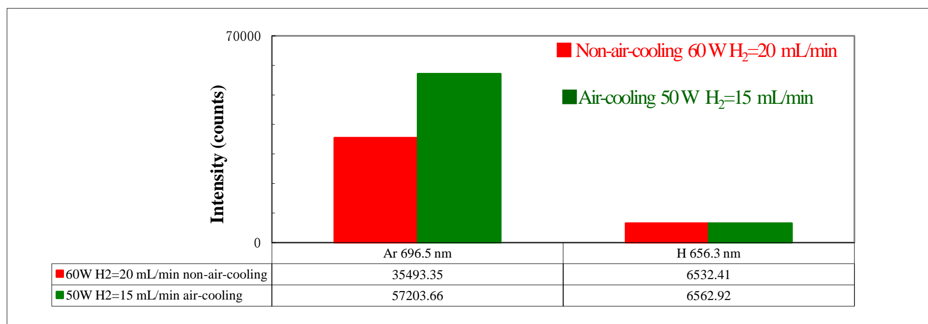

(b)

Fig. 5.3 (a) Comparison of the optical emission spectra of Ar/H_2 plasma jet at the constant Ar flow rate of 25 L/min between the plasma generated by the beam plasma torch without air-cooling at the H_2 flow rate of 20 mL/min and RF power of 60 W (red line) and that generated by the beam plasma torch with air-cooling as H_2 flow rate of 15 mL/min and RF power of 50 W (green line)

(b) Comparison of the optical emission spectra of excited Ar atoms at 656.5 nm and excited H atoms at 656.3 nm in Ar/H_2 plasma jet shown in (a)

The optical emission spectra were collected at the position of 3 mm down from the plasma torch head and 2 mm side from the plasma jet end. The integration time was 20 ns.

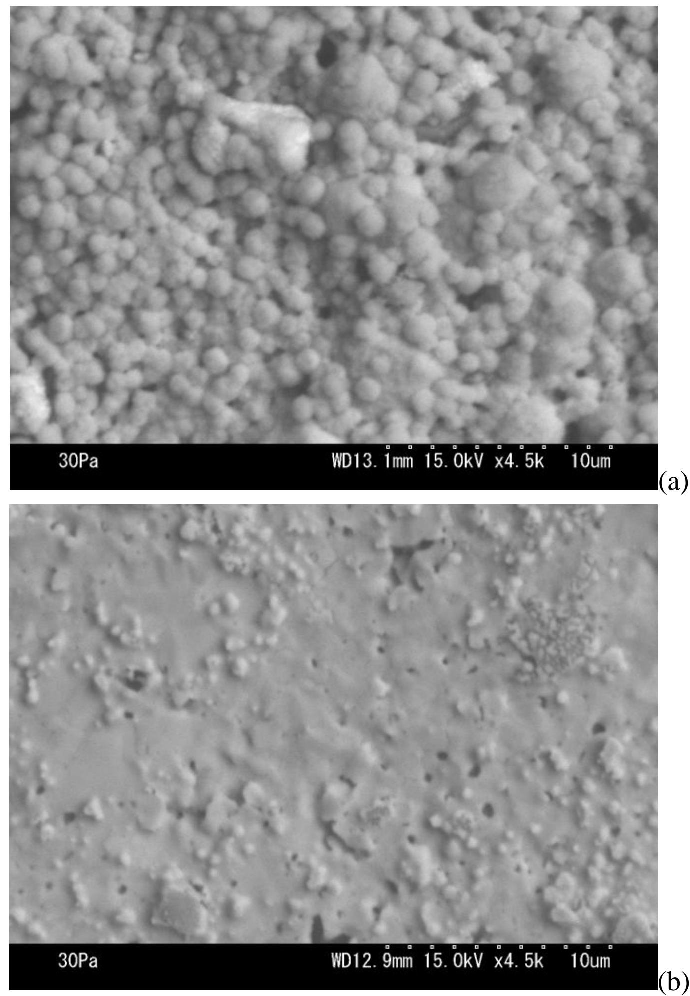

Fig. 5.4 SEM images showing the surface morphologies of the samples treated for 10 minutes as the distance of 1.5 mm down from the plasma torch head. The RF power was set at 60 W for the beam plasma torch without air-cooling at the Ar flow rate of 25 L/min and H_2 flow rate of 20 mL/min (a); The RF power was set at 50 W for the beam plasma torch with air-cooling at the Ar flow rate of 25 L/min and H_2 flow rate of 15 mL/min (b)

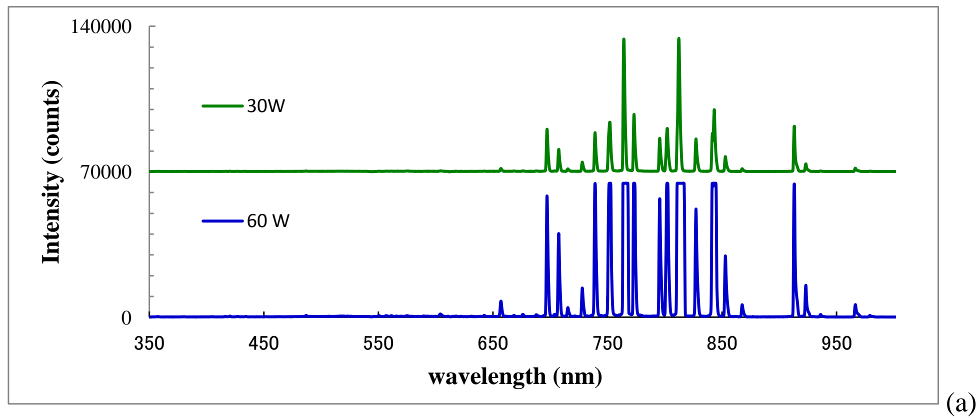

(a)

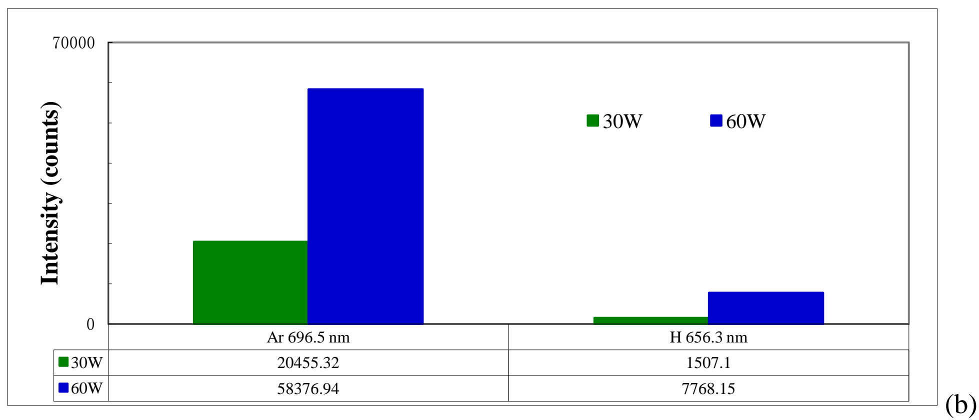

	Ar 696.5 nm	H 656.3 nm
30W	20455.32	1507.1
60W	58376.94	7768.15

(b)

Fig. 5.5 (a) Comparison of the optical emission spectra of Ar/H_2 plasma jet generated by the beam plasma torch with air-cooling as the constant Ar flow rate of 25 L/min and H_2 flow rate of 15 mL/min and the RF power set at 30 W (green line) with the RF power set at 60 W (blue line).

(b) Comparison of the optical emission spectra of excited Ar atoms at 656.5 nm and excited H atoms at 656.3 nm in Ar/H_2 plasma jet shown in (a).

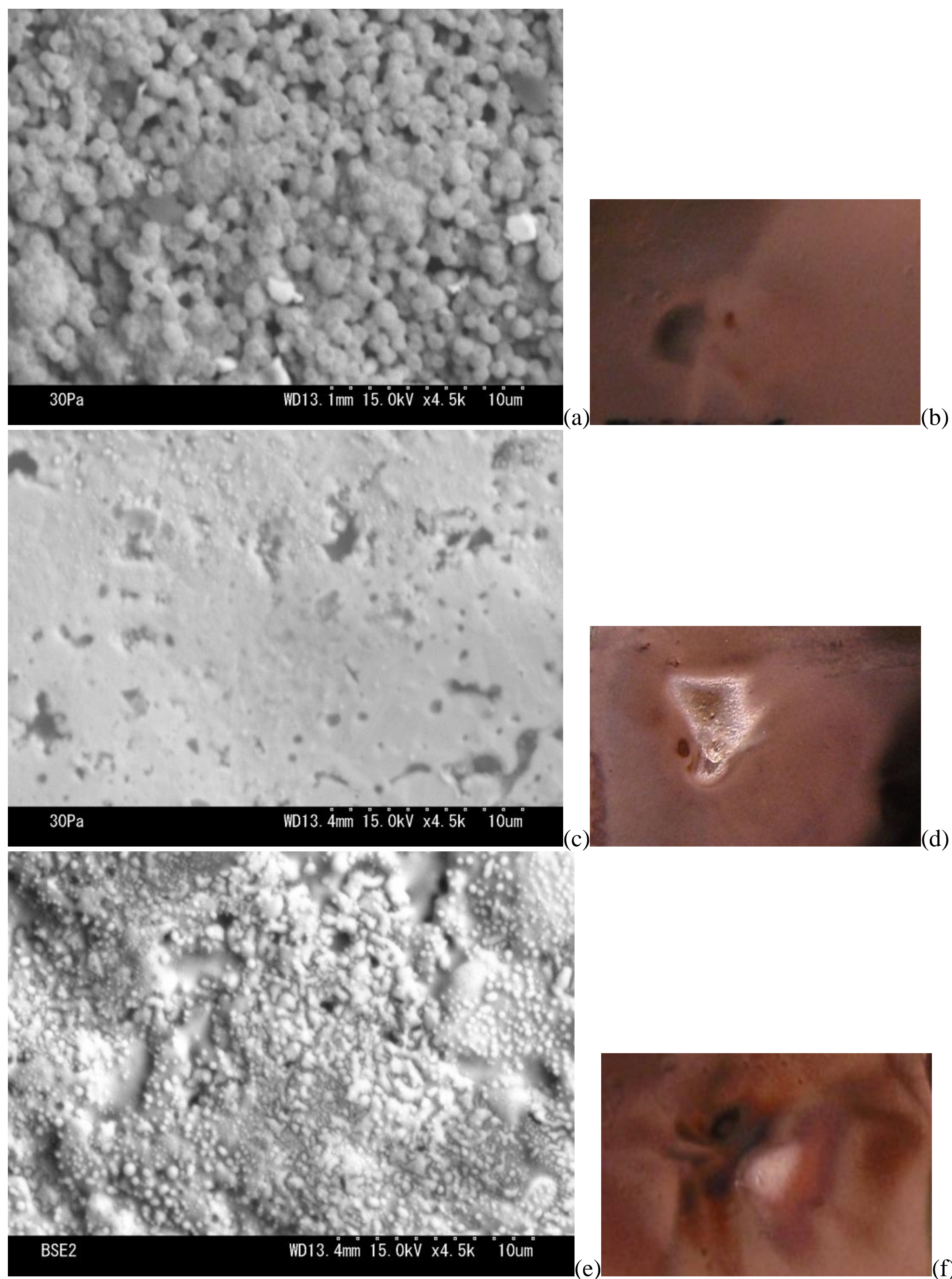

Fig. 5.6 SEM images showing the surface morphologies of the samples treated by the beam plasma torch with air-cooling at the Ar flow rate of 25 L/min and H_2 flow rate of 15 mL/min as the distance of 1.5 mm down from the plasma torch head, for 10 minutes at RF power of 30 W (a); the photograph of the sample (a) (b); for 20 minutes at RF power of 30 W (c); the photograph of the sample (c) (d); for 7 minutes at RF power of 60 W (e); the photograph of the sample (e) (f).

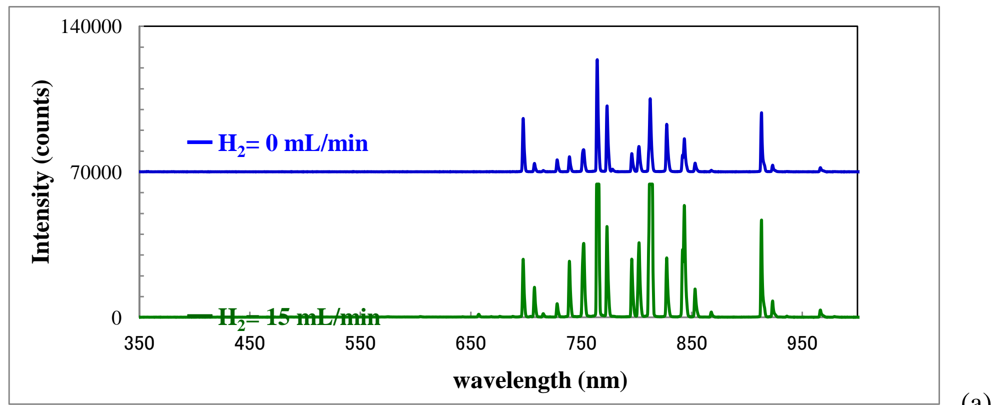

(a)

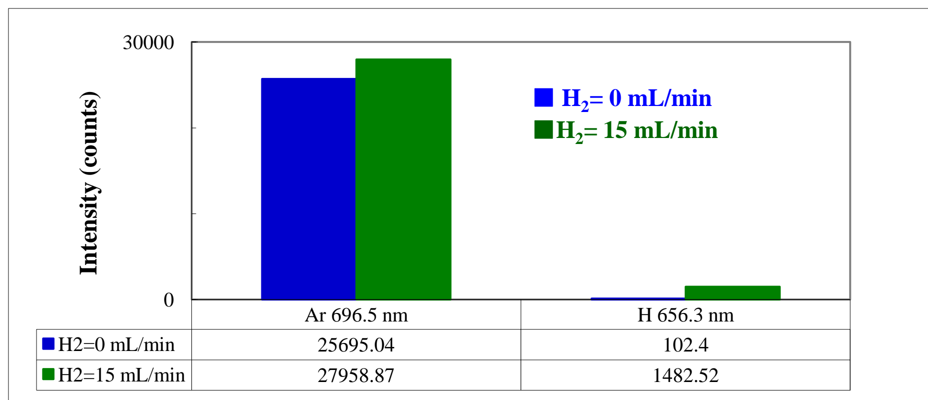

	Ar 696.5 nm	H 656.3 nm
H2=0 mL/min	25695.04	102.4
H2=15 mL/min	27958.87	1482.52

(b)

Fig. 5.7 (a) Comparison of the optical emission spectra of pure Ar plasma (blue line) with Ar/H_2 plasma with H_2 flow rate of 15 mL/min (green line) generated by the beam plasma torch with air-cooling at the constant Ar flow rate of 25 L/min and RF power of 30 W.

(b) Comparison of the optical emission spectra of excited Ar atoms at 696.5 nm and excited H atoms at 656.3 nm in the spectra shown in (a)

The optical emission spectra were collected at a position of 3 mm down from the plasma torch head and 2 mm side from the plasma jet end. The integration time was 20 ns.

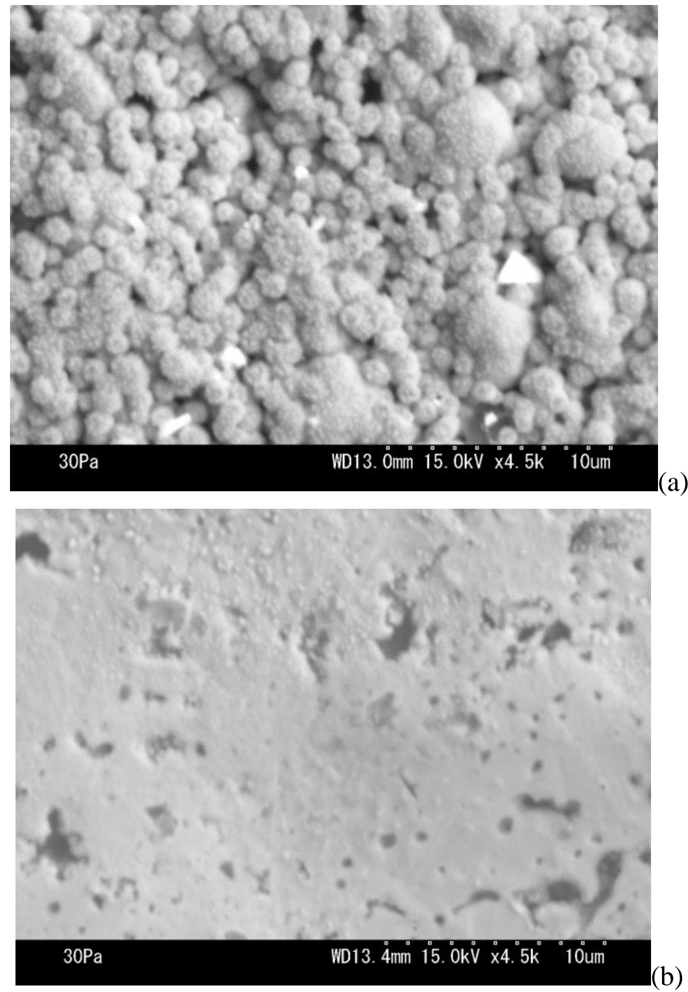

Fig. 5.8 SEM images showing the surface morphologies of the samples treated by the beam plasma torch with air-cooling for 20 minutes at RF power of 30 W and the distance of 1.5 mm down from the plasma torch head with the constant Ar flow rate of 25 L/min, without H_2 addition (a), with the H_2 flow rate of 15 mL/min (b).

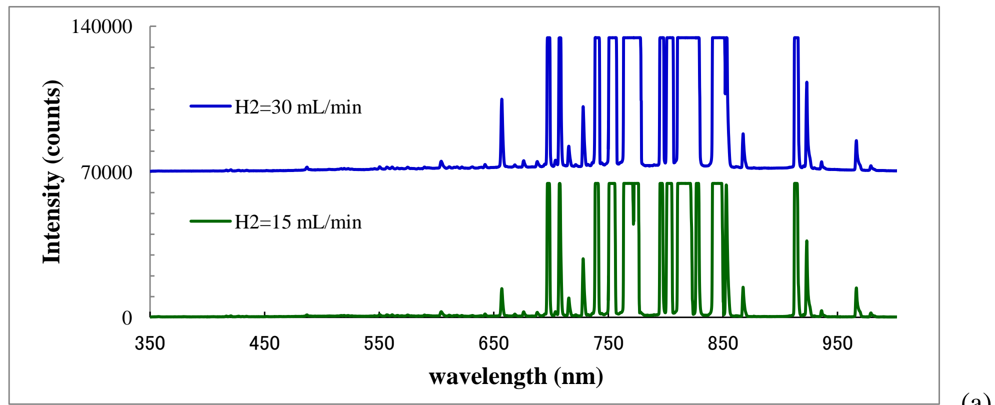

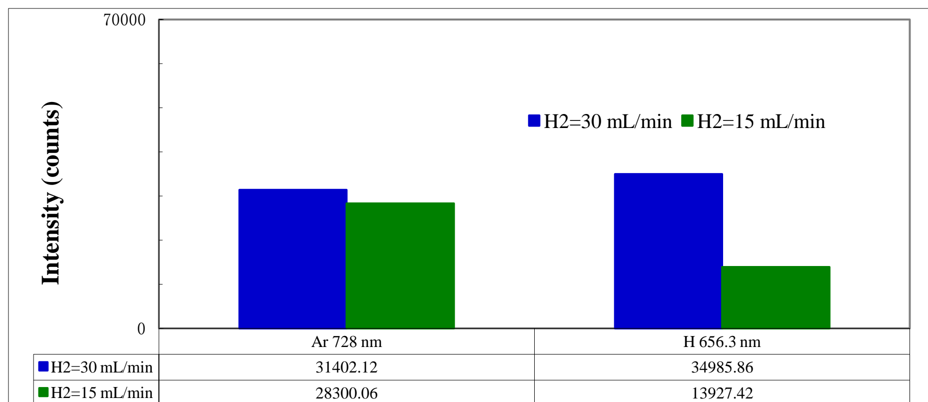

Fig. 5.9 (a) Comparison of optical emission spectra of Ar/H_2 plasma generated by the beam plasma torch with air-cooling at RF power of 60 W and the constant Ar flow rate of 25 L/min, H_2 flow rate of 30 mL/min (blue line), and 15 mL/min (green line).

(b) Comparison of optical emission spectra of excited Ar atoms at 728 nm and excited H atoms at 656.3 nm in Ar/H_2 plasma jet shown in (a)

The optical emission spectra were collected at a position of 3 mm down from the plasma torch head and 2 mm side from the plasma jet end. The integration time was 20 ns.

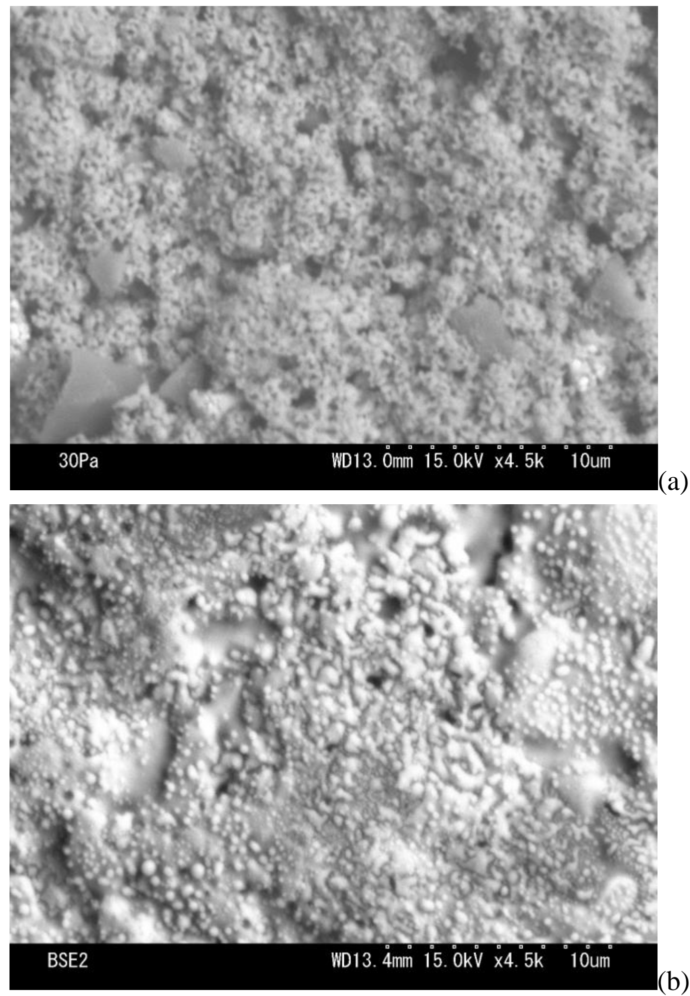

Fig. 5.10 SEM images showing the surface morphologies of the samples treated by the beam plasma torch with air-cooling at RF power of 60 W and the distance of 1.5 mm down from the plasma torch head with the constant Ar flow rate of 25 L/min, the H_2 flow rate of 30 mL/min (a); H_2 flow rate of 15 mL/min (b)

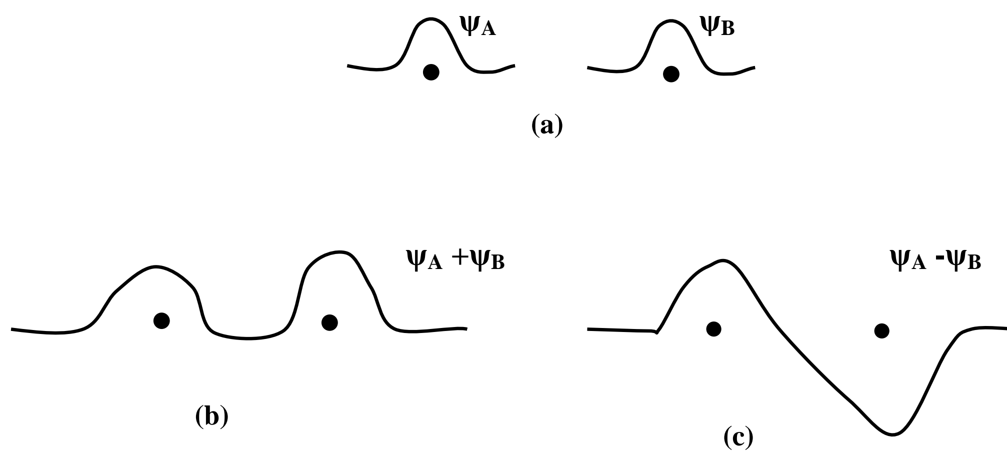

Fig. 5.11 Changes of electron wave function of the H atoms under various conditions. Ground state (a); close to each other by obtaining energy (b); excited state (c).

Chapter 6 Summary

The aims of this study were to apply the copper nano-particles in electronic components area, e.g. the circuit board industry, to reduce the production cost and improve the performance. So in order to overcome the shortcoming that copper is easily to be oxidized in atmosphere, reduce and sinter the copper nano-particles at relatively low temperature to improve the conductivity of the copper nano-paste, and investigate the mechanism and important factors affecting the reduction and sintering of the copper nano-particles, non-equilibrium atmospheric pressure plasma jet generated from three kinds of plasma torches was used, which is an APC plasma torch, a beam plasma torch, and a beam plasma torch with an air-cooling system of electrode. The characteristics of the plasma jets generated by the three plasma torches were investigated and various experiments were carried out for the purpose of reduction and sintering copper nano-particles. It has been confirmed that the oxidized copper nano-particles could be reduced at ambient temperature with 1 minute in atmosphere, and be sintered ambient temperature ambient temperature with in 7 minutes in inner atmosphere.

In chapter 2, the electrical and optical characteristics of both Ar plasma and Ar/H_2 plasma generated by APC plasma torch were investigated. Addition H_2 in to the Ar plasma resulted in a quenching effect on the emission intensity from Ar plasma, and played an important role in reduction and sintering of copper nano-particles by atmospheric pressure plasma. With Ar/H_2 plasma, the sample could be reduced at ambient temperature within 1 minute. At 425 ℃, the copper nano-particles could be sintered to reduce the electric resistance to the bulk copper level with Ar/ H_2 plasma-treatment for 8 minutes and 12 minutes. The conductivity of the plasma-treated films was greatly improved.

In chapter 3, in order to reduce the sintering temperature of copper nano-particles by plasma, beam plasma torch with the plasma nozzle diameter of 1 mm was developed. The electrical and optical characteristics of plasma generated beam plasma torch were investigated. With increasing Ar flow rate from 5 L/min to 25 L/min, both the electrical and optical characteristics were greatly improved, and the plasma jet became more powerful. With addition of H_2 into Ar plasma, the emission intensity from Ar/ H_2 plasma jet was greatly increased. In atmosphere, the Ar/H_2 plasma-treatment with the Ar flow rate of 5 L/min and H_2 flow rate of 10 mL/min at RF power of 60 W for 12 cycles at 425 ℃ could result in the sintering of copper nano-particles, while the surface of the sample was oxidized because of the small nozzle. In order to prevent the sample oxidization, the plasma-treatment was carried out in a glass chamber in inert atmosphere. At ambient temperature, Ar/H_2 plasma with the Ar flow rate of 25 L/min and H_2 flow rate of 5 mL/min at RF power of 30 W could lead the reduction of copper nano-particles, and increasing the RF power to 60 W, it could lead to sintering of copper nano-particles by Ar/ H_2 plasma-treatment for 5 minutes at ambient temperature.

In chapter 4, beam plasma torch with air-cooling system of inner electrode was used to investigate the effect of air-cooling of electrode on the characteristics of plasma jet, and reduction and sintering ability of copper nano-particles. With air-cooling of electrode, both the electrical and optical characteristics were improved. Also, adding H_2 to Ar plasma enhanced the emission intensity from Ar/H_2 plasma jet. As for the air-cooling the beam plasma jet, Ar flow rate of 25 L/min and H_2 flow rate of 15 mL/min were selected as the most suitable experimental condition for reduction and sintering copper nano-particles. At ambient temperature, Ar/H_2 plasma-treatment at RF power of 30 W at a distance of 3 mm could reduce the copper nano-particles. At RF power of 60 W, the copper

nano-particles could be sintered by plasma-treatment for 10 minutes at the distance of 3 mm. It showed the dependence of the sintering of the copper nano-particles on the emission intensity from plasma jet.

In chapter 5, the important factors affecting the reduction and sintering of copper nano-particles by plasma-treatment were investigated. The emission intensity from excited Ar atoms and the emission intensity ratio of Hα/Ar are suggested as two of the most important factors. It is also indicated that the treatment distance and time are greatly affect the sintering of copper nano-particles as the same emission intensity ratio of Hα/Ar.

Base on those mentioned above, the objectives of this study are considered to have been achieved. As for the further study in future, it is necessary to improve the experimental setups used in treating the samples in inert atmosphere, moving the samples, and further improve the conductivity of the copper nano-pastes. In addition, I also hope to further investigate the detailed mechanism of reduction and sintering of copper nano-particles by non-equilibrium atmospheric pressure plasma from the perspective of atomic collisions.

List of publications

1. Reduction and sintering of copper nano-particles by non-equilibrium atmospheric pressure plasma jet

Guiling Zhang, Katsuhiko Hosoi, Shin-ichi Kuroda

Advance Science Letters

Related to Chapter 2

2. Effect of H_2 gas addition on electrical and optical characteristics of RF capacitive atmospheric pressure non-equilibrium argon plasma jet

Guiling Zhang, Xiaomeng Fei, Tamio Mori, Katsuhiko Hosoi, Shin-ichi Kuroda

Journal of Materials Life Society

Related to Chapter 3

Acknowledgements

First and foremost, I would like to show my deepest gratitude to my supervisor, Dr. Shin-in Kuroda, a respectable, responsible and resourceful scholar, who has provided me with valuable guidance in every stage of the writing of this thesis. Without his enlightening instruction, impressive kindness and patience, I could not have completed my thesis. His keen and vigorous academic observation enlightens me not only in this thesis but also in my future study.

I shall extend my thanks to Dr Kawai and Ms. Konoma for their kindness and help during my study in Gunma University.

I wish to give special thanks to Professor Tobita, Professor Sakurai, Professor Takahashi, and Professor Lin for their invaluable suggestions and comments to this thesis.

A deep gratitude is also given to all the members of Kuroda Laboratory, especially to Dr. Hosoi and the members of plasma group, for their kind guidance and assistance. We have formed profound friendship.

Also I hope to express my appreciation to Mr. Mori from Cresur Corporation for providing the plasma devices and the technical support.

Moreover, I wish to give thanks to Japan Students Services Organization for the supply of scholarship and support.

Lastly, my thanks would go to my beloved family for their loving considerations and great confidence in me all through these years. I also owe my sincere gratitude to my friends who gave me their help and time in listening to me and helping me work out my problems during the difficult course of the thesis.